SCIENCE WITH A MILLIMETER ARRAY

MMA DESIGN STUDY VOLUME I

MILLIMETER ARRAY

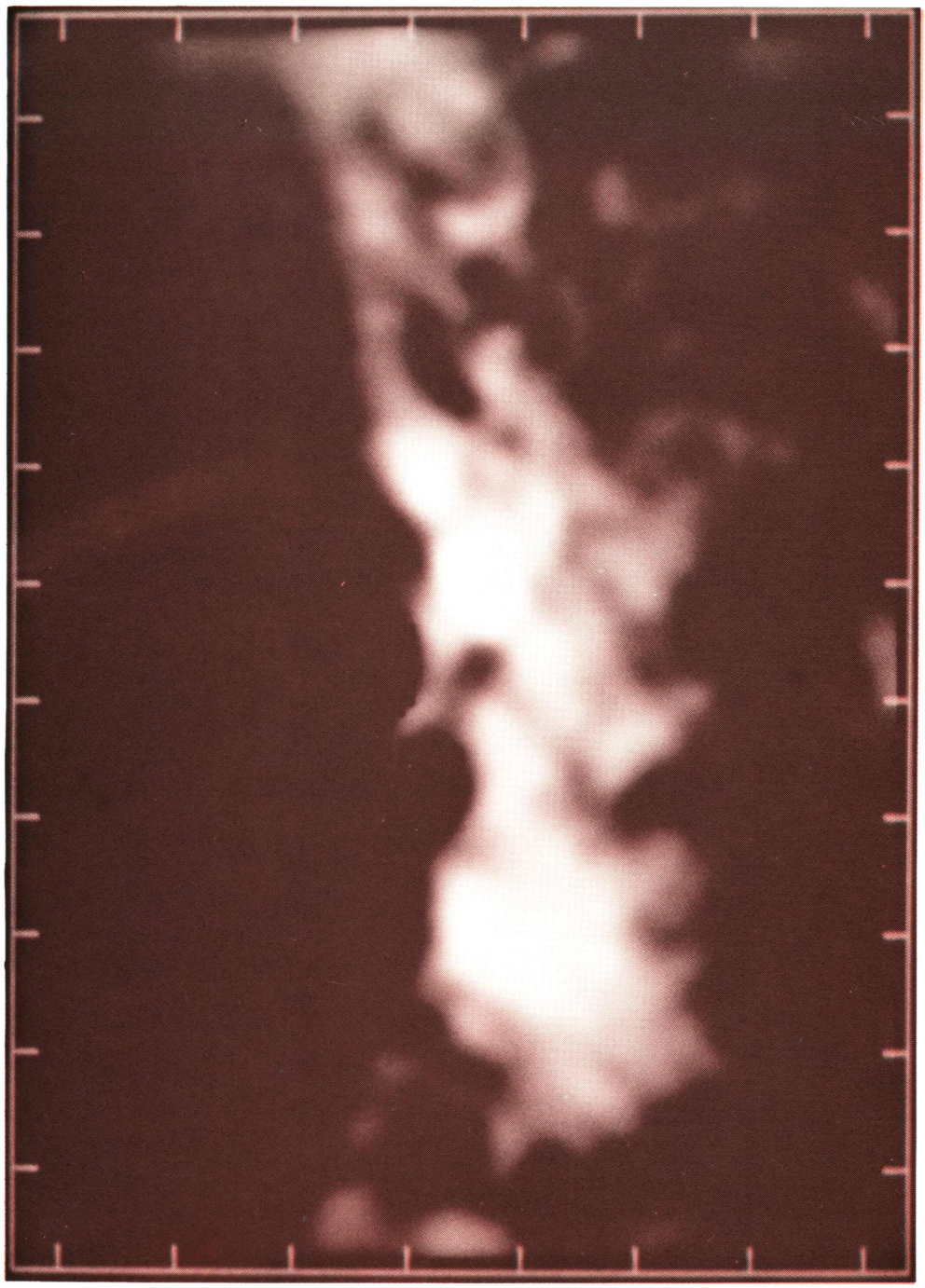

January 1988

The National Radio Astronomy Observatory is operated by Associated Universities Inc., under contract with the National Science Foundation.

Cover Illustration: An image of the integrated CS $J = 2$–1 emission from OMC–1 (L. G. Mundy, T. J. Cornwell, C. R. Masson, N. Z. Scoville, L. B. Baath, and L. E. B. Johansson (1988), *Astrophys. J.*, in press), obtained by maximum entropy processing. This image combines data from several fields mapped with the Owens Valley Millimeter-Wave Interferometer and the 20 meter telescope of the Onsala Space Observatory. This image, in which emission is integrated over the velocity interval -0.2 to 18.2 km s^{-1}, includes all of the flux from the source. The resolution of the image is $7''.5$, and the positional accuracy of the compact features is $1''$ to $2''$.

Science with a Millimeter Array

PROCEEDINGS OF AN NRAO WORKSHOP
HELD AT THE NATIONAL RADIO ASTRONOMY OBSERVATORY
GREEN BANK, WEST VIRGINIA
SEPTEMBER 30–OCTOBER 1, 1985

EDITED BY A. WOOTTEN AND F. R. SCHWAB

Workshop Volume No. 14

MMA Design Study, Volume I

The National Radio Astronomy Observatory (NRAO) is operated by Associated Universities, Inc., under contract with the National Science Foundation.

CONTENTS

List of Participants

T. Armstrong	*National Radio Astronomy Observatory*
J. Bally	*A. T. & T., Bell Laboratories*
T. Bania	*Boston University*
G. Berge	*California Institute of Technology*
J. Bieging	*University of California at Berkeley*
L. Blitz	*University of Maryland*
R. Brown	*National Radio Astronomy Observatory*
J. Condon	*National Radio Astronomy Observatory*
T. Cornwell	*National Radio Astronomy Observatory*
W. Cotton	*National Radio Astronomy Observatory*
P. Crane	*National Radio Astronomy Observatory*
I. de Pater	*University of California at Berkeley*
H. Dickel	*University of Illinois*
G. Dulk	*University of Colorado*
N. Evans	*University of Texas*
J. Gallagher	*National Optical Astronomy Observatory*
D. Gary	*California Institute of Technology*
S. Gottesman	*University of Florida*
E. Herbst	*Duke University*
R. Hjellming	*National Radio Astronomy Observatory*
P. T. P. Ho	*Harvard University*
D. Hogg	*National Radio Astronomy Observatory*
W. Irvine	*University of Massachusetts*
P. Jewell	*National Radio Astronomy Observatory*
G. Knapp	*Princeton University*
M. Kundu	*University of Maryland*
M. Kutner	*Rensselaer Polytechnic Institute*
H. Liszt	*National Radio Astronomy Observatory*
K. Y. Lo	*California Institute of Technology*
R. Maddalena	*National Radio Astronomy Observatory*
H. Martin	*National Radio Astronomy Observatory*
C. Masson	*California Institute of Technology*
D. Muhleman	*California Institute of Technology*
L. Mundy	*California Institute of Technology*
P. Myers	*Smithsonian Astrophysical Observatory*
F. Owen	*National Radio Astronomy Observatory*
B. Partridge	*Haverford College*
S. Reynolds	*North Carolina State University*
L. Rickard	*Howard University*
A. Sargent	*California Institute of Technology*
P. Schloerb	*University of Massachusetts*
P. Schwartz	*Naval Research Laboratories*
N. Scoville	*California Institute of Technology*
G. Seielstad	*National Radio Astronomy Observatory*
L. Snyder	*University of Illinois*
P. Solomon	*State University of New York at Stony Brook*
R. Sramek	*National Radio Astronomy Observatory*
A. Stark	*A. T. & T., Bell Laboratories*

List of Participants

B. Turner	*National Radio Astronomy Observatory*
J. Uson	*National Radio Astronomy Observatory*
P. Vanden Bout	*National Radio Astronomy Observatory*
J. van Gorkom	*National Radio Astronomy Observatory*
S. Vogel	*University of California at Berkeley*
P. Wannier	*Jet Propulsion Laboratory*
S. Weinreb	*National Radio Astronomy Observatory*
W. J. Welch	*University of California at Berkeley*
R. Wilson	*A. T. & T., Bell Laboratories*
A. Wootten	*National Radio Astronomy Observatory*
M. Wright	*University of California at Berkeley*

FOREWORD

On 30 September–1 October 1985 about sixty astronomers gathered amidst the bright fall foliage at Green Bank, West Virginia for the Millimeter Array Science Workshop. This volume constitutes the proceedings of that workshop.

This workshop is part of a process begun in 1983. In that year, the National Science Foundation asked a committee chaired by Alan Barrett[1] for guidance on the priorities for the future of millimeter and sub-millimeter astronomy. Among the committee's three recommendations was a request for a design study for a national millimeter-wavelength array. From this grew the specific ideas for such a benchmark array sketched in Chapter I by R. Hjellming. The purpose of the workshop was to define the scientific goals which a millimeter array loosely conforming to the description in Chapter I might address, and to recommend how the array described there should be modified to address the scientific problems.

To this end, discussion was divided among seven working groups: The Solar System (I. de Pater, chair), The Sun and Stars (G. Dulk, chair), Evolved Stars and Circumstellar Shells (P. Schwartz, chair), Star Formation and Molecular Clouds (N. J. Evans, chair), Astrochemistry (L. Snyder, chair), Low-z Extragalactic Studies (L. Blitz, chair), and High-z Extragalactic Studies (B. Partridge, chair). Most groups found the benchmark array well suited for doing the science that they wanted to do. In the closing session of the workshop, the chairpersons presented reports on the discussions in their groups, stressing the characteristics which they deemed desirable for the array. The importance of dust emission was stressed by several groups, and measurement of dust emission was a goal which drove the frequency requirements of the array upward. Much of the discussion centered on tradeoffs between long baselines and high frequency operation of the array.

Chapter I originally appeared as Number 34 of the Millimeter Array Memorandum Series, but it has been completely rewritten as presented here. The subsequent chapters are the reports of the chairpersons of the working groups. These chapters were distributed as documents in the Millimeter Array Science Memorandum Series. They have been distilled to form the science section of the document requested by the 1983 Barrett report.

Smooth operation of the workshop was assured by the competent engineering of the Green Bank staff. I especially appreciate the help from Becky Warner, Richard Fleming, and the cafeteria staff in ensuring that the meeting flowed in a laminar fashion. I speak for all the participants, I am sure, in thanking George Seielstad for making Green Bank available to us during one of

[1]Other committee members were Charles J. Lada, Patrick Palmer, Lewis E. Snyder, and William J. Welch.

its most delightful seasons. In Charlottesville, Pat Smiley and George Kessler designed and produced the present volume. Phyllis Jackson provided invaluable organizational skills for keeping track of the participants and ensuring their safe arrival in Green Bank.

AL WOOTTEN
NRAO, Charlottesville
15 December 1986

I. The Concept of the NRAO Millimeter Array

R. M. Hjellming

1. Summary of Instrumental Components

This Chapter summarizes the state of thinking on the paradigm Millimeter Array system just prior to the Millimeter Array Science Workshop, held in September–October, 1985. This Chapter is an updated version of Millimeter Array Memorandum No. 34, which was distributed just before the science workshop.

Two arrays are put forth here in order to cover the range of desired resolutions and fields of view. The current paradigm (or so-called "strawman array") consists of a large array of ~ 21 movable antennas of ~ 10 m diameter, together with a small array of ~ 21 antennas of ~ 4 m diameter mounted on a structure ~ 29 m in size in a multi-telescope (M-T) configuration with $\sim 50\%$ filling factor and 25 m resolution. Figure 1 schematically illustrates the major options being discussed for configurations for the two arrays.

Figure 2a shows the relative sampling of the sky by the two sizes of antennas when the multi-element-telescope is used for the complementary instrument. A hexagonal grouping of seven different fields, observed by the large array antennas, will be matched with a single field of view for the small antennas of the multi-element-telescope component. It is essential to the imaging properties of this facility that four different types of observations can be made and used for image reconstruction:

(1) aperture-synthesis observations with the arrays of twenty-one 10 meter antennas with maximum separations of $B_{(\mathrm{km})}$ to obtain data with resolution $(0\farcs19/B_{(\mathrm{km})})\lambda_{(\mathrm{mm})}$;
(2) aperture-synthesis observations with the array of twenty-one 4 meter antennas to obtain data with $8''\lambda_{(\mathrm{mm})}$ resolution;
(3) total-power observations with one or more of the 10 meter antennas to obtain data with $20''\lambda_{(\mathrm{mm})}$ resolution; and
(4) total-power observations with the 4 meter antennas to obtain data with $50''\lambda_{(\mathrm{mm})}$ resolution.

The 10 meter and 4 meter antennas have fields of view of $20''\lambda_{(\mathrm{mm})}$ and $50''\lambda_{(\mathrm{mm})}$, respectively. Imaging at the level of two pixels per resolution element involves arrays of $210^2 B^2_{(\mathrm{km})}$ and 13^2 pixels for the large array with size scale $B_{(\mathrm{km})}$ and the Multi-Telescope array, respectively. The alternative for the complementary instrument is a large single antenna with diameter ~ 25 m that would observe mainly in total-power (or switched-power) mode. However, in order to have comparable speed in imaging the $50''\lambda_{(\mathrm{mm})}$ field of view of the multi-element-telescope, the 25 m antenna must be multi-beamed with $(25/4)^2 \approx 37$ beams, using either multiple feeds at the focal plane or a 37-element focal plane receiver. Figure 2b is a schematic diagram illustrating how the multi-beaming antenna covers approximately the same simultaneous field of view as the multi-element-telescope array.

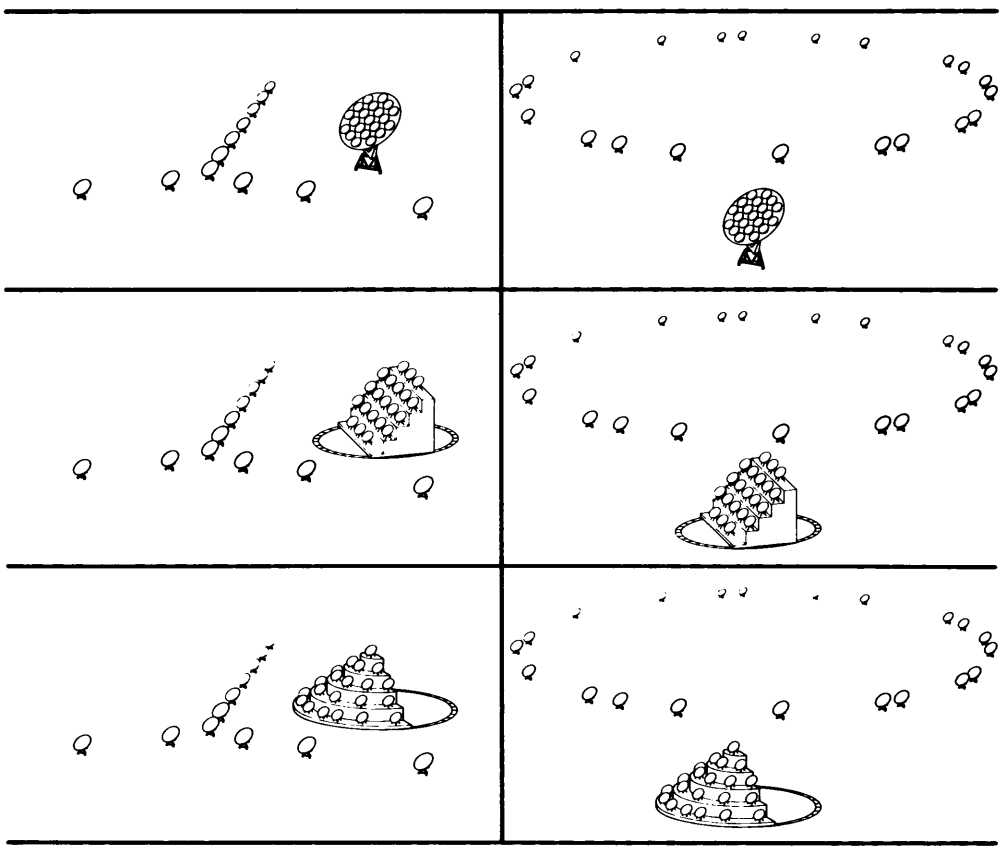

Possible 300 m and Multi-Telescope Configurations

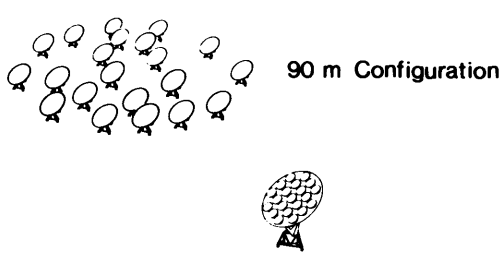

90 m Configuration

Figure 1. Millimeter array configurations.

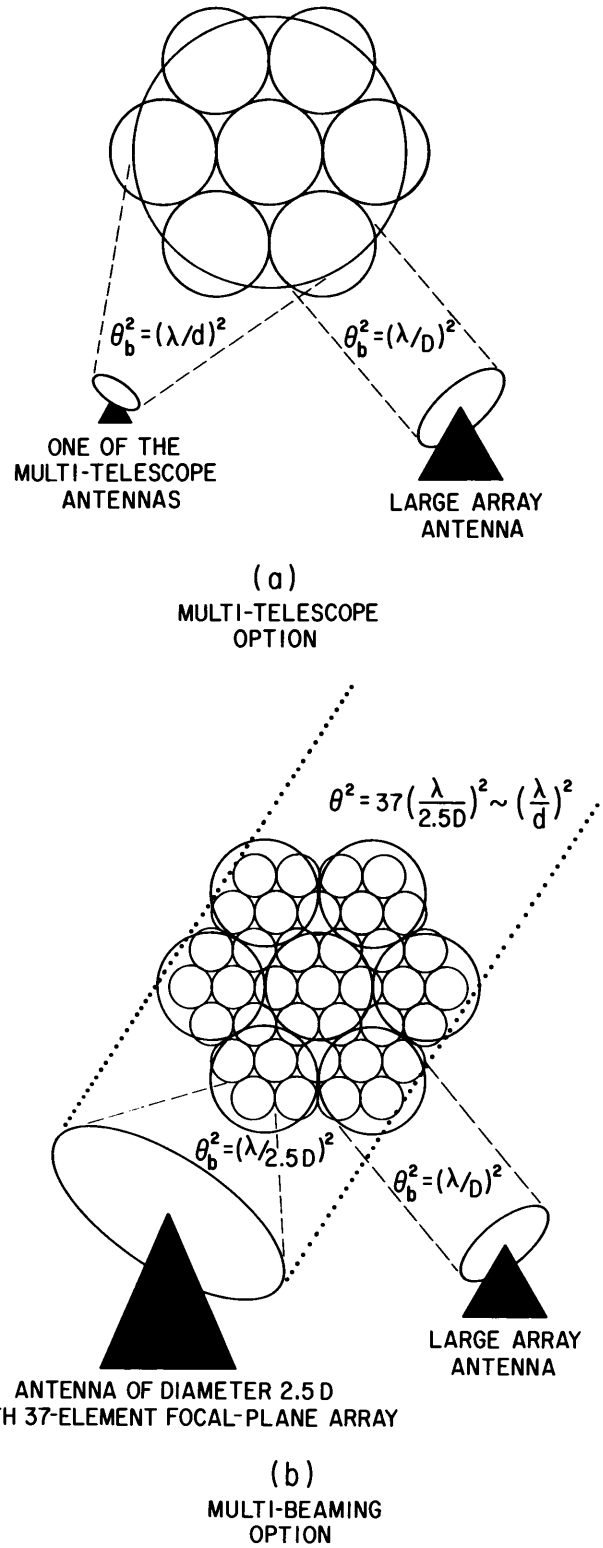

Figure 2. Sky sampling for millimeter imaging.

2. Instrumental Sensitivities

1. Antenna and correlator sensitivity. In order to discuss the sensitivity of individual antennas and that of arrays to both point sources and extended sources, we must define some parameters and, in some cases, assume standard values for these parameters:

ν_s = sky observing frequency,
$\Delta\nu$ = IF bandwidth,
Δt = integration time assumed in sensitivity calculations,
D = diameter of one of the antennas (= 4, 10, or 25 m),
ϵ_a = aperture efficiency of an antenna (= 0.5 assumed),
ϵ_q = correlator quantization efficiency (= 0.82 for 3-level quantization),
ϵ_l = "warm spillover" efficiency of an antenna (= 0.85 assumed),
$\epsilon_{\rm fss}$ = "cold spillover" efficiency of an antenna (= 0.85 assumed),
$T_{\rm sys}$ = system temperature (including receiver temperature, atmospheric absorption/emission, spillover, background),
$T_{\rm rcvr}$ = receiver temperature (ν_s K assumed),
$T_{\rm atm}$ = ambient temperature of the atmosphere (= 280 K assumed),
$T_{\rm sbr}$ = received temperature for rear spillover, blockage, and ohmic losses (= 280 K assumed),
$T_{\rm bg}$ = received temperature due to cosmic background (= 2.7 K),
ζ = zenith angle ($= \frac{\pi}{2}$ minus the elevation),
A = air mass for a particular observation ($\propto \sec\zeta$),
τ_s = atmospheric optical depth for $\zeta = 0$ and sky observing frequency.

We will adopt a convention whereby radiation temperatures are denoted by primes, i.e.,

$$T' = \frac{h\nu/k}{e^{h\nu/kT} - 1}, \tag{1}$$

where h and k are the Planck and Boltzmann constants. We can then express the total system temperature $T_{\rm sys}$ as a sum of individual contributions:

$$T_{\rm sys} = T_{\rm rcvr}e^{\tau_s A} + \epsilon_l T'_{\rm atm}\left(e^{\tau_s A} - 1\right) + T'_{\rm bg} + (1 - \epsilon_l)T'_{\rm sbr}e^{\tau_s A}, \tag{2}$$

which differs slightly from the commonly used $T^*_{\rm sys}$,[1,2,3] such that

$$T_{\rm sys} = \epsilon_l \epsilon_{\rm fss} T^*_{\rm sys}. \tag{3}$$

[1]Kutner, M. L. and Ulich, B. L. (1981), *Astrophys. J.* **250**, 341.
[2]Ulich, B. L. and Haas, R. W. (1976), *Astrophys. J. Suppl.* **30**, 247.
[3]Jewell, P. R. (1985), "Factors Affecting the Sensitivity of a Millimeter Array—Further Discussion", NRAO Millimeter Array Memo. No. 35.

Now that T_{sys} is defined both conceptually and mathematically we express the r.m.s. sensitivity of

(i) an antenna used in total power mode (σ_a) and
(ii) a correlated antenna pair (σ_c)

as[4]

$$\sigma_a = \frac{4kT_{sys}}{\epsilon_a \pi D^2 \sqrt{\Delta\nu \Delta t}}, \tag{4}$$

and

$$\sigma_c = \frac{4\sqrt{2}\,kT_{sys}}{\epsilon_q \epsilon_a \pi D^2 \sqrt{\Delta\nu \Delta t}}. \tag{5}$$

Equations 4 and 5 can be converted into units of Jy/beam by multiplying by 10^{-26} for *mks* units or 10^{-23} for *cgs* units.

Because of the very strong dependence of T_{sys} upon atmospheric transparency and air mass, as seen in Equation 2, it is not possible to discuss the sensitivity of the MMA without adopting the concept of an average system temperature, which we will denote by $\langle T_{sys} \rangle$. This is an average of T_{sys} over the time of observation, which can be computed from Equation 2 for specific values of τ_s and the actual range of zenith angles. Figure 3 shows plots of T_{sys} as a function of zenith angle for τ_s = 0.05, 0.1, 0.2, 0.3, 0.4, and 0.5 using Equation 2 and the parameters indicated earlier in this section. Based upon the assumption of "good" site conditions where $\tau_s \approx 0.2$, this leads us to use $\langle T_{sys} \rangle$ = 200 K for observations at 100 GHz and 500 K for observations at 230 GHz.

2. Array sensitivity. The sensitivity of an array of antennas involves a number of complications that depend somewhat on both the design of the array and alternatives in image processing. An array of N antennas will have $N_B = N(N-1)/2$ independent correlations for each polarization, and we will assume that the number of combined polarizations, N_p, is 1 or 2. Sensitivity to detection of point sources is then described, using the sensitivity per correlator from Equation 5, by

$$\sigma = \frac{\sigma_c}{\gamma \sqrt{N_p N_B}} \tag{6a}$$

$$= \frac{1.71 \langle T_{sys} \rangle / 100}{\gamma \left(D_{(m)}/10\right)^2 \sqrt{\Delta\nu_{(GHz)} \Delta t_{(min.)} N_p (N_B/210)}}\ \text{mJy}, \tag{6b}$$

where $\gamma = \sqrt{\langle n_c \rangle / \langle n_c \rangle_m}$ is a geometry-dependent factor[5] with n_c being the "average" number of data points per occupied cell in the gridded-data plane,

[4] *Cf.* Thompson, A. R., Moran, J. M., and Swenson, G. W., Jr. (1986), *Interferometry and Synthesis in Radio Astronomy*, John Wiley, New York; Equation 6.43.

[5] Hjellming, R. M. (1985), "Sensitivity Criteria for Aperture Synthesis Arrays", NRAO Millimeter Array Memo. No. 29.

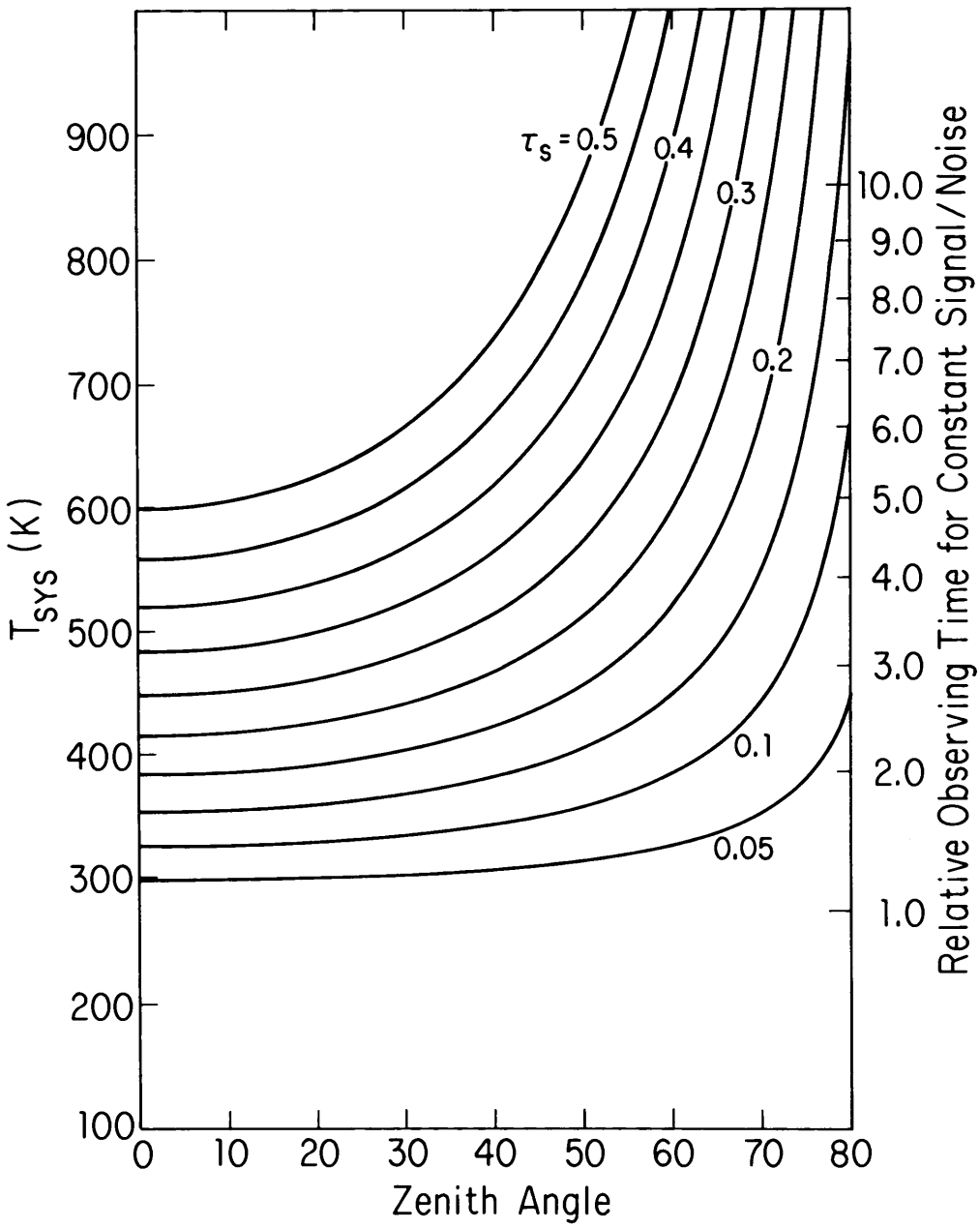

Figure 3. Opacity effects on observing time requirements.

a quantity that depends upon the weighting and tapering adopted during the imaging process, and $\langle n_c \rangle_m$ being the mean number of data points per cell. $\langle n_c \rangle = \langle n_c \rangle_m$ for "natural" weighting; and $\langle n_c \rangle = \langle n_c \rangle_{\rm hm}$, the harmonic mean of the data points per cell, for "uniform" weighting. Thus $\gamma = 1$ for the untapered, naturally weighted case, and $\gamma < 1$ for other cases. In Equation 6b we have evaluated the numerical coefficient for a system temperature of 100 K, bandwidth of 1 GHz, integration time of one minute, and an antenna diameter of 10 meters.

Surface-brightness sensitivity is defined by

$$\Delta T_b = \frac{\sigma_c/2k}{\lambda^2 \Omega_b} = \frac{(\sigma_c/2k)B^2}{\gamma \Gamma \sqrt{\Delta\nu \Delta t N_p N_B}} \tag{7a}$$

$$= \frac{0.62\big(\langle T_{\rm sys}\rangle/100\big)B^2_{\rm (km)}}{\gamma\Gamma\big(D_{\rm (m)}/10\big)^2\sqrt{\Delta\nu_{\rm (GHz)}\Delta t_{\rm (min.)}N_p(N_B/210)}}\,{\rm K}\,, \tag{7b}$$

where Ω_b is the solid angle of the synthesized beam and where we have defined another array-dependent geometry factor, $\Gamma = \Omega_b/(\lambda/B)^2$ with B being the maximum extent of the array. In Equation 7b we have evaluated the numerical coefficient for a system temperature of 100 K, bandwidth of 1 GHz, integration time of one minute, an antenna diameter of 10 meters, and an array with a diameter of 1 km.

3. Observing time for needed sensitivity. Observing times are frequently defined in terms of how long it takes to reach a particular level of sensitivity. For problems defined in terms of point-source-detection-sensitivity we can rewrite Equation 6a so the time needed to reach a sensitivity of $\sigma_{\rm (mJy)}$ is given by

$$\Delta t_{\rm (min.)} = \frac{2.92\big(\langle T_{\rm sys}\rangle/100\big)^2}{\sigma^2_{\rm (mJy)}\gamma^2\big(D_{\rm (m)}/10\big)^4\Delta\nu_{\rm (GHz)}\Delta t_{\rm (min.)}N_pN^2}\,. \tag{8}$$

The dependence of this minimum observing time on the fourth power of the antenna diameter and the second power of N leads one to use the largest practicable diameter for the antennas. However, if one defines the problem differently this dependence changes. If the goal of the array is to obtain the best sensitivity for a large source with solid angle Ω_s ($\gg \Omega_b$), one must observe Ω_s/Ω_b different fields for the time $\Delta t_{\rm (min.)}$, so the source observing time to accomplish this is Δt_s, where

$$\Delta t_s = \frac{\Omega_s}{\Omega_b}\Delta t_{\rm (min.)} \propto \frac{\Omega_s\langle T_{\rm sys}\rangle^2}{\big(\lambda\sigma_{\rm (mJy)}\gamma N D\big)^2\Delta\nu_{\rm (GHz)}\Delta t_{\rm (min.)}N_p}\,. \tag{9}$$

Therefore, the point-source and surface-brightness sensitivities both depend upon the same power of N and D when the total problem of imaging a large object is considered.

4. Analytic aspects of array geometries. The ways in which the array geometry affects the resulting aperture-synthesis images can be simplified in terms of two effects: the degree to which there are "holes", or missing data, in the proper Nyquist sampling of the aperture u-v plane; and the distribution of data points that are measured in the aperture plane. Holes lead to unpredictable defects in the sidelobes of the synthesized beam, as we will discuss later. The distribution of data points in the aperture plane, and the strategies of weighting and tapering used in imaging, affect the size and shape of the final synthesized beam. Because it will illuminate many of the results of the design studies discussed later in this chapter, let us consider the analytic properties of aperture-plane distributions that depend only upon the radius in the two-dimensional aperture plane. If $\mathbf{L}_j$ is the vector location of the jth antenna, then $\mathbf{q} = \mathbf{q}_{jk} = \mathbf{L}_k - \mathbf{L}_j = (u, v, w)$ defines the aperture-plane coordinates of the j-k antenna pair. Since the effects of the w-term can be neglected for most of the arrays of interest for this instrument, we need only consider the relationship between the set of sample complex visibilities, $\{V(u,v)\}$, and the images obtained by Fourier transforming this data set. If we denote the number density of data points in the aperture plane by $N_{uv}(q)$, where $q = \sqrt{u^2 + v^2}$, and if N_{uv} is radially symmetric, and we neglect the effects of data missing according to the sampling theorem, the synthesized beam is the two-dimensional Fourier transform in u and v, or a Hankel transform[6] in q, so the beam is radially symmetric and described by

$$I_{\text{beam}}(r) = 2\pi \int_0^\infty N_{uv}(q) J_0(2\pi q r) q \, dq \,, \tag{10}$$

where J_0 is the first-kind Bessel function of 0-order. Some of the configurations that we will discuss can be described (except for the omnipresent hole at the origin) by simple functional forms for N_{uv}:

(i) VLA-like Y's have distributions close to e^{-q/q_0};
(ii) circular arrays have uniform distributions; and
(iii) non-redundant two-dimensional arrays and highly packed arrays have distributions like the triangle function $(1 - q/q_{\max})$, $q \le q_{\max}$.

It is therefore highly predictable that the beam shapes for these arrays, when "natural" weighting is used, are the Hankel transforms of these functions, giving the following basic beam shapes:

(i) $\left(1 + (r/r_0)^2\right)^{-3/2}$ for VLA-like Y's;
(ii) $J_1(2\pi r/r_0)/r$ for aperture planes with $N_{uv}(q) \approx$ constant, such as circular arrays or any aperture distribution processed using "uniform" weighting; and
(iii) $2\pi \left((r/r_0)^{-3} \int_0^{r/r_0} J_0(x)\, dx - (r/r_0)^{-2} J_0(r/r_0) \right)$ for highly packed arrays and non-redundant 2-D arrays.

[6] *Cf.* Bracewell, R. N. (1966), *The Fourier Transform and its Applications*, Second Edition, McGraw–Hill, New York.

One cannot conclude that any single configuration is "best", because different scientific problems give different amplitude distributions $A(q)$ in the aperture plane, and thus to achieve constant signal-to-noise ratio one would like configurations such that $\sqrt{N_{uv}(q)}$ is proportional to $1/A(q)$.

3. Specific Preliminary Design Study Results

1. Purpose. The purpose of the preliminary design studies for possible configurations of the MMA is partly to understand the imaging characteristics of various arrangements and numbers of antennas and partly to understand the complementarity properties of various multi-element-telescope or multi-beaming instruments. In this summary we focus on three areas:

(1) the large arrays in which N antennas of diameter D are in configurations of size $B = 300$ m, 1 km, and L km;
(2) an array in which these antennas are packed into a $B = 90$ m configuration; and
(3) various complementary instruments with size scales of ~ 29 meters.

For all of these instrumental components we are interested primarily in the quality of the images as characterized by: the r.m.s. sidelobe level, which is a measure of the sampling defects in the aperture plane; the beam shape, which is a reflection of the relative distribution of data in the aperture plane; and the geometry-dependent factors γ and Γ, discussed earlier, that affect sensitivity to point-source detections and surface-brightness.

2. Methods of evaluation of array parameters. Cornwell[7] showed by means of Parseval's theorem that the r.m.s. sidelobe level for any array can be evaluated from the expression

$$s_{\rm na}^2 = \frac{\sum_{j=1}^{M}\sum_{k=1}^{M}\left(T(u_j,v_k)N_{\natural}(u_j,v_k)\right)^2}{\left(\sum_{j=1}^{M}\sum_{k=1}^{M}T(u_j,v_k)N_{\natural}(u_j,v_k)\right)^2}. \qquad (11)$$

Here, $T(u,v)$ is an arbitrarily chosen taper function, and the definition of the function $N_{\natural}(u,v)$, measuring the local density of data sampling, is such that $N_{\natural}(u_j,v_k)$ counts the number of measured data points inside the j-k cell of an $M \times M$ grid of the aperture plane. So the result is the r.m.s. sidelobe level for the case when all measured data points have equal weight, the so-called "natural" weighting. The r.m.s. sidelobe level for cases of "uniform" weighting, $s_{\rm un}$, is obtained from Equation 11 by replacing $N_{\natural}(u_j,v_k)$ by unity if there are any data points in the cell, and by zero otherwise. Sensitivity parameters, the values of $s_{\rm na}$ and $s_{\rm un}$, profiles of computed synthesized beams, and plots of the distribution of data points in the aperture plane provide useful information about the imaging characteristics of aperture-synthesis arrays.

[7]Cornwell, T. J. (1985), "Quality Indicators for the MM Array", NRAO Millimeter Array Memo. No. 18.

The array-dependent factors that affect sensitivity can be simply expressed in terms of the geometry factors γ and Γ as discussed earlier. Hjellming[8] showed that the r.m.s. noise in the image plane can be estimated by the formula

$$\sigma_{\rm na}^2 = \frac{\sigma_c^2}{\sum_{j=1}^{M}\sum_{k=1}^{M} T(u_j,v_k)N_{\natural}(u_j,v_k)} \tag{12}$$

for the case of natural weighting, and by

$$\sigma_{\rm un}^2 = \sigma_c^2 \Bigg/ \frac{\sum_{j=1}^{M}\sum_{k=1}^{M}{}' T(u_j,v_k)/N_{\natural}(u_j,v_k)}{\left(\sum_{j=1}^{M}\sum_{k=1}^{M} N_{\natural}(u_j,v_k)\right)\left(\sum_{j=1}^{M}\sum_{k=1}^{M} T(u_j,v_k)\right)^2} \tag{13}$$

for the case of uniform weighting, where σ_c is given by Equation 5. (The prime denotes that terms which would cause division by zero are ignored in the numerator sum.) If $N_{\rm occ}$ denotes the total number of cells occupied by data, then Equations 12 and 13 reduce to the simple form of

$$\sigma^2 = \frac{\sigma_c^2}{\sqrt{N_{\rm occ}\,\langle n_c\rangle}}, \tag{14}$$

where $\langle n_c\rangle$ is the average number of data points present in occupied cells, possibly including the weight effects of tapering. This is the arithmetic mean, $\langle n_c\rangle_m$, for the case of natural weighting, and is the harmonic mean, $\langle n_c\rangle_{\rm hm}$, for the case of uniform weighting. The result is that $\langle n_c\rangle_m$ and $\langle n_c\rangle_{\rm hm}$ (for the case of no tapering) are two simple parameters for any configuration of antennas, and from them one can compute the geometry factor that affects point-source sensitivity, $\gamma = \sqrt{\langle n_c\rangle_{\rm hm}/\langle n_c\rangle_m}$, for the naturally weighted case.

The geometry factor for surface brightness sensitivity is $\Gamma = \Omega_b/(\lambda/B)^2$, where B is the maximum antenna separation in an array and Ω_b is the beam solid angle for the synthesized beam. For the configurations included in this study, Γ was determined from numerical integration of the beam solid angle over $I_{\rm beam}(x,y)$ (computed from the simulated data set $\{V(u,v)\}$ using a direct Fourier transform); that is, $\Omega_b = \iint I_{\rm beam}(x,y)\,dx\,dy$ with integration from the beam center out to the first null.

3. Results of large array configuration studies. Configurations with $B \geq 300$ m can be considered without serious problems of shadowing, since the antennas are $\sim$ 10 m in diameter, so these are identified as the "large" arrays. The following were evaluated as possibilities for the large arrays:

(1) arrays of antennas in a VLA-like Y with the antennas located radially from the center at distances from the center proportional to $n^{1.73}$, where $n = 1, 2, \ldots$ is the order proceeding from the center;

[8]Hjellming, R. M. (1985), "Factors Affecting Sensitivity for the Millimeter Arrays", NRAO Millimeter Array Memo. No. 33.

(2) Y-configurations with different power laws for the radial distribution, particularly $n^{0.9}$ and $n^{0.5}$;
(3) spiral shapes for the arms of Y's;
(4) non-redundant two-dimensional arrays where antennas have essentially random locations inside a specific area; and
(5) a number of circular configurations.

It was assumed that for all cases the foreshortening problem for low declination objects would be solved by having versions of the adopted configurations that were elongated by about a factor of two in the north–south direction. The estimated weight for each 10 m antenna is $\sim$ 15 tons, which is about a factor of fifteen less than that of the 25 m antennas of the VLA, so it was assumed that transporters with rubber tires would move antennas between stations. The only major cost in having a large number of different configurations is the cost of antenna sites, each requiring its own power and signal distribution systems.

No special advantages were found for non-VLA power laws in Y configurations or "spiralized" arms, and it was concluded that VLA-like configurations with radial power laws near $n^{1.73}$ were representative of this type of configuration. As alluded to earlier in this chapter, the distribution of data points in the aperture plane for VLA-like configurations is very close to an exponential in $N_{uv}(q)$ vs. q (outside of the central hole). Figure 4a shows the antenna locations for a VLA-like Y, and Figure 5a gives the radial aperture-plane distribution for a 300 meter configuration of this type, together with the exponential function $N_{uv}(q) \propto e^{-4.52q/q_{max}}$.

A few examples of non-redundant configurations, with antennas located at "random" locations inside a specific area, were evaluated. These configurations are interesting because they produce a triangular distribution, $N_{uv}(q) \propto (1 - q/q_{max})$ (for $q \leq q_{max}$), and low sidelobes for both extensive observations and snapshots. However, they are not quite as good as the circular configurations that we will discuss next, so they were not deemed worthy of further consideration. In addition, these configurations would be more costly to construct, because of difficulties in extending the power and signal distribution systems to the diverse antenna locations.

While circular configurations were not seriously considered for the VLA because of the high cost of the railroad transportation system, they can be considered for 300 meter and 1000 meter circular configurations because the lighter-weight antennas could be transported by rubber-tired vehicles moving on simple road systems, only a few kilometers or less in length.

Figures 4b and 5b show results for a sample 300 meter circular configuration of 21 antennas for the same cases just discussed for VLA-like Y's. It was necessary to nearly randomly locate the antennas on the circle to avoid high sidelobes, with the result that this configuration has the most even aperture-plane distribution (essentially constant over the outer 95% of the 2-D distribution), the lowest sidelobe levels, and the closest similarity between the beam shapes for the naturally and uniformly weighted cases of any of the configurations

Figure 4. Possible array geometries.

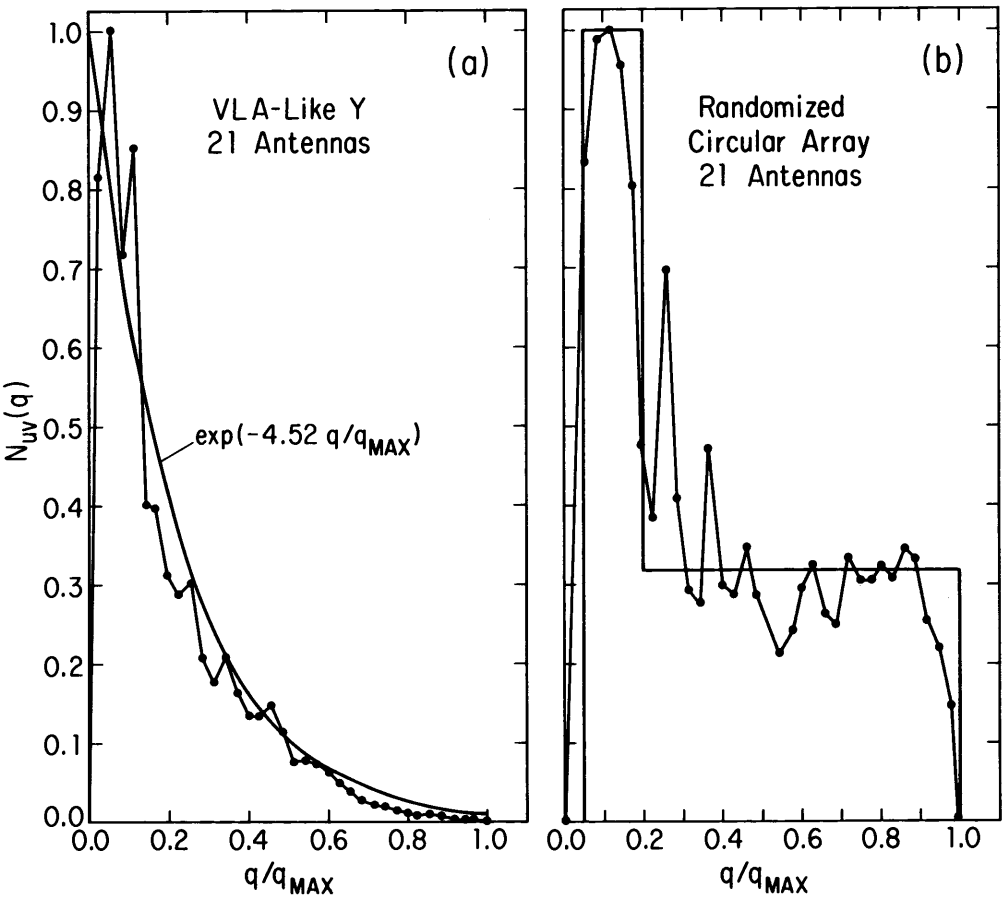

Figure 5. Radial aperture-plane distribution.

studied.

Table 1 summarizes the major array parameters for the two large array configurations that we have discussed, giving all the geometric parameters (γ, s_{na}, s_{un}, and the beam solid angles expressed in terms of the diameters of gaussians with the same 2-D solid angle) and sensitivity parameters (σ_{na}, σ_{un}, $\Delta T_{b,na}$, and $\Delta T_{b,un}$) for both eight-hour observations and snapshots at transit. From Table 1 one can compute $\Gamma = 1.133(\theta_b B/\lambda)^2$. Values of σ and ΔT_b include all the effects of the geometric factors γ and Γ and are given for a system temperature of 100 K and a bandwidth of 1 GHz; they therefore should be multiplied by factors of at least 2 and 5, for 100 GHz and 230 GHz observing situations, respectively.

We conclude that both the VLA-like Y and the circular configuration have good imaging characteristics, and that their differences are advantageous or disadvantageous depending upon the desired signal-to-noise distribution in the aperture plane. The exponential profile in the aperture plane found for the

Table 1. Summary of parameters for observations at $\delta = 60°$ with various arrays of twenty-one 10 meter antennas.

Config.	VLA-like Y		Randomized Circle		Packed Circle	
Config. Diam.	300 m		300 m		90 m	
Gridded Aperture Plane	71 x 71		71 x 71		17 x 17	
Obs. Time	8^h/1 Pol. 4^h/2 Pol.	2^m/1 Pol. 1^m/2 Pol.	8^h/1 Pol. 4^h/2 Pol.	2^m/1 Pol. 1^m/2 Pol.	8^h/1 Pol. 4^h/2 Pol.	2^m/1 Pol. 1^m/2 Pol.
N_{occ}/N_{theo}	0.708	0.091	0.863	0.104	0.890	0.589
γ	0.51	0.96	0.82	0.99	0.42	0.88
s_{nat}	0.0325	0.0565	0.0200	0.0499	0.0717	0.0798
s_{un}	0.0189	0.0526	0.0171	0.0494	0.0570	0.0700
$\theta_{b,nat}/\lambda_{(mm)}$	1".30	1".20	0".51	0".49	2".09	1".99
$\theta_{b,un}/\lambda_{(mm)}$	0".54	0".82	0".48	0".49	1".53	1".75
σ_{nat} (mJy)	0.079	1.22	0.079	1.22	0.079	1.22
σ_{un} (mJy)	0.154	1.28	0.096	1.23	0.187	1.40
$\Delta T_{b,nat}$ (mK)	0.64	11.5	4.07	68.8	0.25	4.2
$\Delta T_{b,un}$ (mK)	7.08	25.8	5.62	69.1	0.46	6.2
Shadowing	1.2%	1.0%	0	0	0.1%	0

VLA-like Y produces a naturally weighted beam that is proportional to $\left(1 + (r/r_0)^2\right)^{-3.2}$, where r_0 is a scaling size. The relatively uniform distributions of data in the aperture plane for the circular arrays lead to beam shapes close to $J_1(2\pi r/r_0)/r$. For both arrays, the beam shapes corresponding to uniform weighting are nearly $J_1(2\pi r/r_0)/r$.

A major question involving configuration studies is always: What is the optimum number of antennas? We have concluded that the improvement in imaging quality for $N > 21$ is gradual, and therefore, while the number of antennas should be at least 21, any number at or above this level is appropriate if dictated by sensitivity considerations. On the basis of imaging characteristics for 300 meter and 1 km configurations, $N = 21$ is the optimum smallest number. This is consistent with VLA experience: in large configurations more antennas have a greater impact on improving imaging quality.

4. The packed array configuration. Experimentation with a number of closely packed configurations in which 21 antennas were placed in an area 90 m in diameter produced the results that would be expected from extrapolation of the "large" configuration studies: placing as many antennas at "random" locations on a circle 90 m in diameter, with the remaining antennas at random

locations inside the circle, produces the "best" result in terms of low sidelobe level and uniform distribution in the aperture plane. Parts (a) and (b) of Figure 6 show one version of a "filled circle" 90 m configuration and the resulting $N_{uv}(q)$ distribution (together with an ideal triangular function) for an extended observation.

In Table 1 the beam and sensitivity parameters for this array, for an eight-hour observation and a 2 minute snapshot observation at transit, are listed. An important property of this array is the ease with which adequate sampling is obtained. According to sampling theorem (and subsidiary considerations) one need only sample data in a grid of size $(2B/D)^2$, which is 18^2 for the array in Figure 7a.

5. The complementary instrument: single antenna with a focal plane array. The most compact array of 10 meter antennas will still need, for most imaging problems with sources larger than $1' \lambda_{(mm)}$, complementary data for spatial frequencies below $\sim$ 20 m/λ. One way to achieve this is with a single antenna multi-beamed with focal-plane arrays of $\sim$ 37 elements (cf. Figure 1b), using imaging techniques that are well established for total-power or beam-switched observations.[9] The multi-beamed antenna needs to be at least 2.5 times the diameter of the antennas in the arrays, so for our 10 meter paradigm array antenna at least a 25 meter antenna is required, and because of cost considerations the complementary antenna should be no larger than necessary. The time needed to image large sources with a single antenna, such as a typical $10'$ galaxy or a small galactic molecular cloud, would be larger than the time needed with the multi-element-telescope that we will discuss next, unless multi-beaming is possible with an instantaneous field $\sim$ 37 times the antenna beam. This allows one to make comparable images in comparable observing time. This would be an excellent solution if the technology of multi-beaming or focal-plane arrays progresses to the point where we can be confident that the technique lacks serious instrumental problems.

6. The complementary instrument: full tracking multi-element-telescope. Using small antennas to observe large fields of view with resolutions the size-scale of $\lambda_{(m)}/30$ radians (or any coarser) requires packing a reasonably large number into as small a region as possible, if we desire to approach the sensitivity of a single dish by attaining filling factors of $> 50\%$. Packing these antennas into a small area on the ground results in serious shadowing and foreshortening problems which can be removed by placing the antennas on a pointable structure. An example that has been examined in some detail is a "full tracking" multi-element-telescope, as sketched in Figure 7a, where $\sim$ 21 antennas $\sim$ 4 m in diameter are mounted on the surface of a $\sim$ 29 m structure that is itself pointed so that the source and the optical axis of the structure coincide when tracking in azimuth and elevation. This instrument has the effective collecting area of an 18.3 m antenna. Table 2 contains a summary of the array, beam, and sensitivity parameters for this instrument.

[9] Emerson, D. T., Klein, U., and Haslam, C. G. T. (1979), *Astron. Astrophys.* **76**, 92.

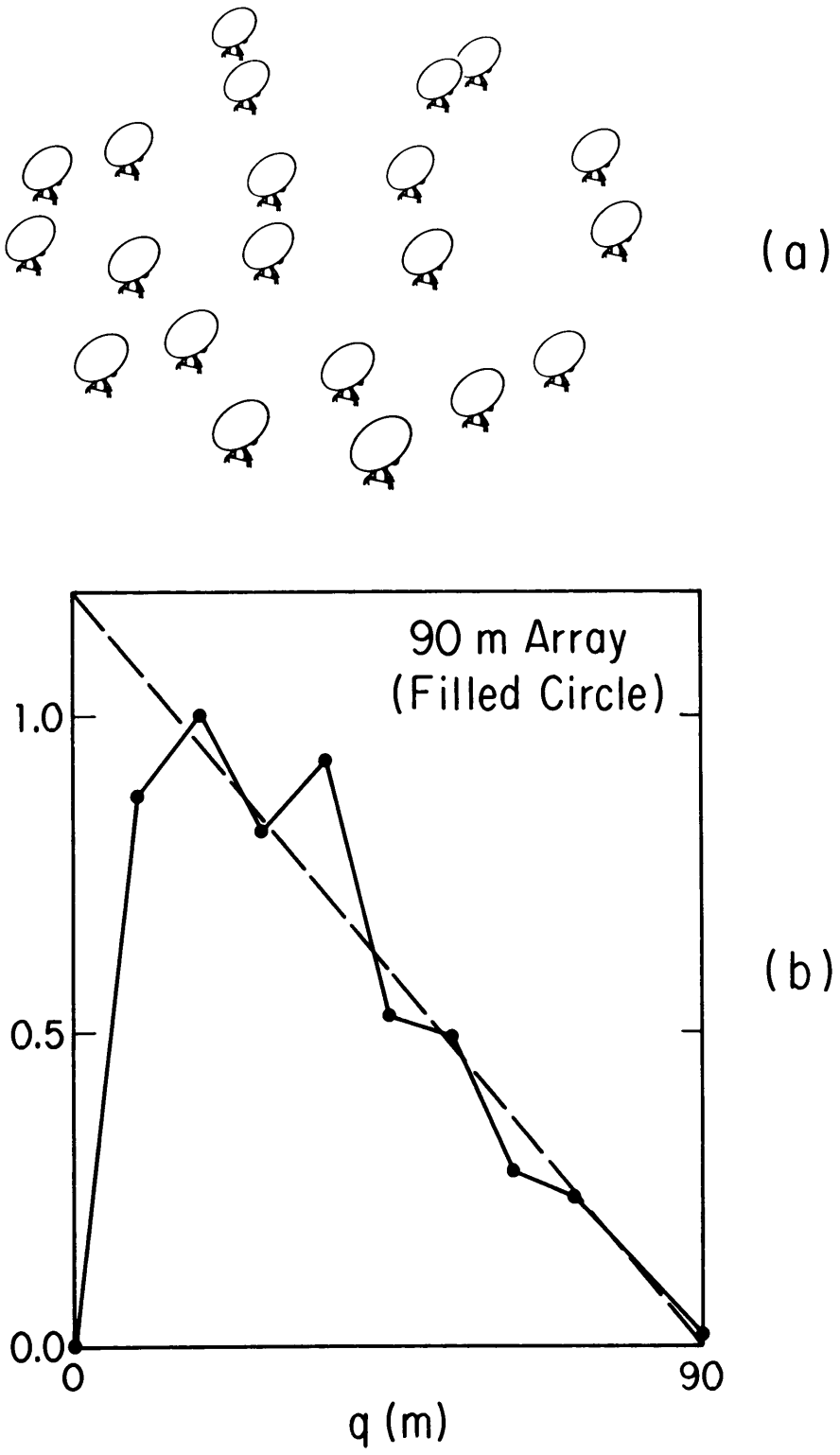

Figure 6. Filled circle 90 m configurations.

Table 2. Parameters for observations at $\delta = 60°$
with multi-telescope arrays of twenty-one 4 meter antennas.

M-T Type	Full Tracking		2-D Rotating Azimuth		3-D Rotating Azimuth	
Config. Diam.	26 m		30.6 m		30.6 m	
Gridded Aperture Plane	15 x 15		15 x 15		15 x 15	
Obs. Time	8^h/1 Pol. 4^h/2 Pol.	2^m/1 Pol. 1^m/2 Pol.	8^h/1 Pol. 4^h/2 Pol.	2^m/1 Pol. 1^m/2 Pol.	8^h/1 Pol. 4^h/2 Pol.	2^m/1 Pol. 1^m/2 Pol.
N_{occ}/N_{theo}	0.996	0.770	0.969	0.511	0.908	0.608
γ	0.36	0.77	0.31	0.81	0.33	0.75
s_{nat} s_{un}	0.101 0.075	0.106 0.086	0.098 0.067	0.109 0.093	0.095 0.070	0.094 0.070
$\theta_{b,nat}/\lambda_{(mm)}$ $\theta_{b,un}/\lambda_{(mm)}$	6.″95 4.″88	6.″90 5.″44	6.″83 4.″27	6.″84 5.″61	6.″60 4.″41	6.″56 5.″10
σ_{nat} (mJy) σ_{un} (mJy)	0.49 1.38	7.6 9.9	0.49 1.61	7.6 9.4	0.49 1.51	7.6 10.2
$\Delta T_{b,nat}$ (mK) $\Delta T_{b,un}$ (mK)	0.14 0.79	2.2 4.5	0.14 1.20	2.2 4.1	0.15 1.05	2.4 5.3

An important property of packed arrays is that nearly complete sampling is obtained with just one snapshot. This is because complete sampling (i.e., the Nyquist/Shannon sampling density, over as large u-v spacings as the geometry allows) for $d = 4$ meter antennas in an array $b = 25$ meters in diameter requires sampling the data only in a $(2b/d)^2$ $(= 13^2)$ array; so, even for short snapshots, adequately dense sampling is nearly achieved in each and every snapshot. This means the results are relatively insensitive to the locations of antennas; and the imaging properties of highly packed arrays are excellent. Therefore the multi-element-telescope approach is a good way to achieve an instrument with the instantaneous field of view of the small antennas, resolution corresponding to the size of the structure, and collecting area that is 40% that of a single antenna of that size. One needs only to empirically calibrate the relative displacements between antennas. The main defects of the multi-element-telescope are: the need for a large correlator system; and the necessity for total-/switched-power observations to obtain sampling for spatial frequencies $\leq 2b/\lambda$.

7. The complementary instrument: azimuth-rotation multi-telescopes. The relative unimportance of exact antenna locations for the full tracking multi-element-telescope indicates that the locations of antennas in two (or three) dimensions are not critical parameters when 21 or so antennas are mounted on any structure of the order of 30 m in size. An example where

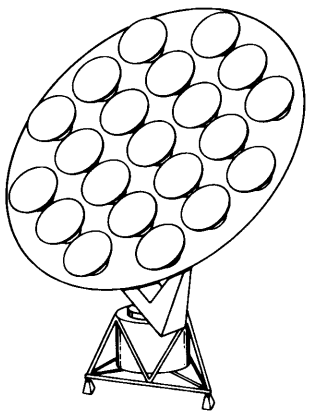

(a)

Full Tracking Array

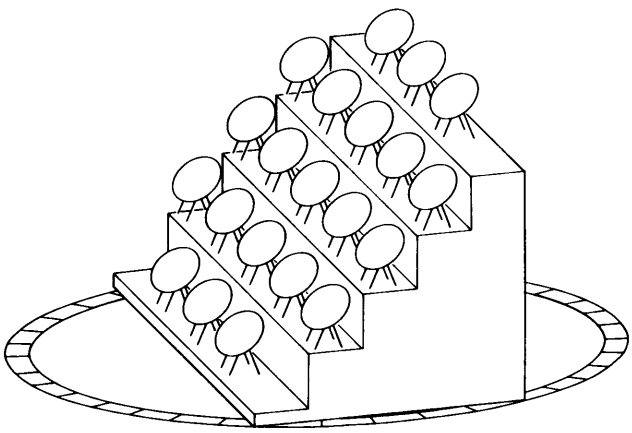

(b)

2-D Rotating Azimuth Array

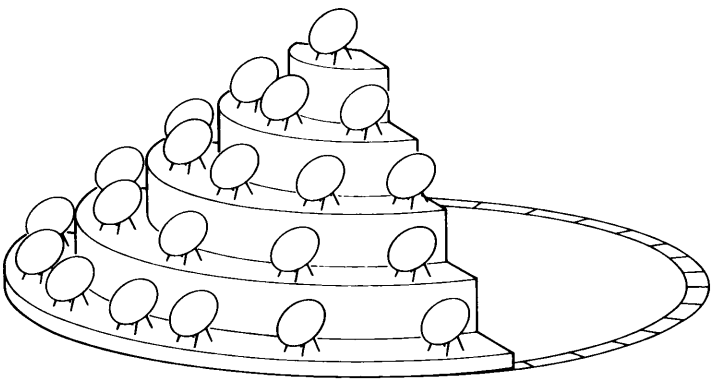

(c)

3-D Rotating Azimuth Array

Figure 7. Complementary instrument configurations.

the antennas are distributed in two dimensions on a tilted plane which rotates in azimuth while individual antennas point only in elevation is sketched in Figure 7b. An alternate possibility where the antennas are distributed in three dimensions on five levels of a structure that looks like a wedding cake is sketched in Figure 7c. Table 2 contains summaries of the array, beam, and sensitivity parameters for these arrays.

The rotating inclined plane, the rotating wedding cake, and the full tracking array all have comparable imaging characteristics. Therefore, should the multi-element-telescope option be chosen for the complementary instrument to the large array, practical engineering considerations of structural stability and cost will be the primary criteria for choosing among the three possibilities. Both the rotating inclined plane and the wedding cake structure can be designed so that co-rotating with each structure is a protective building on the other semi-circle of the railroad track, and when weather or maintenance considerations dictate a shut-down, the structure with the antennas can be rotated inside the slightly larger building structure. In this sense they have more potential for operation in an occasionally hostile environment, while avoiding the standard solution of placing the instrument inside an astro-dome or radome.

8. Sub-illumination of the arrays of large antennas. Although it is not yet a common practice in radio astronomy, there are a number of problems for which it might be worthwhile to under-illuminate large antennas to allow observations with reduced sensitivity but much larger field of view. One obvious use of this mode is study of radio emission from high-energy events on the Sun, where the locations of short-lived, important events are unknown in advance and sensitivity is not a major limitation.

9. Matching total-power and multi-configuration data. The problems of data processing, particularly the mosaicing of images of large fields, are beyond the scope of this document. However, it is appropriate to discuss the overlap of the different kinds of data that are assumed to be produced in the example of the MMA that we have discussed.

Figure 8 shows the normalized contributions of total-power observations and the compact configurations in terms of their proportional sampling in the radial $q = \sqrt{u^2 + v^2}$ space, while Figure 9 shows how these overlap with the sampling obtained in the 300 meter and 1000 meter arrays. Viewed in terms of the aperture plane, adequate image restoration is possible when one satisfies the sampling theorem with the complete data, with adequate sensitivity, for all q less than the $q_{\max}$ associated with the angular resolution desired, given by $\theta_b \approx 1/q_{\max}$. These figures clarify why such a range of configurations and instruments is a major consideration of the design of the MMA.

4. Conclusions

The objective of this discussion has been to discuss in detail the imaging properties of various possibilities for the MMA design. It has been based upon a primary instrument which is an array of large antennas with a collecting

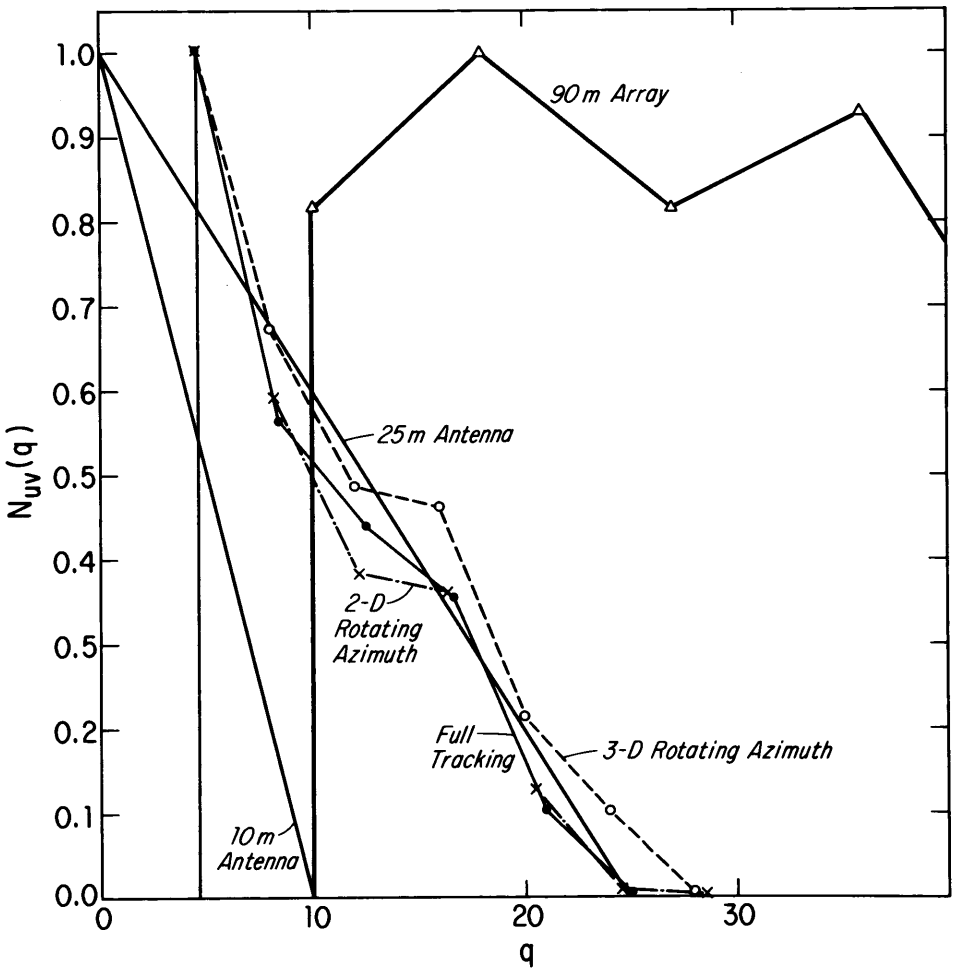

Figure 8. Normalized contributions of total-power observations and compact configurations.

area of 1650 m^2, satisfying the primary recommendation of the Barrett subcommittee.[10] In order to provide the complementary data needed for imaging of extended objects, we have assumed that this array will be supplemented with a complementary instrument which is either a multi-element-telescope or a multi-beamed single telescope. The characteristics of VLA-like Y arrays and circular arrays are found to be excellent for varied types of problems. The multi-element-telescope concept, which has not yet been extensively used in radio astronomy, in any of three types of designs, will work well as a complement to the larger arrays. The multi-beaming concept will work if multi-beamed receivers or focal plane arrays, currently in a rapid state of development, are found to have the desired characteristics; however, no system with more than a few beams is as yet used in radio astronomy.

[10]Barrett, A. H. (1983), "Report of the Subcommittee on Millimeter- and Submillimeter-Wavelength Astronomy", Submitted to the National Science Foundation Astronomy Advisory Committee.

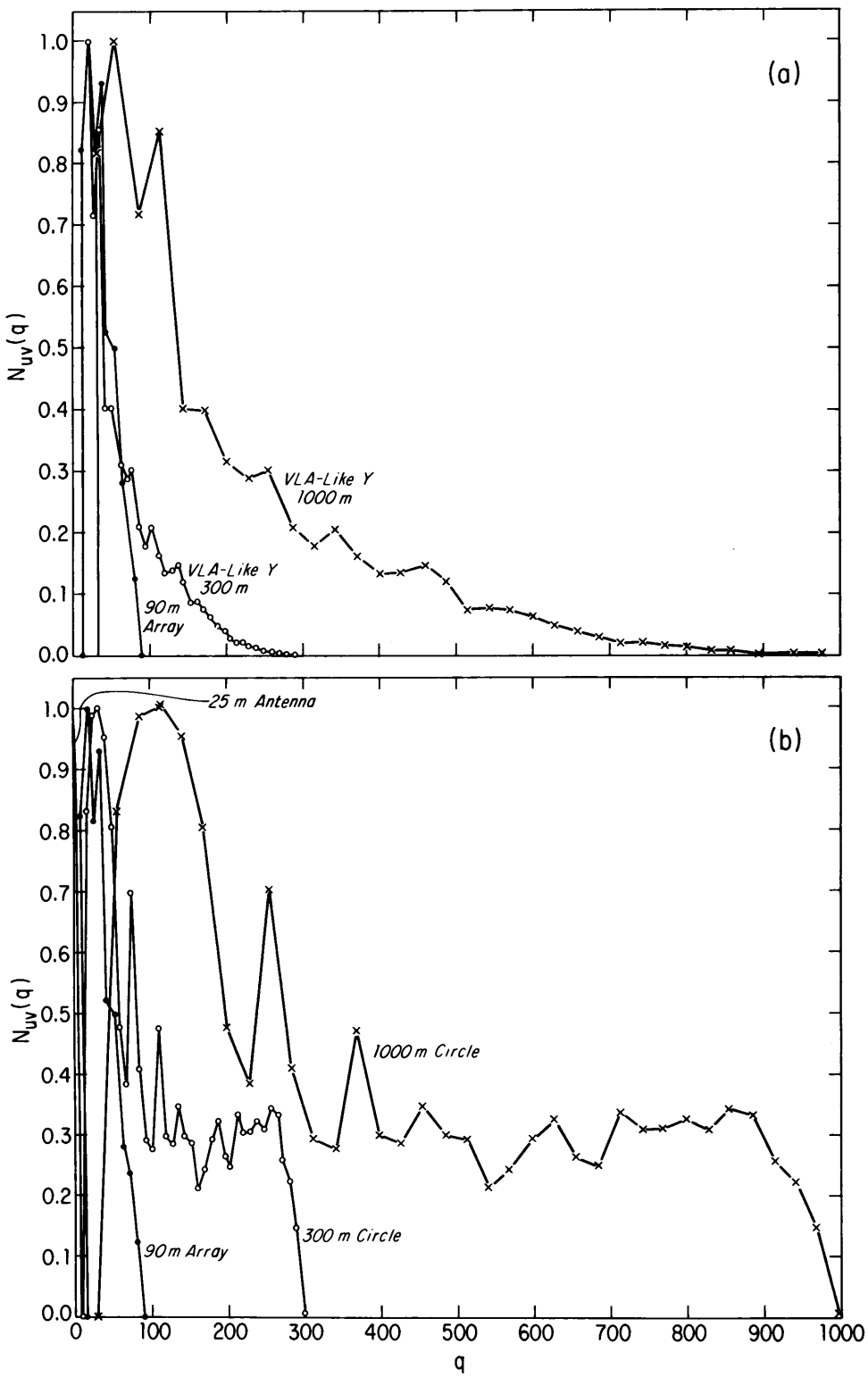

Figure 9. Sampling overlap, all arrays.

In order to evaluate whether the instruments discussed in this chapter have enough sensitivity to carry out particular scientific projects, it is useful to summarize the sensitivity of each instrument for both continuum and spectral line observations, as is done in Table 3.

Table 3. Summary of sensitivity parameters for arrays.

Instrument	Type	$\Delta\nu$	3 mm $\frac{\Delta T_b \Delta t^{1/2}_{(\mathrm{min.})}}{T_{sys}/200}$	1.3 mm $\frac{\Delta T_b \Delta t^{1/2}_{(\mathrm{min.})}}{T_{sys}/500}$	3 mm $\frac{\sigma_{nat} \Delta t^{1/2}_{(\mathrm{min.})}}{T_{sys}/200}$	1.3 mm $\frac{\sigma_{nat} \Delta t^{1/2}_{(\mathrm{min.})}}{T_{sys}/500}$
29 m M-T	Continuum	1.0 GHz	4.40 mK	11.0 mK	15.0 mJy	38.0 mJy
	Line	0.8 MHz	0.16 K	0.39 K		
90 m	Continuum	1.0 GHz	8.40 mK	21.0 mK	2.40 mJy	6.0 mJy
	Line	0.8 MHz	0.30 K	0.75 K		
300 m	Continuum	1.0 GHz	94 mK	233 mK	2.40 mJy	6.0 mJy
	Line	0.8 MHz	3.4 K	8.3 K		
$B_{(\mathrm{km})}$ Array	Continuum	1.0 GHz	1 $B^2_{(\mathrm{km})}$K	2.6 $B^2_{(\mathrm{km})}$K	2.40 mJy	6.0 mJy
	Line	0.8 MHz	38 $B^2_{(\mathrm{km})}$K	92 $B^2_{(\mathrm{km})}$K		

While the instruments discussed have been found to have certain desirable characteristics, that does not mean that the parameters of the arrays are as yet optimal for a major U.S. millimeter-wavelength imaging facility. They simply represent a set of parameters used to allow concrete evaluation. These studies indicate that there are major technical questions to be answered before any choice of antenna size and number can be considered optimal. In this discussion, while using specific numbers, we have attempted to emphasize the principles and generalities involved, because they are most important in furthering our understanding as we progress to the next stage of technical studies.

There are a number of major questions with regard to the MMA that need extensive investigation. One is the optimum ratio of antenna sizes when total-power images and aperture-synthesis data are to be combined in the fashion that is necessary for the facility to be capable of complete imaging. We have adopted a factor of 2.5 throughout the initial design considerations, but examination of the available literature on this subject indicates that only empirical experience has been brought to bear on this problem, with the result that a ratio of three is considered to be conservative, but a factor of two (or less) may be sufficient under some circumstances. A second is whether the collecting area of 1650 m^2, used in the "strawman" design, is sufficient to match both the scientific needs to be discussed in this meeting and the needs of a frontier millimeter imaging facility for the next couple of decades. The third question arises from the considerable dependence of noise upon the atmospheric transparency, leading to the need for detailed evaluations of this need and its impact upon the site(s) for the large array and the complementary

instrument, which could be placed on a good mountain-top site. Finally, it seems essential to simulate the sampling and image reconstruction of complex sources in order to understand: the problems of matching configurations; the problems of matching total power image data and aperture-synthesis data; and the magnitude of the data processing hardware and software needed to accomplish, in an astronomer-friendly manner, the many imaging possibilities intrinsic to the MMA, as currently conceived.

II. The Solar System
Working Group Report[†]

We think that the millimeter array will be a very valuable instrument for planetary science. To be able to achieve any quantitative results, we need high resolution observations with great internal accuracies—besides good absolute calibration measurements. The instrument, as envisaged, offers at least the first two needs—while the latter one can be improved on over the coming years. We think the most valuable observations the instrument will offer us, which cannot be done at any of the existing or proposed telescopes as of now, are accurate ($< 1\%$ accuracy) center-to-limb observations of planets, and observations of large objects ($> 30''$) as well as small $\sim 1''$ objects, such as satellites and asteroids. The unique capability of fast mapping is another feature of particular importance to planetary work, since planets vary on relatively short time scales, due to either rotation, revolution around the sun, or wind effects. We believe strongly that several major alterations of the "strawman" array design are needed—namely,

(1) baselines out to at least 3 km;
(2) submillimeter capability for the central element, and preferably for the entire array;
(3) a better site;
(4) upper- and lower-sideband observational capability; and
(5) the possibility to under-illuminate the large antennas, in order to simulate an array of smaller antennas.

Below, the science which could be done with the instrument is outlined, with the specific requirements of the array summarized at the end.

We shall consider separately *planetary atmospheres*, *"solid" surfaces*, and *comets*.

1. Planetary Atmospheres

Observations at radio wavelengths allow one to derive abundances of gases as a function of altitude, together with the temperature vs. pressure profiles of the atmospheres. The observations should be carried out on lines of different species, and preferably at different transitions. At different transitions one typically probes different altitudes in the atmosphere. Hence, one can derive an altitude distribution for the gas's abundance. The line intensity is a measure of the convolved abundance and temperature profile in the atmosphere. The shape of the line depends upon the pressure and abundance at the relevant altitude levels.

Specific examples of problems in planetary atmospheres are given in the following three sub-sections.

[†]Contributors: G. Berge, California Institute of Technology; I. de Pater (Chairperson), University of California at Berkeley; D. Muhleman, California Institute of Technology; and P. Schloerb, University of Massachusetts.

1. NH_3 on giant planets. A broad, blended line (many GHz in width) is centered at 1.3 cm. The opacity for continuum (i.e., broadband) observation at millimeter and centimeter wavelengths is dominated by NH_3 gas. Observations at these wavelengths, thus at both sides of the line center, allow an independent determination of the altitude distribution of NH_3 gas and the temperature vs. pressure profile (assuming the line shape is known!). Observations at these wavelengths pertain to depths of cloud formation which occur in a region which cannot be observed at other wavelengths. High resolution observations (0.05–0.1 planetary radii) allow determination of NH_3 gas abundance as a function of altitude and determination of the behavior of temperature vs. pressure profiles across the disk. We basically think of latitude distributions, but with high enough sensitivity the longitudinal distribution can be defined. A latitudinal variation of NH_3 gas on Jupiter has been found, which corresponds to the belt–zone structure seen at optical and IR wavelengths. So this gas apparently plays a role in the formation of the belts and zones, due both to dynamics and to condensation effects in the atmosphere. Similar effects may exist on other planets for condensable gases.

2. CO on Venus and Mars. Mapping studies of CO in the atmospheres of Venus and Mars offer the possibility to study the diurnal, latitudinal, and seasonal variations of the atmospheric temperature and CO abundance in a direct way. In the upper atmosphere of Venus strong diurnal CO abundance gradients exist. Maps of the J = 1–0, 2–1 and 3–2 lines may be inverted to yield the longitudinal and latitudinal CO abundance and temperature variation in the atmosphere in the 80–120 km altitude region. Such studies provide the fundamental input to models of the general wind circulation and photochemistry of this region in the atmosphere. Direct measurement of winds would substantially improve wind-circulation theories. Such measurements are possible by observing the Doppler shift of lines near the limb of the planet. These shifts can be measured at the limb if wind velocities are of the order of > 100 km s^{-1}.

The CO abundance in the atmosphere of Mars is not strongly altitude dependent, and, therefore, one can use the CO lines at millimeter-wavelengths to sound the atmosphere for its temperature profile. Maps of the planet Mars can then be used to produce global maps of the Mars temperature profile, in order to study latitudinal and seasonal variations as well as the effect of large scale meteorological phenomena (e.g., global dust storms) on these profiles.

3. Trace constituents. Besides just determining the presence of trace elements, it is important to define their altitude distribution in order to define their place of origin—e.g., in the deep atmosphere, brought up by convection; or outside the atmosphere via influx from outside (e.g., oxygen from rings or satellites); or high up in the atmosphere due, for example, to photolysis lightning.

In particular, center–limb observations of such gases will contain a clue as to the level in the atmosphere at which they exist. If we think of a typical

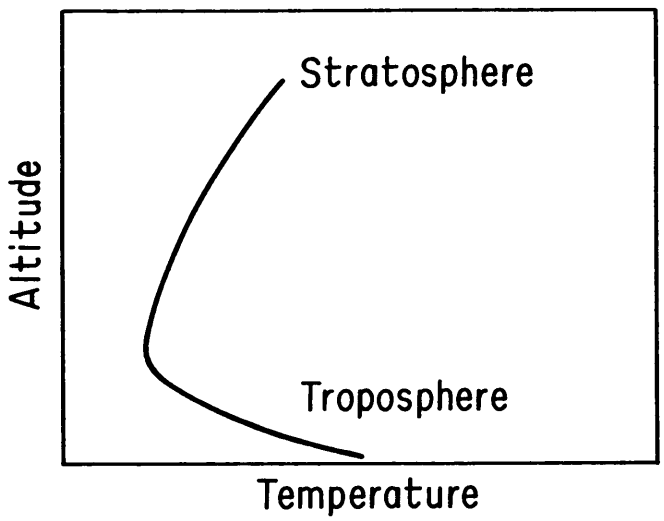

Figure 1. A typical planetary atmosphere temperature vs. pressure profile.

temperature vs. pressure profile as shown in Figure 1, then gas which is distributed near and above the troposphere (so in the stratosphere) may appear in absorption at the center of the planet, while appearing in emission at the limb. So center–limb observations may seem limb-brightened in the line center, while they seem limb-darkened outside the line. Examples of some interesting molecules are: (a) PH_3, H_2S, CO, and HCN, on the giant planets; (b) sulfur molecules (SO_2 and SO) and ozone, in Earth-like atmospheres (Venus and Mars); (c) nitriles and hydrocarbons like HCN, HC_3N, and organic molecules, on Titan; and (d) SO_2 and SO on Io.

One typically probes pressure levels from 1/100 of a millibar to 1 bar in planetary atmospheres. Hence, linewidths are of the order of 1 MHz to 1 GHz. The essentials required to obtain necessary scientific results are:

- high resolution ($\approx 0\farcs1$–$0\farcs2$) for center–limb variations;
- broad bandwidth (> 2 GHz) with 10 bands of 40–80 MHz which can be spread out over a 2 GHz total band;
- separate and simultaneous upper- and lower-sideband observations (one band on, and one band off the line center for broad lines);
- a submillimeter capability; and
- increased resolution if submillimeter receivers are on the entire array; submillimeter observations are also necessary to determine the effective temperature of "cold" planets like Uranus and Neptune.

2. Solid Surfaces

At different wavelengths one probes to different depths in the crust—roughly anywhere from a depth of several wavelengths, to several hundreds of wavelengths deep (for pure water ice). The measured brightness tempera-

ture depends upon the physical temperature of the subsurface layers, and on the radiative transport of the thermal emission outward. The physical temperature depends upon the solar insolation and the thermal conductivity and inertia of the material. Radiative transfer outward is limited by the emissivity and the absorption/scattering characteristics of the material, both of which are highly dependent upon wavelength. Thus, probing the surface layers at different wavelengths allows mapping of the temperature distribution with surface depth. This, together with high resolution maps in intensity, as well as in polarization, will ultimately allow one to deduce the substance and composition of the material (e.g., solid rock, loose dust, gravel; ice in clumps, wet ice; etc.). The importance of submillimeter and millimeter observations is that one typically probes in the region of the diurnal solar heat wave—this gives the information necessary to derive the thermal characteristics (conductivity, thermal inertia, and dielectric constant) of the material, properties unique for each substance.

In the following sub-sections, we elaborate upon several examples.

1. Satellites and asteroids. The Galilean satellites each have their own unique properties. We have only to recall pizza-like Io with its volcanoes and hot spots, and the Voyager photographs of each satellite. Spectra of the satellites at infrared to centimeter wavelengths give the information on the subsurface layers of the bodies—information which cannot be derived in any other way except by drilling a hole in their "ground." In particular, the spectra of Europa and Ganymede are exceptional when compared to that of the moon. Brightness temperatures at centimeter wavelengths are about three times lower than at infrared wavelengths, while it usually is only 10%–20% colder. Additionally, Europa's spectrum seems to increase more rapidly toward shorter wavelengths than does Ganymede's spectrum. To really unravel the composition one needs center–limb variations and polarization characteristics, plus better accuracies for the existing disk-averaged brightness temperatures.

2. Titan. Observations at wavelengths between 3 mm and a few centimeters can be used to probe Titan's surface layers. Continuing heated debates exist on whether the surface is solid, or an ocean of liquid ethane. Radio data form the only means to answer this question, other than sending a probe to land at the surface. (Sail the sea!)

3. Pluto and Charon. With the millimeter array it will finally be possible to measure Pluto's brightness temperature. Even to observe Pluto and its moon Charon separately (they are separated by only $\sim 0\farcs5$) will be a worthy task.

4. Terrestrial planets. Larger objects like Mars and Mercury can be mapped in detail. In particular, Mars' poles are interesting: 2 cm and 6 cm maps clearly distinguish these features and show different brightness contrasts at the different wavelengths. Mapping Mercury's night side or dark crescent seems interesting: this has never been "seen" before at any wavelength, much less mapped.

5. Rings (Saturn, Uranus, Neptune?). Observation over the entire submillimeter to centimeter spectrum allows determination of particle composition and size distribution in the various parts of the rings (information complementary to Voyager results!).

The essentials needed for these observations are:

- high resolution (0.″1–0.″5) at different wavelengths;
- polarization capability;
- long spacings to "filter out" the nearby planet; and
- a submillimeter observing capability, preferably for the entire array.

3. Comets

Comets are the most pristine samples of early solar system material. Hence knowledge of the cometary composition is very important for models of the early solar system, and of star formation in general.

Direct detections of parent (or primary) constituents is only feasible at radio- and millimeter through infrared wavelengths, since transitions at optical and UV wavelengths are excited by photons which dissociate the entire molecule—hence those transitions don't exist. Thus, observations at millimeter-wavelengths are an excellent potential probe of those molecules.

Some likely candidates are: HCN, HC_3N, and other nitriles and hydrocarbons which may be parents of CN radicals; C_2 and C_3 molecules (all detected at optical wavelengths); and CO and CS (both observed at UV wavelengths). Comets are known to contain significant quantities of a nonvolatile material (dust). Radar observations of Comet IRAS–Araki–Alcock showed the existence of large (> 2 cm) grains around the comet, a previously unknown class of particles.

Continuum observations at millimeter–submillimeter wavelengths form the potential means to derive information of millimeter–submillimeter sized particles, about which little is known.

4. Summary: Array Design Requirements

Frequency Windows:	**1, 2, and 3 mm bands (both continuum and line);** **30–50 GHz (only 1 continuum band);** **345 GHz (continuum and line);** **Submillimeter capability, down to 350 μm (continuum and line).**
Bandwidth:	**$\gtrsim$ 2 GHz with $\sim$ 10 bands of 40–80 MHz which can be spread out over entire band;** **50–100 kHz spectral linewidth;** **Upper- and lower- sideband observation to allow difference measurements at line center and away from it.**
Polarization:	**Full polarization capability.**
Baselines:	**Long baselines ($\gtrsim$ 3) km are needed to resolve satellites—Uranus, Neptune, Pluto–Charon.**

Dish Size: Small weak objects require the 10 m dishes; large planets (Jupiter, Saturn, and Venus) require 4 m dishes. With lenses in the big dishes to illuminate only the inner part of the dish our problem can be solved, but with some loss of sensitivity;

Note: For planetary observations we do not believe in either self-calibration or mosaicing—we need, e.g., accuracies better than 1% in center-to-limb observations, which might be obtained in single maps, but likely not in mosaics.

Site: High, dry, and wind-quiet site required for entire instrument—so that good phase stability, low optical depth, and accurate pointing can be obtained. Again, we do not think that self-calibration will do us much good, due to the absence of any feature which is both unresolved at all spacings and relatively strong (at least detectable at all spacings). So we urge the community to choose a high site in preference to the VLA. Solar system objects are always south of 30° N latitude (thus are usually at high zenith angles). Observations down to at least two air masses are required.

Central Structure: Design seems fine for planetary work, but nearly useless as a separate instrument, due to the low resolution. It may be usable as a mapping instrument at 350 μm.

Design: 10 m dishes (plus lenses);

Priority 1: Randomized array to minimize sidelobe levels;

Priority 2: Circular design to get uniform u-v plane filling, so fine structure can more readily be detected.

Final comments: Mapping of the moon offers a unique possibility to test mosaicing and self-calibration techniques. Moreover, the moon itself is the best site we can think of for this millimeter instrument—in that case although losing the moon as a target, we can observe the earth, its atmosphere (in the mosaicing way, however), and interesting portions of the Soviet Union.

III. The Sun and the Stars
Working Group Report[†]

1. The Sun

1. Gamma-ray–millimeter-wave flares. The most important solar problem that can be addressed with a millimeter-wave array (given the present state of knowledge) is probably that of γ-ray–mm-wave flares. As the instrumental requirements for this problem equal or exceed those for any other solar problem, it acts as a driving force on the millimeter array design.

In γ-ray–mm-wave flares, recent evidence (mostly from the Solar Maximum Mission spacecraft and millimeter-wave radiometers) has demonstrated that electrons and protons are accelerated almost simultaneously to very high energies. In particular, electrons attain energies of 10 to 100 MeV within one or two seconds of flare onset, and emit both millimeter waves and continuum gamma-rays of high intensity. This continuum radiation is accompanied by nuclear gamma-ray lines at energies less than about 10 MeV due to protons, and neutrons are sometimes detected at Earth.[1]

At the present time there is no widely accepted explanation for this very rapid acceleration. Some argue that a "first phase" process must be the cause because of the very short time scale, possibly a process involving electric fields in double layers. Others argue[2,3] that stochastic acceleration can act on short enough time scales.

With the firm evidence that some physical process produces relativistic electrons on the Sun so rapidly, we must accept that the same process operates at other locations where magnetic energy is available—i.e., on a wide range of stars including flare stars, interacting binaries, and X-ray binaries. Possibly, but less surely because of the uncertain role of magnetic fields, the same process may be important in the centers of active galactic nuclei.

In the radio range, the special characteristic of γ-ray–mm-wave flares is that the flux density increases with frequency into and perhaps beyond the millimeter-wavelength regime. Figure 1 shows spectra of several flares, most of them recorded before the γ-ray connection was realized. Observations at millimeter wavelengths are obviously of great interest: there have been no spatially resolved studies in either millimeter waves or γ-rays. Instruments being designed may achieve arcsecond resolution in hard X-rays of a few hundred keV energy, but not in the energy range > 10 MeV of greatest interest here.

[†]Contributors: G. A. Dulk (Chairman), University of Colorado; D. E. Gary, California Institute of Technology; R. M. Hjellming, NRAO; and M. R. Kundu, University of Maryland.

[1] *Cf.* Chupp, E. L. (1984), *Ann. Rev. Astron. Astrophys.* **22**, 359.

[2] Melrose, D. B. (1983), *Solar Phys.* **89**, 149.

[3] Bai, T. *et al.* (1983), *Astrophys. J.* **267**, 433.

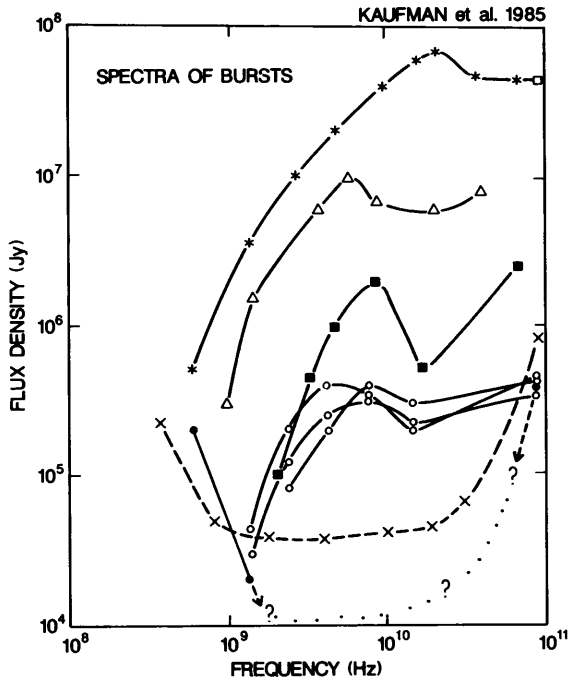

Figure 1. The spectra of several solar flares. (Adapted from Kaufman, P. *et al.* (1985), *Astron. Astrophys.* **157**, 11.)

Hence the millimeter-wave array is of utmost importance in the elucidation of these most energetic of solar flares.

We now list some of the most important characteristics of γ-ray–mm-wave flares, together with the implied instrumental requirements.

Characteristic: $\lesssim$ 1 *s time scales* — This time scale is characteristic of the ion-acoustic travel time in a magnetic flux tube of length $\sim 10^9$ cm, which is somewhat longer than the fast electron travel time in that flux tube.

Requirement: $\lesssim$ 0.1 *s time resolution* — This is needed to distinguish between the ion-acoustic travel time and the electron travel time. For the former we need to resolve the temporal expansion of a source, and for the latter to observe the near simultaneous brightening of footpoints of a flaring flux tube. The high data rate suggests that data compression is desirable, going automatically to high time resolution when a flux or brightness threshold is exceeded.

Characteristic: $\lesssim 1''$ *size scales* — Source sizes in millimeter waves are probably smaller than $1''$, as judged by scaling from $30''$ at 20 cm, to $10''$ at 6 cm, to $3''$ at 1.3 and 2 cm, and then to millimeter waves.

Requirement: array sizes 300 m to 1 km.

Characteristic: complex background sources — Solar active regions in which γ-ray–mm-wave flares occur are bright and have multiple structures which

are time-varying. Millimeter bursts may sometimes be less bright than these background sources.

Requirement: good u-v coverage in the snapshot mode — It would be desirable to have more than 21 antennas (30 or more) to give good snapshots in the 1 km array and to provide redundancy for self-calibration.

Characteristic: burst location uncertain beforehand — Exact flare locations within active regions of size 3 arcminutes or more cannot be predicted.

Requirement: large field of view of 3 arcminutes or more — Three possible solutions are:

(1) Mosaicing, with 3 by 3 mosaics completed every 0.1 s.

(2) Make an image with the 4 m antennas of the central element, determine the burst source position to $\sim 10''$, and use this information to position the 10 m antennas, all within 0.1 s of burst onset.

(3) Under-illuminate the 10 m antennas, making the equivalent of 3 m to 4 m antennas, perhaps with a flip-out lens. This is the preferred solution because it would allow imaging from the first 0.1 s when the most illuminating phenomena begin to occur.

Characteristic: changing brightness spectrum — Measurement of the rapidly varying brightness spectrum in millimeter waves is very important in order to define the energetic electron spectrum as a function of position and time. In particular there is a need for simultaneous measurements at two frequencies in the millimeter wavelength band.

Requirement: simultaneous imaging at 1 and 3 mm, or at 3 and 9 mm.

Characteristic: circularly polarized radiation — We expect a degree of circular polarization $\lesssim 10\%$ for $\gtrsim 10$ MeV electrons radiating in a 100 gauss field at the 300th harmonic of the gyrofrequency. Circular polarization is an excellent diagnostic of magnetic field strength and direction when the electron energy spectrum is known from gamma-ray or millimeter-wave spectra. (Neither spectral lines nor linear polarization have ever been incontrovertibly detected in solar radio radiation.)

Requirement: accurate circular polarization — An accuracy of about 1% is required. Thus either linear feeds or "clean" circular feeds (on axis?) are desirable.

2. Penetration of electron beams into the lower atmosphere. In many flares, brightenings occur in Hα, EUV, and even white light simultaneously with hard X-ray bursts. There is a controversy over the cause of these brightenings, whether due to electrons, to protons, or to an ion-acoustic conduction front. For the first it is uncertain whether they are able to penetrate deeply enough into the dense atmosphere; for the second it is unknown how an adequate number can be accelerated in the required 1 s; and for the third it is uncertain whether heat conduction can be fast enough.

Observations in millimeter waves can help answer these questions because they originate in the relevant region of the atmosphere, the low chromosphere,

in contrast to centimeter waves that, during flares, originate in the corona. The millimeter-wave emission mechanism in most flares is probably thermal bremsstrahlung from the heated plasma, so it is relatively straightforward to relate radio wave brightness to the density–temperature structure in the heated regions. The relative timing of millimeter-wave vs. centimeter-wave bursts should help distinguish among the possible causes.

The instrumental requirements for the millimeter array for this problem are nearly identical to those for the γ-ray–mm-wave flare problem. Flares amenable to study here are much more frequent than γ-ray–mm-wave flares, with several per day (vs. one per few weeks) occurring during sunspot maximum.

3. Thermal phase of flares. In some flares, energy continues to be released over durations of tens of minutes, and energetic particles are continually accelerated. The source of this energy is controversial. Magnetic energy stored in the corona seems to be insufficient to account for the total in some large flares, arguing for storage below the photosphere. If so, there should be a signature in the low chromosphere, where millimeter waves arise.

The instrumental requirements are similar to those of γ-ray–mm-wave flares, but with relaxed time scales.

4. Mapping of solar active regions. Millimeter-wave emission from active regions is due to free–free bremsstrahlung, and is partially polarized due to the difference between **x** mode and **o** mode emissivities. It therefore gives information about the magnetic field strengths and topology in the low chromosphere, whereas most magnetogram data apply to the photosphere, below the supposed region of magnetic dissipation in coronal heating and flares. Changes in magnetic field topology, pre- to post-flare, should be much larger in the chromosphere than in the photosphere, and hence much more evident at millimeter wavelengths. Instrumental requirements are similar to those above, but with relaxed time constraints, tightened polarization accuracy, and, because of active region complexity, best possible u-v coverage.

5. Mapping of solar filaments and prominences. The variation of brightness temperature with frequency in the centimeter-/millimeter-wave domain provides easily interpretable information on the temperature and density structure of the transition sheath surrounding filaments, those dense clouds of cool gas suspended high in the corona. From the temperature gradient observable at millimeter wavelengths the thermal energy conducted into the filament from the corona can be calculated. Mini-flares whose cause is unknown occur in filaments: magnetic reconnections and thermal instabilities are possibilities. Comparison of high spatial resolution observations at millimeter and centimeter wavelengths can relate the geometry of the filament and its surrounding coronal cavity, leading to a determination of the density–temperature structure of the sheath and coronal cavity, and to reasons for their existence.

For this problem it is necessary to image a field of about 1 arcmin with a resolution of about 1 arcsec at 1 mm. This is feasible with a 3×3 mosaic, or by under-illuminating the 10 m dishes. Quasi-simultaneous observations at 1,

3, and 9 mm are required, with intermediate bands near 2 and 6 mm being desirable. Scaled arrays, e.g., the central element at 1 mm and the array at 3 mm, would provide the great advantage of having identical resolution at two frequencies.

6. Mapping of the quiet Sun: quiet regions and coronal holes. At 36 GHz, recent Japanese 45 m results[4] demonstrate that coronal holes are brighter than quiet regions, contrary to what is observed at almost all other frequencies (e.g., 10 and 98 GHz). Earlier reports of this highly unexpected effect came from U.S. and Russian observers, but seem not to have been taken seriously, perhaps because of the relatively poor spatial resolution. The cause of the anomalous brightening is unknown: it is possibly related to a lower gradient of density and temperature in the transition region of coronal holes compared with average quiet regions, or to a wider temperature plateau in the upper chromosphere. Maps with arcsecond resolution are desirable to determine whether the brightness difference is related to fine structure or widespread emission, and to compare brightness distributions at the solar limb where the emission scale height is only about $1''$.

Instrumental requirements include simultaneous mapping at 9, 3, and 1 mm, with intermediate wavelengths near 6 and 2 mm being desirable. Mosaics of fields 3 arcmin or more are required.

7. Miscellaneous, speculative.

Coronal heating: Mechanisms that cause heating of the outer atmospheres of the Sun and stars is not understood. For the Sun we know that mechanical energy deposition due to sound waves is inadequate. The magnetic field comes through the photosphere in small bundles with strength greater than 1000 gauss, and these field lines spread out by the time they get to the corona. Parker[5] and others have demonstrated that there is no equilibrium topology for helical bundles in the general case, and hence there must be dissipation of energy. Proof that this heats the corona is lacking.

Millimeter maps of brightness and polarization with better than $1''$ resolution might reveal the emergent magnetic flux topology and its spreading in the chromosphere. Sites of heating in the low corona may be evident in a series of maps spaced about 1 s apart. If so, temperatures and densities of heated pockets could be derived.

The instrumental requirements for this study include excellent u-v coverage in the 300 m and 1 km configurations; the latter might require $\gtrsim 30$ antennas. The small field of the 10 m antennas, $\sim 20''$, is adequate.

Oscillations and pulsations: Some modes of oscillation and pulsation may be observable at millimeter wavelengths by metrology. For example, if radial and torsional oscillations of low order could be observed, they would reflect the structure of the deep solar interior.

---

[4]Kosugi, T., Ishiguro, M. and Shibasaki, K. (1986), *Publ. Astron. Soc. Japan* **38**, 1.
[5]Parker, E. N. (1983), *Astrophys. J.* **264**, 635.

The instrumental requirements include accurate measurements ($\lesssim 0\farcs1$) of the relative positions of opposite solar limbs as a function of time (tens of minutes to many hours). Two subarrays would be needed, pointed at opposite limbs.

2. The Stars

Radio astronomy of the stars has recently become of major importance, largely because of the availability of a new instrument, the VLA, with its factor of 10 to 100 increase in sensitivity and resolution. The MMA, as conceived, would be another giant step upward in sensitivity and resolution in its wavelength band, and results of major importance are to be anticipated. Some problems that would be attacked are given below. Summaries of the present state of knowledge are given in the book edited by Hjellming and Gibson[6] and the review article by Dulk[7].

1. Outbursts from active stars and close binary systems. Here we are mainly concerned with flare stars (dwarf stars with emission lines of spectral class dMe) and close binaries such as those of type RS Canes Venatici (RS CVn). Millimeter observations offer the important advantage of allowing detection of fast electrons much closer to the acceleration site, in the same way as for the Sun and many other objects. Thus it is to be expected that the correspondence between optical/UV flare emission and millimeter-wave emission will be close. It is likely that centimeter-/decimeter-wave flare emission arises in fairly large, optically thick sources located high in a stellar corona, perhaps at a distance of $\sim R_\star$ above the photosphere, whereas millimeter-wave sources should be only a small fraction of a stellar radius in size and located much lower. Hence flares can be associated better with centers of activity (starspots or active longitudes) than has been possible at centimeter wavelengths.

Flare spectra of stars sometimes have a positive slope at least to short centimeter wavelengths. The frequency of peak flux (where the optical thickness of the radiating source changes from thick to thin) may then be in the millimeter band. The location of the peak is mainly sensitive to the magnetic field strength (typically $\gtrsim 10^3$ gauss) and the energy of the radiating electrons (typically $\lesssim 1$ MeV), hence measurements of the peak frequency greatly constrain these parameters.

Flare emission may occur in millimeter waves at low harmonics of the gyrofrequency if the field strengths attain values of $\sim 10^4$ gauss. Certainly strong fields exist on many active stars, as evidenced by flare activity and quiescent emission in centimeter waves. Fields of 10^4 gauss have not been observed directly, but several kilogauss fields have been observed on G to M dwarf stars. When these same techniques are applied to dMe stars they usually give only limits consistent with the existence of 10^4 gauss fields, and the dMe star AD Leo has measured fields of ~ 4 kG over about 70% of its surface.[8] If in

[6]Hjellming, R. M. and Gibson, D. M. (1985), *Radio Stars*, (D. Reidel: Dordrecht).
[7]Dulk, G. A. (1985), *Ann. Rev. Astron. Astrophys.* **23**, 169.
[8]Saar, S. H. and Linsky J. L. (1985), *Astrophys. J. (Letters)* **299**, L47.

fact peak fields of 10^4 G do exist, it is possible that cyclotron maser emission, occurring at low harmonics of the gyrofrequency, occurs at millimeter wavelengths. Such emission is characterized by high degrees of circular polarization ($\gtrsim 90\%$), high brightness temperatures ($\gtrsim 10^{14}$ K), and rapid time variations (< 10 ms). Bursts with these characteristics have been observed at frequencies up to 5 GHz from the Sun, the Earth, Jupiter, Saturn, the RS CVn system HR 1099, the dMe flare stars L726-8A and AD Leo, and the cataclysmic variable binary AM Herculis. (Not all of these characteristics have been observed in all objects; e.g., high time resolution has only rarely been achieved for stars, and planetary masers occur only at low frequencies.) If observed in the millimeter band, such bursts would offer strong evidence of magnetic fields near 10 kilogauss.

In addition to "normal" flares that accelerate electrons to the range 100 keV to 1 MeV, some solar flares exhibit evidence for electron energies of 10 to 100 MeV, and these radiate intensely in the millimeter band even with low field strengths. Millimeter observations of flare stars and RS CVn's will reveal whether stellar counterparts of such flares exist. Normal flares on a star 5 pc distant would give fluxes of order 10 mJy at 3 mm, whereas γ-ray–mm-wave flares should give fluxes more than ten times larger. While these unusual flares might not be identifiable at centimeter wavelengths, they would stand out in millimeter waves and allow determination of the electron energy spectrum.

The requirements on a millimeter array that will ensure appropriate observations include the following:

(i) High sensitivity in the continuum mode: better than 1 mJy at 1 mm. This is the overriding consideration, one which requires the largest possible collecting area, the lowest system temperatures, and the largest bandwidths.
(ii) High time resolution, better than 1 s.
(iii) Accurate circular polarization, better than 10%.
(iv) Operation at two frequencies simultaneously is highly desirable.

2. Quiescent emission from chromospheres/coronae of active, late-type stars. Quiescent emission is observed in the centimeter/decimeter band from a number of nearby dMe stars, late type stars, and close binaries. There is no accepted model for this emission—it may be due to gyrosynchrotron radiation from predominantly thermal electrons or from nonthermal electrons in a power-law tail. Observations in the millimeter band can distinguish between these possibilities since there are many more fast ($\gtrsim 1$ MeV) electrons in a nonthermal tail (able to emit millimeter waves) than there are in a thermal electron distribution with its exponential cutoff at high energies. Extrapolations from observed microwave fluxes indicate that dMe quiescent emission is undetectable (~ 0.05 mJy) for thermal gyrosynchrotron radiation, while the nonthermal tail model predicts detectable emission (~ 0.5 mJy).

For active late type stars and RS CVn systems, the flux levels at all frequencies are higher than for dMe stars, due to the larger source areas. Millimeter-wave fluxes greater than 10 mJy are predicted from a nonthermal tail of ener-

getic electrons.

Instrumental requirements for this study are similar to those of Part 1 above. The longer integration times possible here are mostly offset by the lower flux densities expected for quiescent emission compared with outbursts.

3. Winds of hot stars. Observations at 1.3 mm and 3 mm are of fundamental importance to studies of winds from hot stars. Current problems with wind fluxes at centimeter wavelengths (e.g., variability, spectrum oddities, and failure to fit expected visibility curves with model temperatures) argue that millimeter-wave data will be critical in sorting thermal from nonthermal radiation.

The simple theory of radio emission from winds predicts:

$$S_\nu \propto \nu^{0.6} \qquad \text{and} \qquad R_\star \propto \nu^{-0.6};$$

and typical values at 2 cm are: $S_\nu \approx 100$ mJy and $R_\star \approx 0\farcs1$. As shown below, this rising spectrum allows many wind sources to be detected at millimeter wavelengths. Effects of nonthermal electron populations are much smaller at millimeter wavelengths than at centimeter wavelengths, so that "pure" wind radiation should be more common, and uncertainties in derived mass loss rates should be smaller.

Because of the $\nu^{0.6}$ spectrum, the flux density S_ν of wind sources is roughly ten times larger at 1.3 mm than at 6 cm. The mass loss rate $\dot{M}$ goes as $\dot{M} \propto S_\nu^{3/4}$. If the sensitivity at 1.3 mm were the same as currently available at 6 cm, this would imply that six times smaller mass loss rates would be observable. Alternately, sources with the $\dot{M}$ now detectable at 6 cm with the VLA would be observable out to a distance about three times farther than is now possible.

How many stellar wind sources would then be detectable with the millimeter array?

(i) Wolf–Rayet (W–R) stars: 24 W–R stars have been detected with the VLA at 6 cm, roughly all such stars within 2.5 kpc. With the millimeter array, all known galactic W–R stars at observable declinations will be detectable, roughly doubling the sample size, depending somewhat on atmospheric attenuation vs. declination.

(ii) O–B stars: About 16 O–B stars thought to be wind sources have been detected with the VLA at 6 cm. This number will be increased with the millimeter array because of two factors: First, stars of lower $\dot{M}$ will be detectable within the present limiting distance. Given the relation $\dot{M} \propto L_\star^{1.6}$, the luminosity threshold for detection will be lowered by about a factor of 3. With the estimated initial mass function for O–B stars, roughly 70 new sources will be detectable. Second, stars like those presently observable will be detectable at larger distances. This factor is not as important as might be thought because all O–B stars are near the galactic plane (i.e., in a cylindrical volume a few hundred parsecs thick rather than a spherical volume), but some 20 new, distant sources should be detectable.

An increased sensitivity beyond the paradigm array, due to a larger $A_{\rm eff}$, larger bandwidth, or smaller $T_{\rm sys}$, would lead to a correspondingly larger number of detections, going roughly as $S_{\rm lim}^{-0.8}$.

We list two main reasons why detecting more stellar winds represents an important scientific goal: First, with the relatively small number now observable there are uncertainties related to small number statistics. More importantly, the presently known objects may be the outliers of a population, unusual objects not representative of the whole. Second, lowering the $\dot{M}$ threshold will enable both UV and radio analysis techniques to be applied to the same stars. Currently, almost all stars with $\dot{M}$ large enough for radio detections have UV resonance lines that cannot be analyzed because they are completely saturated.

We turn now to the importance of having long enough baselines in the millimeter array to resolve wind sources. The character of wind sources leads to two components: an optically thick central core, and an optically thin outer region. To date, no core has been resolved; the largest, P Cygni, has a diameter of about $0\farcs1$ to $0\farcs2$ at 6 cm. If the millimeter array has baseline lengths comparable to those of the VLA, P Cygni and one or two other wind sources may have resolvable cores.

Optically thin outer parts of two stellar winds have been resolved with the VLA for two stars, the O–B star P Cygni and the W–R star γ^2 Vel; the "resolution" was accomplished by comparing visibility versus baseline. From such data, four vital pieces of information can be derived:

(i) The temperature of the wind.
(ii) A verification that the radio emission is indeed bremsstrahlung from wind material.
(iii) Isotropy on the plane of the sky can be established.
(iv) If accomplished at multiple frequencies, the temperature can be derived as a function of radius.

Resolution of the optically thin outer parts of winds requires a signal-to-noise ratio of about 50 : 1, a value that would be achieved for essentially all stars currently detected at 6 cm. In addition, nearly all of these would be resolvable at 1.3 mm, giving a strong justification for long baselines in the millimeter array.

In summary, the instrumental requirements for the study of wind sources are similar to those listed in Part 1 above, but here baselines of 35 km to 70 km are required in order to resolve a significant number of stars.

4. Main sequence stars. About 600 stars, a few main sequence but mostly giants, will be detectable with a millimeter array simply because of the thermal radiation from their photospheres or low chromospheres. Figure 2 is an HR diagram showing the detectable stars and the limiting distances at which stars of various spectral and luminosity classes could be detected with the paradigm millimeter array. It also shows the approximate number of stars expected to have flux densities of various levels. The star numbers are probably lower limits because any effect that increases the effective temperatures or stellar radii

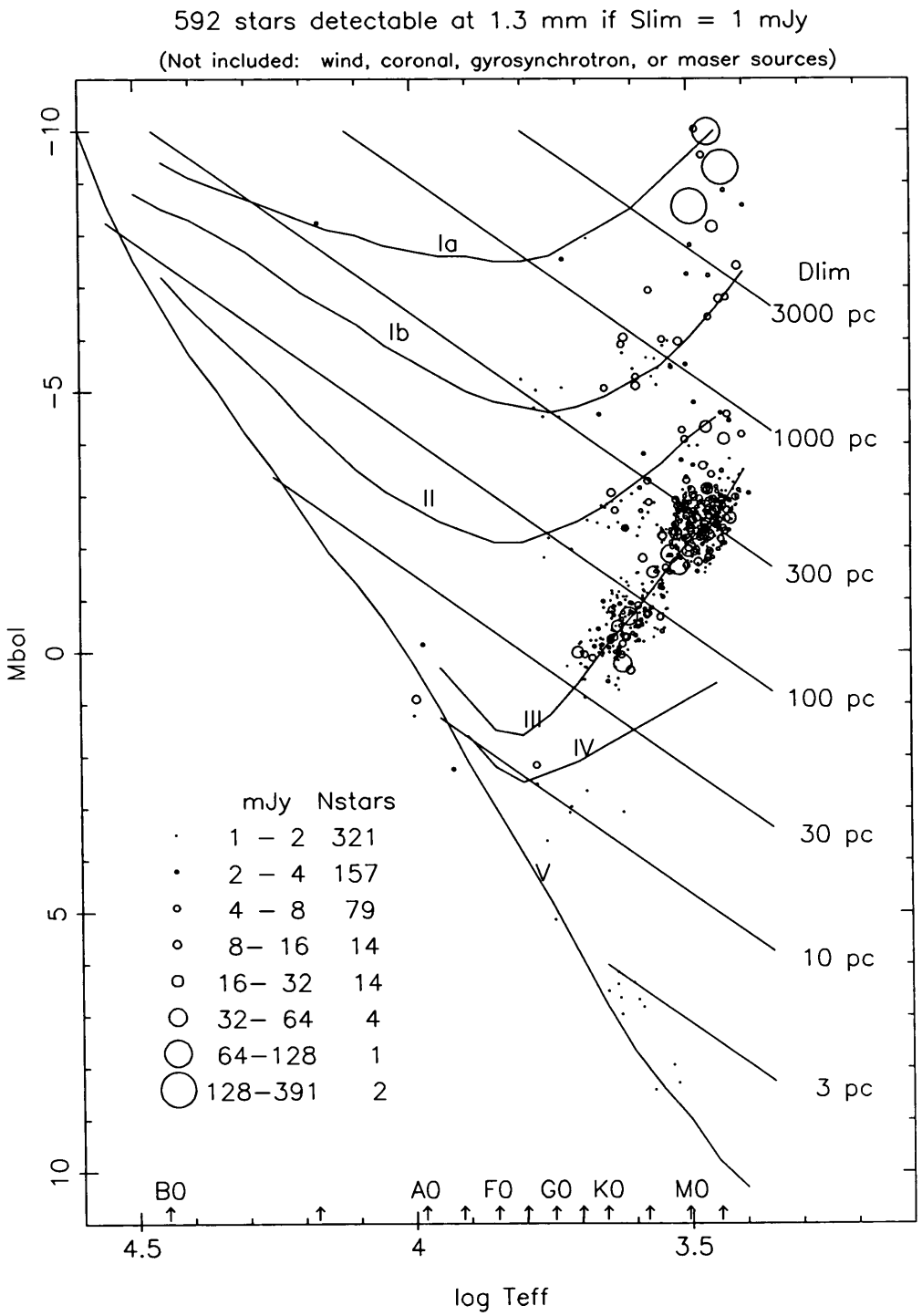

Figure 2. HR diagram showing stars that will be detectable with the paradigm MMA at $\lambda = 1.3$ mm if the minimum detectable flux density is 1 mJy.

(e.g., dense transition regions, coronae, or winds) would allow more stars to be detected. Figure 2 was derived from the 9110 stars of the Yale Bright Star Catalog; catalogued values of spectral class, luminosity class, apparent magnitude, and color index were used to derive bolometric magnitudes, effective temperatures, distances, and stellar radii. From these, the 1.3 mm flux density was derived.

Because $S \propto T_{\rm eff} R_\star^2$, millimeter-wave observations can check on the canonical values (mostly inferred indirectly, few measured) of $R_\star$, or with less sensitivity, $T_{\rm eff}$. One should expect surprises, with radio sizes or effective temperatures being different from canonical.

In addition to simple detections, several other studies become possible if the array sensitivity is high enough—for example:

(i) Sixty or more nearby stars should be resolvable with VLA-like baselines, providing a direct check on the stellar radii. Figure 3 is an HR diagram showing 63 stars that can be resolved with 35 km baselines. About ten stars have diameters of two or more beamwidths. Stellar winds, common on red giant stars but not included in these estimates, would increase the number and resolvability of such stars. Criteria for resolving stars have been presented by Mutel.[9]

(ii) Starspots and/or active regions would modulate the flux at the stellar rotation period. Long-term monitoring allows a direct measurement of how stellar activity cycles relate to spot numbers and sizes.

(iii) Stellar pulsations such as are expected in some parts of the HR diagram may modulate the flux enough to be detected.

(iv) Metrology of star positions over periods $\gtrsim$ 1 year, with a few milliarcsecond resolution, may reveal the binary nature of some stars, and perhaps demonstrate the existence of low mass (planetary) companions.

The requirements for these studies are again high sensitivity and long baselines. The need for high sensitivity is emphasized by the realization that the number detectable is proportional to $S_{\rm lim}^{-1.5}$, where $S_{\rm lim}$ is the limiting sensitivity (e.g., 4σ); for example, in Figure 2, more than half of the stars have flux densities in the 1–2 mJy range. The precision of positions, sizes, etc. is proportional to the signal-to-noise ratio. Hence there is an overriding need for high $A_{\rm eff}$, wide bandwidth (> 10 GHz), low system temperature, and self-calibration of weak sources (which may require the redundancy provided by a number of antennas larger than 21).

5. Cool supergiant chromospheres. In the millimeter band, radiation of these stars comes from locations where energy deposit (mechanical?) causes partial ionization of the winds, whereas centimeter-wave radiation arises outside of that region where the limiting ionization of 1% to 2% has been attained. Betelgeuse and Antares are strong sources with flux densities of 200–300 mJy, spectral indices of about 1.2 to 1.4 and angular sizes of about 50 mas in the

[9]Mutel, R. L. (1985), in *Radio Stars*, Eds. R. M. Hjellming and D. M. Gibson, *op. cit.*, 359.

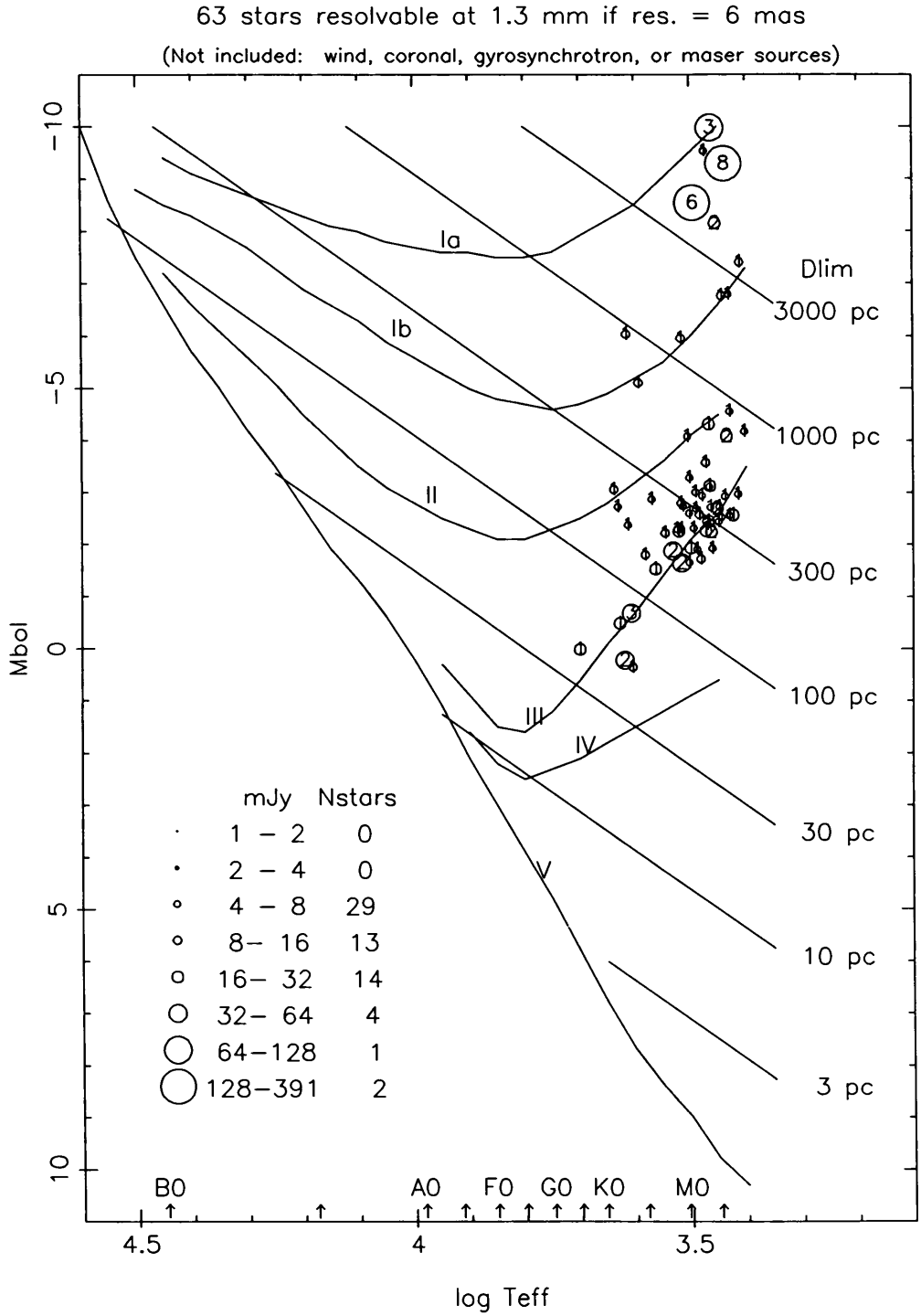

Figure 3. HR diagram showing stars that will be resolvable with the millimeter array at $\lambda = 1.3$ mm if baselines to 35 km are available. The sizes of the circles are proportional to flux density, and the numbers inside the circles indicate the number of resolution elements across the star.

millimeter range. Imaging of these two stars with $\gtrsim 6 \times 6$ pixels is possible at 1.3 mm with a 35 km array (they are represented by the two large circles at the upper right of Figures 2 and 3). One then expects asymmetries, starspots and possibly pulsations to appear in the data. With a sensitive millimeter-wave array, it will be possible to measure the spectrum of several other cool supergiants.

Regarding requirements on the millimeter array, this is an excellent example of a project for which baselines of 30 km and more are essential.

6. Miscellaneous. A number of stars exhibiting very interesting phenomena are observable at millimeter wavelengths; many of these are in the area of overlap between this Working Group and the Working Group on Evolved Stars. Here we will briefly mention some of these objects; a few of them are reviewed in more detail by the Evolved Star group.

Time variations of X-ray binaries: Cyg X-3, SS 433 and LSI+61°303 are binary stars with strong X-ray and γ-ray emission. Their radio sources, particularly Cyg X-3, exhibit shorter and shorter time scales as frequency increases, e.g., tens of minutes at 70 GHz. Observations in millimeter waves, especially if nearly simultaneous at 1 and 3 mm, will directly reflect the energetic electron spectrum as a function of time at a location very close to the region of particle acceleration.

Novae and recurrent novae: At millimeter wavelengths, one can observe nova shells in the early stages of expansion, in the months coinciding with optical studies. The combined data will be much more powerful than either by itself in constraining models of shell density and velocity. Outbursts such as that on RS Ophiuchus in January 1985 would be especially revealing if observed with a millimeter array. In that case there were two components, an extended shell and a compact component that had a spectrum still rising at 22 GHz and an observed brightness temperature $T_B \gtrsim 10^6$. Possible causes for the radiation include synchrotron emission from shock-generated fast electrons, and fast electrons trapped in some sort of stellar magnetosphere. Millimeter-wave observations, spectra, and resolution of source sizes and positions, are essential in distinguishing among models.

Ejected shell/wind objects and small planetary nebulae: Some kinds of circumstellar shells and compact planetary nebulae produce bremsstrahlung radiation which is optically thin only at millimeter wavelengths, hence only there amenable to certain kinds of diagnostics. A significant number are large enough to be imaged with a millimeter array, allowing the determination of the density profiles. As some of these sources are associated with shocks moving into fossil red giant winds, parameters of the shocks will be derivable. Source sizes are typically a few arcseconds, so the optimum resolution (consistent with source brightnesses) is about $0\farcs1$.

VV Cephei and symbiotic star binaries: Here we deal with ionized, optically thick sub-regions of supergiant stars (VV Cep binaries) and giant stars (symbiotic binaries). The ionized regions are associated with relatively small,

hot, ionizing stars orbiting deep inside dense, mostly un-ionized winds from cool primary stars. The HII regions thus produced are exceptionally dense ($n \gtrsim 10^7$ cm^{-3}) and almost certainly hot ($T_e \gtrsim 10^5$ K); somewhere in the millimeter band they change from being optically thick to optically thin. Models of these ionized regions are very dependent on the orbital parameters of the binaries and on asymmetries or temporal variations in the winds. Millimeter-wave observations are ideal for the probing of the ionized sub-regions, and of fluctuations and asymmetries that exist deep within the cool winds.

Acknowledgments. This Working Group has greatly benefited from discussions with and comments from G. Hurford, D. Abbott, and R. Mutel.

3. Summary of Desired Instrumental Properties

Sun.

- Good snapshot imaging in arrays of ≤ 1 km ($\lesssim 1''$ resolution);
- Integration time: $\lesssim 0.1$ second;
- Fast frequency switching among 1 mm, 3 mm, and 9 mm ($\lesssim 1$ s); bands near 2 mm and 6 mm are desirable;
- Simultaneous observations at two frequencies are highly desirable.
- Accurate circular polarization: better than 1%;
- Field of view of 3 arcmin or more at 3 mm by:
  - (i) mosaicing at ~ 0.01 sec, or
  - (ii) feedback of pointing from MT to 10 m dishes in ~ 0.03 sec, or
  - (iii) under-illumination of 10 m dishes (preferred solution).

Stars.

- High sensitivity: large $A_{\rm eff}$, large bandwidth, low $T_{\rm sys}$;
- Long integration times: self-calibration on weak sources;
- Moderate time resolution: $\lesssim 1$ second;
- Two frequencies simultaneously highly desirable;
- Accurate circular polarization: better than 10%;
- Long baselines (35 to 70 km) required for some studies.

IV. Circumstellar Shells and Evolved Stars
Working Group Report[†]

1. Overview

Evolved stars and their envelopes are the most natural target for observations with a millimeter-wave array. This assertion is proved by the facts that current millimeter-wave interferometers at Hat Creek and OVRO have been used extensively to study their structure, that a large amount of work on them is conducted with the VLA at centimeter wavelengths, and that they are almost the only use of VLBI techniques in galactic astronomy. Two reasons can be cited for this interest. The study of star-like sources obviously requires high spatial resolution and the ability to map a complex region. If a stellar envelope has dimensions of 10–1000 A.U., then at the typical distance of one kiloparsec its angular size will be between $0''.01$ and $1''$. The more important reason, however, is the increasing realization of the importance of these objects in galactic evolution and of the process which produces an extended envelope—namely, mass loss—in the life of many stars. We now know that mass loss accompanies giant branch evolution and modifies stellar evolution both in terms of rates and masses. We are also becoming aware of the presence of a galactic bulge component which is largely composed of stars similar to those in the solar neighborhood which have been assumed to be an extreme case of giant branch evolution with mass loss. Studies of mass loss and of the resultant envelopes seem to show that late type stars are a significant contributor of processed material to the ISM. They could return as much as $0.3 M_\odot$/yr, which would nearly match the star formation rate. If they do return that much mass, then an understanding of these objects and their mass loss mechanism is a prerequisite to analysis of the entire star formation process. Taken to the extreme, late type star evolution and mass loss may be the key to galactic evolution.

In the following discussion the major scientific issues concerning evolved stars and circumstellar shells will be reviewed, as will be some of the current results in this field. A specific millimeter-wave array design is not tested against these issues, but rather a series of experiments for a millimeter-wave array are developed. These experiments are listed in Section 5. The resultant requirements for a millimeter-wave array are presented in Section 6 as the major conclusions of our study.

[†]Contributors: J. H. Bieging, University of California at Berkeley; D. E. Hogg, NRAO; P. R. Jewell, NRAO; G. R. Knapp, Princeton University; S. P. Reynolds, NRAO; P. R. Schwartz (Chairman), Naval Research Laboratory; and P. Wannier, Jet Propulsion Laboratory.

2. Astrophysical Issues

1. The evolutionary state of late type stars. Toward the end of their lifetimes, low and intermediate mass stars ($1M_\odot \lesssim M \lesssim 10M_\odot$) go through a high mass loss phase. As a result, a circumstellar envelope is formed that can often be detected with millimeter-wave spectral line and continuum observations. In general, these stars are cool giants or supergiants or are hotter objects that may be in even more advanced phases of evolution. Several categories of objects can be identified:

(1) Classical Mira and semi-regular variables (periods $\gtrsim$ 1 year);
(2) OH/IR and carbon stars;
(3) Objects with warm central stars (Sp = F through B); and
(4) Planetary Nebulae.

Current stellar evolution theory places stars from categories 1 and 2 in the asymptotic giant branch (AGB) stage of evolution.[1] Category 3 and 4 objects have evolved beyond the AGB. AGB stars are characterized by a degenerate carbon/oxygen core with He- and H-shell burning zones. They experience episodes of rapid He burning, resulting in thermal pulses. A consequence of these thermal pulses is that processed material (C) from the He burning zone may be mixed into the H envelope in a series of "dredge-up" phases.

Category 1 and 2 stars lose mass at often very high rates (up to $10^{-5}M_\odot$/yr) in nearly continuous mass loss flows or possibly in more episodic outbursts. The process producing mass loss in these stars is not well understood, but radiation pressure on grains condensing in their cool, extended atmospheres is suspected. Atmospheric shock waves driven by envelope pulsations may also contribute. The mass loss flows of these stars can often be detected by a variety of millimeter-wave observations, including molecular line spectroscopy, dust, and free–free continuum.

AGB stars are the suspected progenitors of Planetary Nebulae (PN). It has been held that near the end of red giant evolution, the stars' envelopes can be ejected by a sudden cataclysmic event. Alternately, there may be a smooth transition from a mass loss outflow into the PN phase. Current speculation is that there is a point in AGB evolution at which the steady mass loss outflow switches from a "normal" level to a "superwind" level. This increase in the outflow rate may be induced by a pulsation mode switch from first overtone to fundamental mode pulsation. After a sufficient portion of the stellar envelope is blown off, the star begins a blue-ward journey across the H–R diagram—which, if the star reaches ionizing temperature before the remnant envelope is dispersed, ultimately results in a classical PN.

Certain objects are conjectured to be in the transition between red giant and PN (e.g., GL 2688, IRC+10420, and GL 618). A few PNs have neutral envelopes (e.g., NGC 7027 and Vy2–2) which are interpreted as remnants of the expelled red giant circumstellar envelope. Although this picture is appealing, some problems exist: almost all of the transition objects and 50% of PNs

[1]Iben, I. Jr. and Renzini, A. (1983), *Ann. Rev. Astron. Astrophys.* **21**, 271.

have non-spherical envelope morphology, while the envelopes of their supposed progenitors are usually spherically symmetric.

2. Stellar mass loss. Mass loss from red giants was inferred from observation of OH, H_2O and SiO masers, but is more directly shown by the detection of CO (1–0) and (2–1) emission lines. About 120 stars are known CO sources, and as many as 300 are detectable with current technology. Detections are about evenly divided between oxygen- and carbon-rich objects (O/C $\gtrsim$ or $\lesssim$ 1) of all categories, from Miras through PN-like objects.

These observations yield well-defined values of the mass outflow velocity and stellar systemic velocity. Line fitting allows the stellar velocity to be determined with great precision, and the average and terminal velocity of the outflow to be estimated. The stellar velocities, considered together with optical and infrared line velocities, are of value in analyzing the pulsations of the stellar atmosphere. They can also be used to study the galactic kinematics of the group of stars in order, for example, to estimate progenitor masses. Observed outflow velocities are in the range 4–60 km/s, with some indication of a correlation with luminosity. By careful analysis of the CO profile, the envelope mass and mass loss rate $\dot{M}$ can be estimated. Mass loss rates in the range 3×10^{-8} to $3 \times 10^{-4} M_\odot$/yr are inferred, but with considerable uncertainties because of uncertainties in the CO/H_2 conversion ratio, the distance, and the assumed temperature and radial distributions. Oxygen rich stars span this range of mass loss rates, while the carbon stars cluster near a few times $10^{-5} M_\odot$/yr.

The composition of the stellar envelopes produced by these mass outflows can be estimated for C, N, and O isotopes from observation of CO isotope substituted transitions. Some of these results will be discussed in Part 3 of this Section. The gas-to-dust ratio can also be estimated by comparing CO and continuum observations. The gas-to-dust ratio appears nearly constant and is approximately equal to the interstellar value.

Circumstellar chemistry appears to be dominated by photospheric chemistry, particularly in carbon stars. It is, therefore, quite different from interstellar chemistry. Large abundances of SiS and carbon rich molecules (HC_XN) are seen, but molecular ions are absent.

The morphology and extent of circumstellar envelopes is determined by the dynamics of the mass loss process and by the stellar and interstellar radiation field (ISRF). Stellar envelopes are, thus, an unparalled astro-chemistry and radiative transfer laboratory because: (a) the envelopes' density structure is approximately known, (b) the time of exposure to the ISRF can be estimated, and (c) the distribution of photoproducts (CN, C_2H) can also be observed.

Except for a few pathological objects and PN, mass loss from evolved stars appears to be primarily radiatively driven. This conclusion results from the observation that $\dot{M}V/(L/c) \equiv B$ peaks at unity with a scatter of about a factor of 3. Oxygen rich stars usually have $B \lesssim 1$. Stars with $B \lesssim 1$ usually have shorter periods than those with $B = 1$, probably because their envelopes are more tightly bound (and thus have lower mass loss rates). PN are the

exception to this rule (i.e., $B \gtrsim 1$) suggesting that the stellar luminosity drops substantially after the beginning of PN formation. Otherwise, the molecular clouds associated with PN and PN precursors are similar to those associated with cool stars.

3. Mass loss and the ISM. The total rate of mass loss by late stars could be as large as $0.35 M_\odot$/yr, making them a significant contributor to the cycle of star formation and return of processed material to the ISM. The cores of red giant stars support a variety of H and He reactions which produce the CNO nucleides. If dredge-up of neutron rich core material accompanies mass loss, significant consequences to galactic chemical evolution result. Individual stars with CNO abundances which are very different from either solar or interstellar values are observed with prodigious mass loss rates (up to $10^{-4} M_\odot$/yr). Fully 50% of extreme mass loss objects are carbon rich (C $\gtrsim$ 0), implying that freshly synthesized carbon enriches the ejected material. The relative abundances of the CNO isotopes are a much more sensitive indicator of the operating nucleosynthesis processes than chemical abundance ratios such as C/O or N/O. Isotope ratios are both sensitive to specific reaction cycles and more easily measured because they have similar physical and chemical properties. Spectroscopically, isotope-substituted molecular transitions are usually easily separable, yet they are not separated by such large frequency increments as to jeopardize precision measurements.

CNO isotopes are the products of several different processes: ^{12}C, ^{16}O, and probably ^{18}O are the products of He burning, and can thus be cycled into the ISM by red giant mass loss or by supernovae. ^{14}N, ^{13}C, ^{15}N and ^{17}O are thought to be the products of H burning either by equilibrium CNO cycles or explosive H burning. The relative abundances of these isotopes in the CNO cycle are determined by initial nuclear composition and nuclear reaction cross sections. CNO processed material should have enhanced ^{14}N, ^{13}C, and depleted ^{15}N and ^{18}O relative to the solar abundance. The observable shell abundances depend upon a variety of factors including both the history and activity of the stellar interior, the degree and rate of mixing to the surface, and the mass loss process. For the purpose of determining the effect of red giant mass loss on galactic evolution, the entire history of enrichment by single stars must be studied. It is important to observe objects at all stages of red giant evolution to determine what, if any, effects stellar evolution has upon isotope abundances.

The comparison of red giant predicted and observed abundances with observed galactic abundances is a test of the hypothesis that red giants actually cycle significant amounts of processed material back into the ISM. Table 1 shows the observed abundances of four types of material: solar system, GMCs in the disk $\gtrsim$ 3 kpc from the galactic center (GC), GMC near the GC, and an average in red giants.[2,3]

[2]Wannier, P. G. (1980), *Ann. Rev. Astron. Astrophys.* **18**, 399.
[3]Wannier, P. G. (1985), in preparation.

Table 1.

Region	$^{17}O/^{18}O$	$^{12}C/^{13}C$	$^{16}O/^{17}O$	$^{16}O/^{18}O$	$^{14}N/^{15}N$	$^{32}S/^{34}S$
Solar	0.186	89	2630	490	272	23
Disk	0.27	60	2400	700	333	21
GC	0.29	26	900	250	$\gtrsim 550$	18
Red Giants*	1.6	15	460	545	$\gtrsim 515$	22**

*Straight average of available observations
**IRC+10216 only

The solar values represent abundances at the formation of the solar nebula ($\gtrsim 10^9$ years ago), while the disk GMCs probably represent the current disk values. The clouds in the GC probably represent more evolved material which has been subject to more recycling through stars (as evidenced by the higher stellar metallicity and older stellar population and the smaller gas fraction). Although a strict sequence is not proven, some evidence for nuclear processing by red giants is suggested by these data. Red giant processed material may be enriching the ISM in ^{13}C and ^{17}O. The large spread in observed red giant abundances however is a problem, as is the essentially identical value of the disk and GC.

3. Observational Aspects

Circumstellar envelopes are intensively studied phenomena in millimeter-wave astronomy. Current activities, and results obtained using high resolution instruments such as the Hat Creek and OVRO interferometers, together with the limited VLBI results that have been obtained to date, are an important guide to the future investigation of circumstellar envelope phenomena.

1. Stellar masers. Astrophysical masers are a valuable but sometimes difficult to interpret probe of the structure and kinematics of high density regions. A complex spectrum of very high surface-brightness velocity components is observed. Each velocity component usually originates from a single spatial spot which is separated from others in a larger masering region. The SiO maser is observed only in the cool, extended envelopes of late type stars and Orion. These late type stars, Mira variables and even more extreme oxygen rich types, are, as we noted in Part 3 of Section 2, a significant galactic population and lose mass at very high rates. They could be a primary source of processed material returned to the ISM. OH and H_2O masers are observed in a few transitions and are usually viewed as test particles in the stellar envelopes, but the SiO millimeter spectrum exhibits a rich variety of bright lines in many rotational and vibrational states. The diversity of observable excitation states may make the eventual interpretation of SiO possible; individual maser spots may tag specific densities, so that we may correlate differences in various observational properties of the spots with the different densities.

Stellar masers do not appear to be strictly coincident in individual stellar envelopes, and the SiO masers originate inside the OH maser region. OH

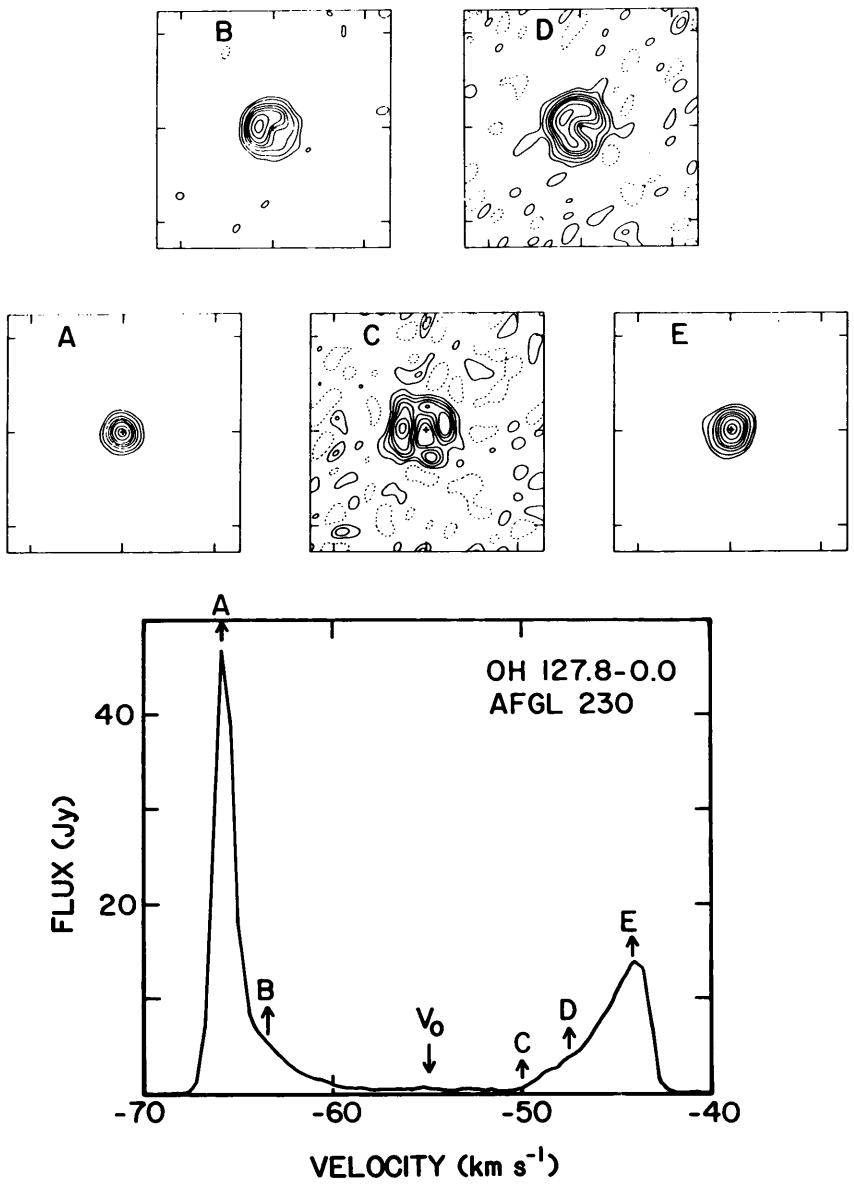

Figure 1. VLA maps of 1612 MHz maser emission from OH127.8−0.0, showing its symmetric shell structure. (Bowers, P. F., Johnston, K. J., and Spencer, J. H. (1983), *Astrophys. J.* **274**, 733.)

and H_2O maser maps are consistent with a picture of emission from different portions of a nearly spherical expanding shell, as shown in Figure 1. Only the SiO $J = 1$–0, $v = 1$ and 2 masers have been observed with better than single antenna resolution, and the maser regions and spots appear to have sizes 10–100 A.U. By observing both the distribution and variation of maser structure as a function of several transitions, the base of the mass loss region and the driving mechanism for the outflow may be studied.

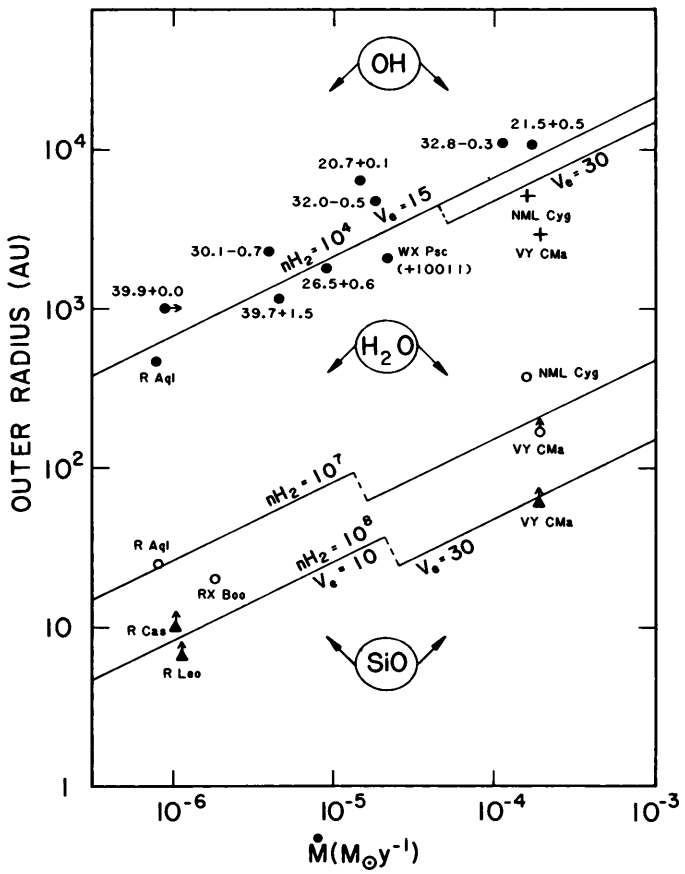

Figure 2. Radius of the maser region as a function of CO or IR mass loss rate. (Bowers, P. F. (1985), in *Mass Loss from Red Giants*, Eds. M. Morris and B. Zuckerman.)

Maser excitation is still not understood, but the existence of OH, H_2O, and SiO masers in the same stars hints at a common mechanism. Infrared pumping via similar vibrational/rotational transitions in the intense part of the stellar continuum may be the common factor. SiO, with its large number of observable transitions, may be the only maser which can be ultimately explained. If so, the absolute coincidence of, or spatial relationships between, different velocity and transition spots must be mapped in detail.

Astrophysical masers may be a statistically significant indicator of stellar mass loss. The size of maser regions correlates with several independent indicators of mass loss (see Figure 2). Currently this correlation is best for extreme OH/IR star objects, which, although important, are only a small part of the larger picture. The brightness of SiO masers in the "normal" population of Mira variables makes it possible to extend this correlation to a sample of objects which is vastly larger and more significant on a galactic scale.

2. Observation of the molecular envelopes of late type stars. Most of the information concerning the envelopes of late stars discussed in Section 2

was determined from single antenna observations, but at least one object, IRC+10216, has also been studied with the Hat Creek 3-element interferometer. IRC+10216, is approximately symmetric, is strongly centrally peaked and has 6′ diameter in ^{12}CO, but is smaller ($\sim 1'$) in other molecular lines. Eleven transitions of eight species (HNC, SiS, HC_3N, C_2H, HCO^+, CH_3OH, $H^{13}CN$ and SO) have been observed.[4] Figure 3 shows an example of the spectra of HNC, SiS and HC_3N simultaneously observed on short baselines (corresponding to 45″ and 35″ fringe spacings). Even at these spacings, resolution effects are apparent in the spectra, implying different sizes and/or brightness distributions. IRC+10216 is a carbon star with many detected molecular species, and these data show that different species may have different relative abundances and/or excitation as a function of radius from the central star. Observations of a single species, therefore, gives an incomplete picture of the stellar envelope. IRC+10216, it appears, requires imaging on angular scales from 6′ to $\lesssim 1''$ in a large number of molecular lines which reflect a range of physical conditions.

An important aspect of the study of molecular envelopes is that because of the high IR flux of the central source, many molecules are radiatively (rather than collisionally) excited. Since the stars are also variable, some transitions should be time variable. SiO masers, for example, are time variable. Bieging *et al.*[5] suggested such variability in the HCN 1–0 lines of IRC+10216, based upon a detailed excitation model and fits to their synthesis maps. The effect is best observed when a complete synthesis map can be made at a single epoch; knowledge of this effect is vital to establishing the relative importance of collisions and radiation in molecular excitation.

3. Mapping of proto-planetary nebulae. It is believed that as the evolution of the red giant star continues, it will eventually become a PN. It will pass from the red giant stage to the PN stage by a short-lived process that is not now understood. By studying the few objects believed to be in transition between the two stages, it may be possible to measure some of the characteristics of the PN formation process.

One prominent object that is probably in transition is the infrared source CRL 618. It is notable for having bipolar reflection nebulosities, between which is situated a strong radio continuum and infrared source. VLA maps[6] have shown that the central star is surrounded by a compact HII region of size $0''.4 \times 0''.1$ (1×10^{16} cm by 2.5×10^{15} cm) which perhaps delineates the interaction between the "old" wind of the red giant and the recently developed fast wind of the transient stage. To explore this further, high resolution continuum maps at 1.3 mm and 3 mm are needed to measure the physical conditions of the ionized region near the star. In addition, the cool molecular envelope of the old wind should be mapped, especially in molecular species which trace regions of high density, to see if the bipolar flow indicated by the ionized material and by the

[4]Bieging, J. H. and Nguyen-Q.-Rieu (1985), unpublished.
[5]Bieging, J. H., Chapman, B., and Welch, W. J. (1984), *Astrophys. J.* **285**, 656.
[6]Kwok, S. and Bignell, R. C. (1984), *Astrophys. J.* **276**, 544.

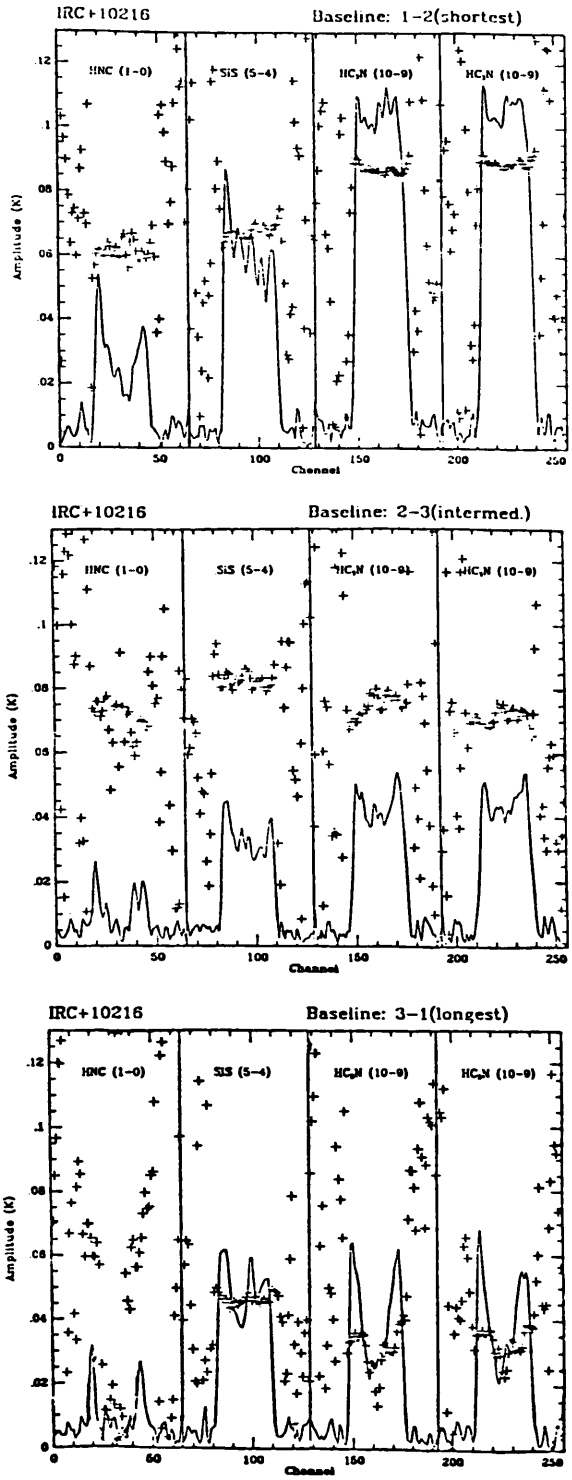

Figure 3. Simultaneous observations of molecular lines in IRC+10216, made with the Hat Creek Interferometer. Fringe amplitude is represented by the solid lines, and fringe phase by crosses.

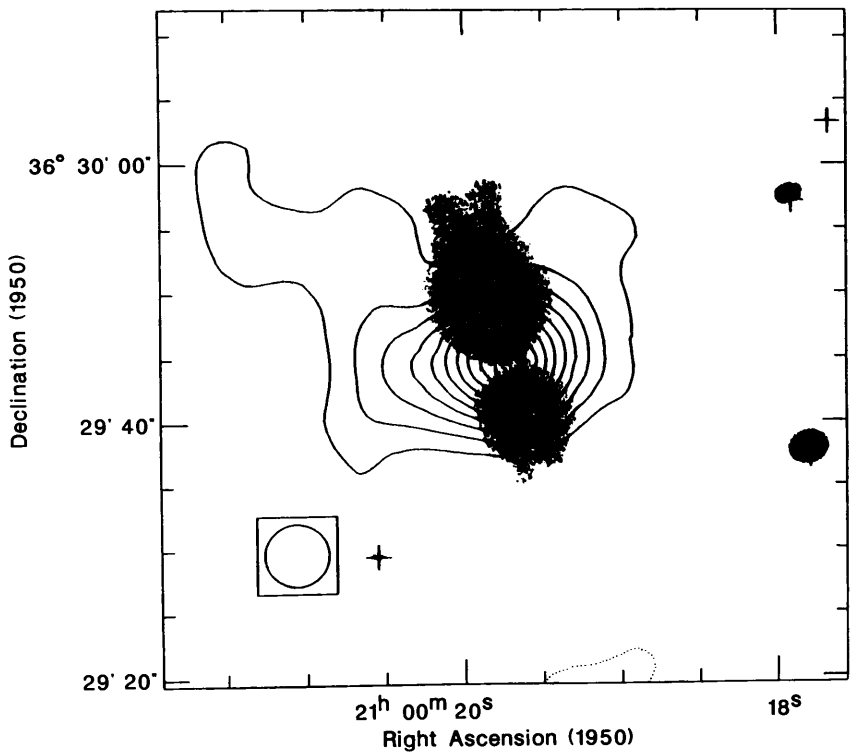

Figure 4. A contour plot of the HCN emission from CRL 2688 (integrated over all of the available channels, 64), shown superimposed on the optical photograph of Cromwell (Ney, E. P. *et al.* (1975), *Astrophys. J. (Letters)* **198**, L129.). The contour interval is 10% of the peak intensity. Crosses mark the astrometric positions of four field stars; the cross near the center of the nebula is the IR position given by Ney *et al.* The inset shows the half-power width of the synthesized beam.

reflection nebulae is being collimated by a dense molecular disk. In the latter regard, the first CO maps of CRL 618 are as yet inconclusive, but preliminary maps of HCN in the closely related object CRL 2688 are more encouraging.

An example of high resolution observations of proto-PN is the recent study of CRL 2688 made with the Hat Creek 3-element interferometer.[7] A total of ten different transitions of six species (HCN, C_4H, HNC, SiS, HC_3N, and C_2H) were mapped. Figure 4 shows a CLEANed map of the average over the HCN line with $5\farcs6 \times 7\farcs8$ resolution overlaid on an optical photograph. The HCN distribution is clearly non-circular and appears to be aligned with the optical dust lane. The HCN is evidently outlining a dense circumstellar disk surrounding the central IR source (i.e., star) but the resolution is not sufficient to determine its thickness. The HCN brightness temperatures are $\gg$ 10 K, showing that the disk is not only quite dense ($n(H_2) \gtrsim 10^5$ cm^{-3}) but also warm. The molecular line maps of CRL 2688 demonstrate that a picture of a proto-PN can be constructed if complete maps with $1''$ resolution over a field of

[7]Bieging, J. H. and Nguyen-Q.-Rieu (1987), *Astrophys. J.*, in press.

view of one arcminute can be made in several transitions. Velocity information over a wide range, probably at least 100 km/s should also be included.

Similar considerations apply to the next stage of evolution—in which the PN is well-formed, but there remains a trace of the molecular material from the red giant envelope. There are only a few objects of this type now identified (Vy2–2, NGC 6302, and NGC 7027 are examples), but they offer an important testing ground for theories of evolution. The impact of high-resolution observations is illustrated by the beautiful maps of the CO distribution made with the Owens Valley millimeter interferometer (see Figure 6). The neutral envelope, presumably the result of the red giant wind, is oblate in structure and inhibits the growth of the ionized region (the PN) in the equatorial plane. The CO observations also show the presence of a high velocity gas near the ionized nebula. This gas may be in a shocked neutral shell surrounding the expanding ionized gas. The existence of a shocked region is inferred from the observation of emission from neutral H_2.

We anticipate that the millimeter array will be used most extensively in the study of the distribution of molecules in the neutral envelopes and in the shock regions of recently-formed planetaries. Continuum maps will be useful in those cases where the ionized structure is so compact as to be optically thick at wavelengths accessible to the VLA.

4. The evolution of young massive stars. It is now well established that an important feature of the evolution of O and early B stars is the loss of material in strong, fast stellar winds. The mass loss rate, of order $1 \times 10^5 M_\odot$ yr^{-1} for a B1Ia supergiant, is a function of luminosity, suggesting that the wind is driven by radiation pressure. Extreme examples of this phenomenon are the Wolf–Rayet stars which, with masses in the range $10–20 M_\odot$ and mass loss rates of $2 \times 10^{-5} M_\odot$ yr^{-1}, are in a short lived stage that may precede a supernova explosion.[8] The mechanism for the mass loss is not known since the momentum of the wind is large compared to that available from the luminosity of the star. Interest in these stars is great because they may be supernova progenitors. For this reason it is important to get good estimates of properties of the stellar wind, such as the duration of the wind, the total mass lost in the wind, and the extent and chemical composition of the wind-blown shell.

Thermal radio emission has been observed from more than 30 Wolf–Rayet stars using the VLA. These measurements have given estimates of mass loss rates for these stars. Similar estimates could be made from radio flux densities measured at millimeter wavelengths. Of more importance, however, is that millimeter wavelength interferometry offers the possibility of exploring in detail the physical conditions in the wind. If the visibility function of the wind can be measured at a number of wavelengths between 20 cm and 1 mm the temperature and density of the wind can be estimated for distances from the star of 50–1500 stellar radii. From these data we can hope to answer the

[8]Abbott, D. C., Bieging, J. H., Churchwell, E., and Torres, A. V. (1986), *Astrophys. J.* **303**, 239.

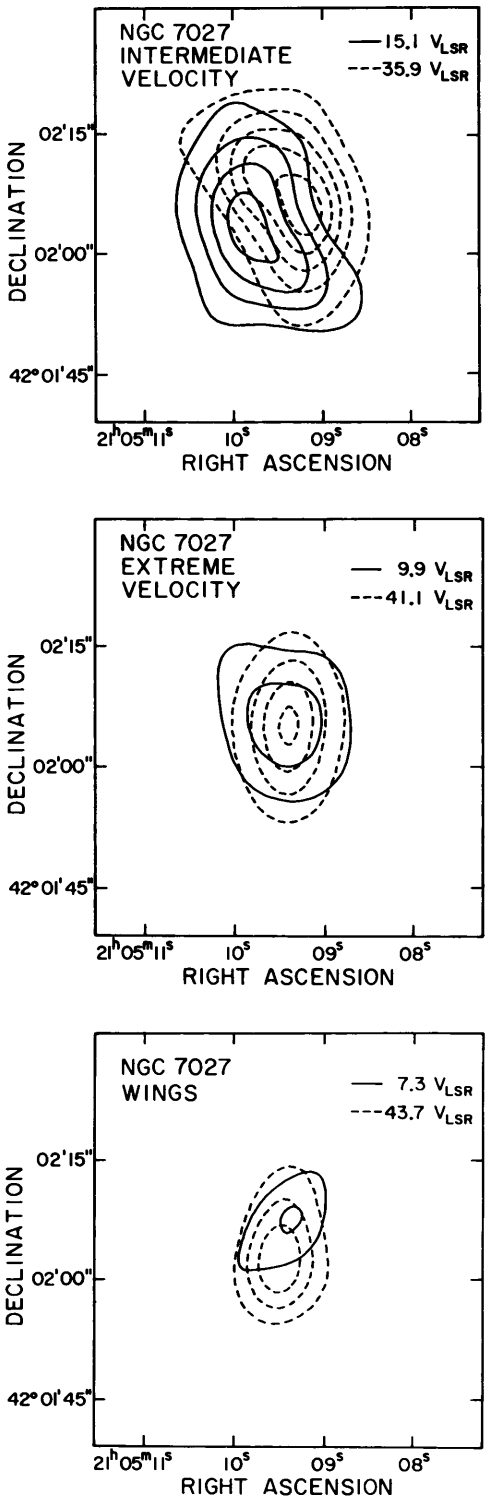

Figure 6. Morphology of different CO velocity components in NGC 7027 observed with the OVRO interferometer. (Masson *et al.* (1985), *Astrophys. J.* **292**, 464.)

following questions:

(1) Is the outflow spherical?
(2) Has the outflow reached terminal velocity at a distance of $50R_\star$?
(3) Is the flow isothermal?
(4) Are the ions in the flow recombining?

Knowledge of the physical conditions in the wind will provide important constraints on the models of the wind mechanism that have been proposed.

Similar considerations apply to the case of the winds from OB stars, except that they are in general much more difficult objects to observe, because the mass loss rates cover a much broader range than those of Wolf–Rayet stars. Nevertheless, there are a few stars which are bright at radio wavelengths, either because they are close or because they have unusually high rates of mass loss. For these objects, millimeter wavelength interferometry will enable exploration of the radial distribution of temperature and density in the wind.

4. Related Astrophysical Problems

1. The Vega phenomenon and millimeter-wave photometry. The continuum resolution and sensitivity projected for the Millimeter-Wave Array will make it a powerful extension and complement to the far infrared and sub-millimeter photometry being planned for the 1990s and to IRAS. The "Vega Phenomenon" is an excellent example of this point. Very large grains (size $\approx$ 1 mm) orbiting main sequence stars produce a far infrared excess in their spectra. These grains are a permanent relic of the star formation process and are related to the sun's cometary and planetary system. In Vega this component results in a spectral component with blackbody temperature = 85 K and $S_\nu(100\ \mu\text{m}) = 7$ Jy. Since the grains are larger than the wavelength, the spectrum is blackbody, so that the expected flux at 1.3 mm, 40 mJy, is well above the detection limit of the MMA, as currently conceived. In fact, the MMA would be about an order of magnitude more sensitive than IRAS for detecting Vega-like objects.

A related project is the photometry of unidentified IRAS 100 μm objects to determine their spectra and positions. If the unidentified objects have cool dust emission spectra, then all IRAS sources with $S_\nu(100\ \mu\text{m}) \gtrsim 1$ Jy will be detectable with the MMA and their positions determinable with arc-second precision. Identifications should follow easily at this positional accuracy (IRAS positions are good to $\lesssim 1'$ so that identifications with distant objects are confused).

2. Supernova remnants. The explosion of the supernova typically results in the ejection of up to the ten solar masses of material into the surrounding medium. These ejecta interact first with ambient circumstellar material, and then with the interstellar medium at large, producing a rich complex of phenomena. In addition, if a magnetized neutron star is formed, its energy input may drive a further interaction with the surrounding supernova ejecta.

If the supernova progenitor or its companion produced a stellar wind typical of red giants, the explosion will take place in a relatively dense medium. This

interaction results in the acceleration of relativistic particles, perhaps accompanied by turbulent amplification of magnetic fields, with resultant production of nonthermal emission. This is the phenomenon of the radio supernova. Considerably later, the remnant shock wave is interacting with ambient interstellar medium. Again, the collisionless shock wave appears to cause some combination of acceleration of particles and amplification of magnetic field. The detailed physical processes are not well understood. In young remnants, observational evidence suggests magnetic field amplification at the shock wave, though the plasma physics remains obscure. In older remnants, magnetic pressure may limit the compression in cooling filaments.

In the pulsar-driven (Crab-like) supernova remnants the particle acceleration is even more obscure. However, evolutionary processes cause the initial, presumably pulsar-produced spectrum to develop structure. This structure, in the form of spectral steepening, makes potentially observable such quantities as the pulsar's characteristic energy-loss time and the mass of material currently interacting with the pulsar's injected bubble of relativistic particles and magnetic field.

The extension to millimeter wavelengths of high-sensitivity imaging capability can be a powerful tool in the investigation of these problems. Radio supernovae become visible first at high frequencies; a powerful millimeter interferometer could detect and identify new supernovae without confusion problems, providing information on the density of the circumstellar medium and the spectrum of accelerated particles. In older remnants, synchrotron-loss effects on particle energy spectra can begin to appear at millimeter wavelengths. In middle-aged remnants such as the Cygnus Loop, optical filaments identify cooling shock waves and are also often coincident with radio filaments. Optical spectra provide information on compression and shock velocity; a break in the radio spectrum of a filament can then give the magnetic field and the energy in particles, allowing a direct determination of the efficiency of the shock at accelerating particles, and magnetic field. These effects are not detectable at centimeter wavelengths, and their analysis requires resolution of a few arcseconds or better.

Evolutionary models of Crab-like remnants predict the appearance of a spectral break in the millimeter region. Inhomogeneities in magnetic field strength can then appear as structure in spectral-index maps. In the Crab, possible correlations with optical filaments should be investigated. In other Crab-like remnants, finding such a break can better determine the evolutionary stage of development, with implications for the ejected mass and the age.

5. Experiments for a Millimeter-Wave Array

The astrophysical issues and the growing body of observational experience discussed in the previous sections lead to a group of experiments obviously well-suited to a millimeter-wave array. These experiments are perceived as finite observing programs for any potential array, and they probably will represent

the highest priority proposals for such an instrument:

(1) Detailed multi-spectral mapping of about 30 C- and O-rich late type stars at resolutions 1″–1′, to determine the structure, chemistry, and excitation of their mass outflows;
(2) A survey of about 100 late type stars in various isotopic lines to study, statistically, the chemical and abundance trends over galactic radius and stellar type;
(3) Very high resolution ($\lesssim 1''$) multi-molecular mapping of a sample of about 20 proto-PNs to detect asymmetry or characteristic structures;
(4) Very high sensitivity and resolution ($\lesssim 0''.01$) maps of dust continuum and selected molecular lines in a small sample of O and C giants to detect the inner and outer boundary of the flows, dust formation radius, and dissociation edge;
(5) Very high resolution ($\lesssim 0''.01$) mapping of the SiO maser structure of about 50 stars, to map out the base of the mass loss outflow in Mira variables;
(6) Monitoring of the time-dependent structure of radiatively excited molecules in several variable stars;
(7) Observation of the total dust continuum in a sample of C- and O-rich stars to determine total dust mass;
(8) Detailed mapping of the HII cores of several proto-PNs;
(9) Measurement of the visibility function of Wolf–Rayet stars out to 2 kpc, to determine the temperature structure of their outflows;
(10) Mosaic mapping of about 10 SNRs;
(11) Observing the radio turn-on of extragalactic supernovae.

6. Requirements for a Millimeter-Wave Array

The scientific issues and proposed experiments discussed above set certain requirements on a millimeter-wave array. These requirements are listed below.

- Operating frequencies: 100–1000 GHz; preferred frequency range is 230–345 GHz.
- Effective area: a minimum of 2000 m^2 at 230 GHz.
- Maximum sensitivity mode for continuum observations should be near 300 GHz.
- Maximum IF bandwidth $\gg 1$ GHz and facility for spectral multiplexing, to allow simultaneous observations of many spectral features.
- Available resolving power for complete maps from 1′ to 0″.1, with some facility for even higher resolution. No preferred baseline orientation is required; most likely targets are at declinations $\gtrsim 0°$.

V. Molecular Clouds and Star Formation
Working Group Report[†]

The Working Group on Molecular Clouds identified many scientific problems that can be uniquely addressed with a millimeter array. Most of these are related to a central theme: understanding the processes which precede and accompany the formation of stars and planetary systems. While other instruments (both existing and planned) will make important contributions on this theme, the MMA appears to provide the combination of sensitivity, spatial resolution, and spectral resolution which is best suited to this problem.

1. Characterization of the Turbulent Structure of Interstellar Clouds

Understanding star formation begins with understanding the structure of a molecular cloud before stars form. The simplest scenario, in which a cloud simply collapses to form a star, does not seem realistic, in general. Instead the velocity field of molecular clouds is dominated by supersonic turbulence, the source of which is not clear. Thus we are led to our first scientific problem: *to characterize the turbulent structure of molecular clouds.* A powerful probe of turbulence is the study of velocity fields as a function of scale size. For example, do they follow a Kolmogorov spectrum? Existing studies cover only about one order of magnitude in size. The MMA provides a unique capability to provide information over a much larger range of scales. Experiment No. 1 of Section 5 outlines a plan for studying the turbulent velocity field on scales ranging from 3″ to 1° (0.008 pc to 9 pc at 500 pc). While the upper end of this range could be reached with existing instruments, an MMA using a mosaicing capability allows coverage of this three order of magnitude range in a single experiment. The speed provided by a synthesis array would allow an experiment in turbulent scales to be done on several clouds with different properties (e.g., those forming high mass stars, those forming low mass stars, quiescent clouds, and Bok globules). More importantly, the present data indicate that line widths decrease with decreasing scale size, so that the transition to subsonic turbulence can be explored only with an array's capability for high spatial resolution. An interesting aspect of this experiment is that the relevant domain for investigation of the problem is not the map plane, but rather the spatial frequency plane which is naturally provided by an array. The spectral

[†]Contributors: T. Armstrong, NRAO; J. Bally, AT&T Bell Laboratories; R. Brown, NRAO; H. Dickel, University of Illinois, N. J. Evans II (Chairman), University of Texas; P. T. P. Ho, Harvard University; M. Kutner, Rensselaer Polytechnic Institute; H. Liszt, NRAO; R. Maddalena, NRAO; L. Mundy, California Institute of Technology; P. Myers, Smithsonian Astrophysical Observatory; A. Sargent, California Institute of Technology; P. Vanden Bout, NRAO; S. Vogel, California Institute of Technology; W. J. Welch, University of California at Berkeley; and A. Wootten, NRAO.

lines that seem best suited to this project are the ^{13}CO and $C^{18}O$ $J = 2$–1 lines. For denser regions, the CS lines (e.g., $J = 2$–1 or 3–2) may be desirable, in order to select shorter line-of-sight distances.

2. Identification and Characterization of "Protostellar" Fragments

In pursuing the turbulent structure to smaller scales, one hopes to begin isolating individual turbulent elements (fragments) which could eventually become individual stars. In particular, the distribution of angular momentum on small scales can be studied. The second scientific problem is to *identify and characterize "protostellar" fragments*. By protostellar, we mean that no luminous condensed object (a main-sequence star or pre- main-sequence star) has yet formed. Since the gravitational energy released by contraction is effectively radiated away during the phases we wish to study here, we assume that the temperature remains low. These objects are in the natural domain of a millimeter array. We find (see Experiment No. 2 of Section 5) that the best way to identify these fragments is through their dust emission at short wavelengths. As long as the dust temperature does not drop too low, the brightness temperature will be proportional to the dust temperature and the column density. Then, in the absence of temperature gradients induced by internal sources, the interferometer will respond primarily to enhancements in the column density which occur as a fragment contracts. Since the opacity of the dust is so low at 1 mm, it will remain a good tracer of column density up to $N = 4 \times 10^{25}$ cm^{-2}. A $1M_{\odot}$ protostar in spherical collapse would reach an average column density sufficient to make $\tau_{1\,\mathrm{mm}} \approx 1$ only at radii approaching 165 A.U. ($\approx 1''$ at the distance of the nearest clouds).

3. Characterization of Kinematic and Physical Parameters of Protostars

Once having identified candidate protostellar condensations, we would then want to characterize their kinematic and physical parameters. For kinematic studies (see Experiment No. 3 of Section 5), any spectral line would serve, so one would choose CO $J = 2$–1 for maximum sensitivity, once again using the interferometer's ability to resolve out the ambient cloud. If opacity in the surrounding cloud distorts the emission from the fragment, then lines of lower opacity or higher characteristic density could be used to discriminate against the emission from the ambient cloud. As the fragment shrinks, these lines will become comparable in brightness to the CO emission from the fragment. Convincing evidence that a fragment is truly protostellar will require the kinematic signature of collapse, probably combined with rotation. For this purpose, high spectral and spatial resolution is required in order to map the line centroid and shape across the object. The ordered motions of collapse and rotation are quite small at early stages and will only emerge from the turbulent velocity field when the object is quite small. The free-fall velocity reaches 3 km s^{-1} when a $1M_{\odot}$ protostar reaches a radius of 140 A.U. ($1''$ at the distance of the

nearest clouds). Consequently, only the high spatial resolution of an array will be capable of mapping the velocity fields in these objects.

Determination of the physical properties (temperature, density, ionization state, and chemical abundances) is also necessary for testing models of protostellar collapse. In particular, one would want to map these properties across the object. The same probes (see Experiment No. 4) that have been used in extended clouds (CO for temperature, rarer CO isotopes for column density, and high dipole species like CS for density) could be used on the protostellar fragments until the fragment density becomes so great that these probes become optically thick or thermalized. Once these probes fail, only the dust continuum will remain as a column density probe. To determine the density, multiple transitions of a single molecule are required[2]; the ability to observe simultaneously in several frequency bands would be very useful for this project (see Experiment No. 4).

Do we now have any evidence that such protostellar condensations exist? The answer is yes. The IRAS survey has found hundreds of sources in nearby clouds, generally embedded in dense clumps of gas, which have no optical counterpart. Those with very low 60–100 μm color temperatures are likely to be the youngest objects. Notable among these sources is the isolated globule B335. Observations with arcsecond resolution of objects like B335 would be able to determine the structure very near the forming star, discriminating between disks and proto-binary stars.

Special opportunities exist in regions where massive stars have already formed, since these stars will warm their surroundings enough that many molecular transitions will be excited in nearby, still proto-stellar, condensations. For example, the warm (T_K = 30–50 K) cores of the S140, M17, and NGC2024 clouds appear to have regions of very high density ($n \approx 10^6$ cm^{-3}). This dense material is probably clumped, and preliminary results from the VLA and millimeter interferometers suggest clump sizes of 5–10 $\times$ 10^3 A.U., with masses in the range 0.5 to 5$M_\odot$—within the range expected for protostellar condensations. A still more extreme example of these regions is the Orion "hot core." The brightness of this source in many spectral lines has allowed detailed study with existing arrays, and these form a paradigm for what would become possible with an MMA. However, the presence of massive stars and protostars in the vicinity of the hot core may have distorted its properties. Observations of less highly evolved regions are therefore desirable.

Another interesting possibility is to make absorption line measurements against background HII regions or dust emission regions (see Experiment No. 5). The velocity in these absorption features would allow discrimination between infall and outflow on scales very close to those of the forming object.

[2] *Cf.* Snell, R. L., Mundy, L. G., Goldsmith, P. F., Evans, N. J. II, and Erickson, N. R. (1984), *Astrophys. J.* **276**, 625.

4. Identification and Characterization of Disks Around Young Stars

There is growing evidence that disks are common features around young stars, although most of the evidence so far obtained is circumstantial. For an understanding of star and planet formation we would like to know when such disks form, and we would like to study their kinematic and physical properties. Thus we are led to the scientific problem of *identifying and characterizing disks around young stars.* A related phenomenon is that of high velocity (often bipolar) outflows from young stars. The disks are invoked as a mechanism to channel the flows into the bipolar form that frequently is observed. In other models, the disk itself is the source of the outflow. Magnetic fields may play an important role in driving or channeling the outflows. In turn, the outflows may have a major impact on subsequent star formation, by disrupting surrounding material, sweeping up dense shells, compressing pre-existing clumps, or by regenerating the general turbulent field in the cloud.

Addressing first the nature of the outflowing material seen as broad wings on the CO lines, we note that several arguments suggest that the outflowing matter is strongly clumped. Resolution of the clumps spatially would be possible with a millimeter array. It seems clear that the matter seen in the broad CO wings is generally matter swept-up from the ambient cloud. The stellar (or disk) wind is presumably faster, less massive, and at least partially ionized, as reflected by the detection of infrared recombination lines or radio continuum emission from many of the stars driving outflows. Study of these winds would become possible with a synthesis array. Many winds appear to be quite optically thick at centimeter wavelengths, so observations of the free–free emission at millimeter wavelengths may be more effective. Also the recombination lines (e.g., H39α or H40α near 2.6 mm) may be strong enough to detect, providing velocity information on the ionized component (see Experiment No. 6). If part of the wind is neutral and molecular, then very broad wings ($\Delta V \approx 300$–1000 km s^{-1}) may appear on the CO profiles. Such wide lines, while consistent with many models, would rule out some disk-driven wind models.

One of the few disks studied in detail so far is that in the Orion hot core.[2,3] Using the Wright and Vogel estimate[2] that dust opacity varies as $\lambda^{-1.3}$, assuming the gas density is proportional to n^{-2}, and adopting the relation[4] $N(\mathrm{HI+H_2}) = 1.2 \times 10^{25} \tau_{0.4\,\mathrm{mm}}$, Wootten[5] has calculated the source structure as a function of frequency, and finds that

$$T_b(r, \lambda) = 1448 \lambda_{(\mu\mathrm{m})}^{-1.3} r_{(\mathrm{pc})}^{-1}\ \mathrm{K}\,.$$

Measurements of the chemical structure of these disks can also be made if several species are observed. A recent interferometric study of Orion has

[2]Wright, M. C. H. and Vogel, S. N. (1985), *Astrophys. J. (Letters)* **297**, L11.
[3]Masson, C. R. (1985), private communication.
[4]Keene, J., Hildebrand, R. H., and Whitcomb, S. E. (1982), *Astrophys. J. (Letters)* **252**, L11.
[5]Wootten, A. (1986), NRAO Millimeter Array Science Series Memorandum No. 1.

shown that, since different molecular species are differently distributed, the physical conditions must vary across the source.[6] If observations with an array are made in a double-sideband mode and if a 1.5 GHz intermediate frequency is available, the sidebands can be placed so that one is at 259 GHz and the other at 262 GHz. Synthesis of as many as fifteen lines, probing different conditions, can then be carried out. Among them are: $H^{13}CN$, which can be compared with $H^{12}CN$; several hyperfine components of C_2H, which generally avoids hot cores and so traces the ambient gas; SO, which is found in turbulent outflow regions; two lines of SO_2, which probes hot outflows; HDCO; and dimethyl ether. The required baselines and velocity resolutions are similar to those that would be needed for the previous experiment.

Perhaps one of the most intriguing questions which can be addressed with an array is that of the magnetic structure of the dense cores at the centers of the outflow sources. During the time it will take to map out disks in HCN as described above, continuum observations in two polarizations can be carried out in the other sideband with sufficient sensitivity to measure polarizations of 1–2%. If the dust grains in the disk are elongated, and aligned by the magnetic field, these observations should indicate the direction of the field in the disk and cloud core. It will then be possible to study whether field and polarization alignments become more ordered in denser regions and whether there is any overall relation between the directions of the high velocity outflows and those of the magnetic fields. By differencing the left- and right- circularly polarized parts for the line emission of such a molecule as SO and measuring the frequency shift, the magnitude of the magnetic field can be mapped, so that it should be possible to trace the variation of field strength and compare it to density morphology. In addition to the dual polarization capabilities, spectral resolution of at most a few times 10 kHz will be necessary for this project, as well as sensitive continuum and line performance at $\sim$ 1 mm.

As a result of improved infrared detection techniques, in particular speckle interferometry, it has been shown that in a number of cases the dust around low mass stars is distributed in a disk.[7,8] The sizes of these disks are usually a few hundred A.U.—that is, comparable to the size of the pre-planetary solar system.[9] However, the infrared observations provide only indirect measurements of the disk mass, and no velocity information. Initial 7″ resolution observations of the HL Tau disk with the OVRO interferometer failed to resolve the CO source, but a lower limit of $\sim 10^{-3} M_\odot$ was obtained, comparable to the mass of the pre-planetary solar system.

For HL Tau, the peak flux in the J = 1–0 CO line was $\sim$ 4 Jy and the

[6]Vogel, S. N. (1985), private communication.

[7]Beckwith, S., Zuckerman, B., Skrutskie, M. F., and Dyck, H. M. (1984), *Astrophys. J.* **287**, 793.

[8]Grasdalen, G. L., Strom, S. E., Strom, K. M., Capps, R. W., Thompson, D., and Castelaz, M. (1984), *Astrophys. J. (Letters)* **283**, L57.

[9]*Cf.* Aumann, H. H., Gillett, F. C., Beichman, C. A., de Jong, T., Houck, J. R., Low, F. T., Neugebauer, G., Walker, R. G. and Wesselius, P. R. (1984), *Astrophys. J. (Letters)* **278**, L23.

2.7 mm continuum flux was 100 mJy. The sensitivity and resolution of the MMA should permit the routine detection of such objects. For example, with a 1 km baseline, the resolution of J = 2–1 CO, at 1.3 mm, is $0\farcs25$. At 160 pc, the Taurus cloud distance, this corresponds to 40 A.U. Thus it will be possible to compare the speckle infrared dust measurements ($\sim 0\farcs3$ resolution) directly with the gas properties, since an eight hour integration time should lead to a map with reasonable signal-to-noise ratio ($\approx$ 10). It will also be possible to sample the velocity structure much closer to the star and determine if we are observing gas in Keplerian orbits. Adopting a typical stellar mass of $1M_\odot$, the velocity at $0\farcs13$ radius and 160 pc distance should be 6 km s^{-1}. With 20 kHz filters, the velocity resolution will be 0.05 km s^{-1}, and velocity gradients will be readily discernible. Extrapolating from the HL Tau case, it should be possible to observe a reasonable statistical sample of such objects and ascertain their properties. In particular, it may be possible from the velocity information to ascertain which are likely to be protoplanetary disks and which are incipient binary systems. Numerous T Tauri stars and related objects are obvious candidates for such studies. In addition, it may be possible to make at least continuum measurements at 1.3 mm of the nearby disk-like structures around β Pictoris, Vega, and Fomalhout and further investigate their nature.

We note that the great sensitivity of the array will make possible the detection of many of the objects discussed above, throughout our galaxy. Thus one can imagine undertaking an entire class of projects involving galactic structure. And thus one could use a millimeter array to *identify protostellar clumps, bipolar outflows, or disks throughout our galaxy* (see Experiment No. 7). These would serve first as test points for galactic kinematic studies. Since the interferometer would resolve out most of the extended emission along the line-of-sight, revealing only the compact structures, some of the confusion in current CO surveys could be alleviated. In a similar way SiO masers could be used to trace the velocity field in the galactic bulge, addressing questions of bulge rotation and velocity dispersion. The star formation rate could be studied as a function of galactocentric radius R_{GC}, using the MMA to count protostellar cores and bipolar outflows. With sufficient statistics, one could also use the observed $\dot{M}_{CO}$ vs. $M_\star$ relations to investigate the initial mass function and its variation with R_{GC}.[10]

Of particular interest to galactic structure studies will be the investigation of the inner regions of our galaxy, particularly the inner several hundred parsecs, where gamma ray observations suggest that the usual relation between CO luminosity and mass breaks down.[11] The nature of the gas and that of star formation in this region are vital to efforts to understand nuclear starbursts in other galaxies. Again, protostellar fragments or bipolar outflows could be used to probe the velocity field, thus constraining the gravitational potential and mass distribution, as well as the star formation activity, in this region.

[10]Levreault, R. M. (1985), Ph. D. Thesis, The University of Texas at Austin.

[11]Blitz, L., Bloemen, J. B. G. M., Hermsen, W. and Bania, T. M. (1985), *Astron. Astrophys.* **143**, 267.

The array will also prove a valuable probe of the inner 3 pc of the galaxy, where many fascinating phenomena have been discovered. The array will be able to probe the major components in this region (ionized gas, neutral molecular gas, and dust). For this work, one would like 0.″1 resolution. Finally, a more speculative possibility is to study the accretion disk around the black hole. Maps with very high angular resolution of the H and He recombination lines could push the studies of rotational velocities much closer to the center than possible with infrared techniques, constraining the mass of the central object. In addition, hyperfine lines (analogous to the 21 cm line but at millimeter wavelengths) may be produced from H-like ions of heavy elements (via the Sunyaev–Curasov effect) in the very hot gas of the accretion disk.

5. Examples

The following are some examples of fruitful lines of research into molecular clouds and star formation which could be undertaken with the MMA.

Experiment 1. Characterization of the turbulent structure of molecular clouds. The objectives of this project are the following:

(1) To determine the turbulent velocity spectrum over three orders of magnitude in spatial scale (0.01 pc to 10 pc, at a distance of 500 pc) and to investigate the energy cascade from large turbulent cells within a cloud into the smaller cells (e.g., is the turbulence described by a Kolmogorov spectral law?);
(2) To determine when supersonic line widths are important, and to determine the source of the line widths (e.g., what role do magnetic fields play in supporting clouds? When and how do the young stars affect the line widths throughout the cloud?); and
(3) To investigate the differences between active, high mass star-forming regions and non-flamboyant regions, and to see why they differ.

The relevant observations fall into three classes, according to scale size:

(1) Smallest scales (3″–30″) —

Instrument: 90 meter array in a circular/random configuration;
T_{sys} = 500 K;
Spectral line mode of operation;
Frequency = ^{13}CO (J = 2–1 transition) (Simultaneous observations of other lines could be beneficial. For the denser regions C^{18}O and ^{13}CO observations may be needed.);
Spectral resolution = 125 kHz (0.17 km s^{-1});
Bandwidth: 256 channels would suffice;
Field size = 30″.

Objects: A few (4?) molecular clouds within 1 kpc of the Sun (Orion, Taurus, and Rho Ophiuchus, for example) which represent different classes of clouds, and a Bok globule.

Project: Map six fields in each cloud, to an r.m.s. noise level of 0.1 K;
Integration time = 6 hours per field;

The fields would be chosen at random within a 1 square degree sub-section of the cloud. Four clouds would be observed each day. A total of six days would be needed for this phase of the project;

The Bok globule would require an additional day.

Why this instrument? It is the only instrument capable of reaching the small scale structures in a reasonable amount of time.

(2) Intermediate scales (10″–90″) —

Instrument: The Multi-Telescope Array;

T_{sys} = 500 K;

Spectral line mode of operation;

Frequency = ^{13}CO (J = 2–1 transition) (Simultaneous observations of other lines could be beneficial. For the denser regions C^{18}O and ^{13}CO observations may be needed.);

Spectral resolution = 125 kHz (0.17 km s^{-1});

Bandwidth: 256 channels would suffice;

Field size = 90″.

Objects: Same objects as above.

Project: Map 24 fields in each cloud, to an r.m.s. noise level of 0.1 K;

The Bok globule could be done with fewer fields, since globules are much smaller than clouds;

Integration time = 1.5 hours per field;

Four fields surrounding each of the fields mapped with the 90 meter configuration;

A total of six days would be needed for this phase of the project.

Why this instrument? While comparable in resolution to present day instruments (e.g., Nobeyama if it could reach this frequency, and if it had the same receiver, atmosphere, etc.), the MMA would be 80 times faster.

(3) Large scales (45″–1°) —

Instrument: 4 meter dishes used like a single-dish telescope (i.e., the phase information is not needed);

T_{sys} = 500 K;

Spectral line mode of operation;

Frequency = ^{13}CO (J = 2–1 transition) (Simultaneous observations of other lines could be beneficial. For the denser regions C^{18}O and ^{13}CO observations may be needed.);

Spectral resolution = 125 kHz (0.17 km s^{-1});

Bandwidth: 256 channels would suffice;

Objects: Same objects as above.

Project: Sample 100 positions per cloud, chosen so as to sample as wide a range of spatial scales as possible;

Map each position to an r.m.s. noise level of 0.1 K;

Integration time = 1 minute per position;

Four clouds would be observed each day. A total of a few hours would be needed.

Why this instrument? Faster than any single-dish telescope by a factor of 5 (i.e., the square root of the number of individual dishes). Common calibration, etc., with other phases of this project.

Data reduction: Data analysis would be restricted to the u-v plane only; no conversion to maps would be needed. Data reduction would not require a large computer, and probably would be simpler than is typical for the VLA.

Experiment 2. Identification of protostellar fragments. The MMA will be intrinsically more sensitive to continuum emission than to line emission, because of the larger bandwidth. For a one percent bandwidth in continuum observations (e.g., $\Delta\nu = 1$ GHz at $\nu = 100$ GHz) the signal-to-noise ratio will equal that of a line 55 times stronger than the continuum (assuming a line of width 1 km s^{-1}). For example, if dust and gas temperatures are equal and if one observes a thermalized, optically thin line (e.g., ^{13}CO or C^{18}O), then an optical depth of dust which is 55 times smaller is equally detectable. If $T_D > T_K$, if one compares to a non-thermalized or a thick line, or if larger continuum bandwidths are achievable, then the advantage of continuum observations increases. Since the opacity of dust rises steeply with frequency, the advantage of dust emission also grows rapidly with frequency. Consequently, we have developed our thought experiment so as to detect protostellar fragments in the continuum at 1 mm.

We assume that $\tau_{1\,\mathrm{mm}} = 2.5 \times 10^{-26} N_{\mathrm{tot}}$ and $T_D = 20$ K so $T_B = 5 \times 10^{-25} N_{\mathrm{tot}}$, and we compute a minimum central N_{tot} by assuming that the protostar is spread uniformly throughout a sphere of radius r. Then $\langle N \rangle = 1.1 \times 10^{30} \frac{M M_\odot}{r^2_{(\mathrm{A.U.})}}$, so $\tau_{1\,\mathrm{mm}} = 1$ at $r = 165$ A.U. for a $1 M_\odot$ protostar.

To calculate what we could detect, we use the basic equation given by Hjellming (Chapter I)

$$\Delta T_b = \frac{0.64(T_{\mathrm{sys}}/100)\left(B_{(\mathrm{km})}/(D/10)\right)^2}{f_{\mathrm{geom}}\sqrt{\Delta t_{(\mathrm{minutes})}\Delta\nu_{(\mathrm{GHz})}(N_B/210)(n_a/n_m)}}\,\mathrm{K}\,,$$

and set $T_{\mathrm{sys}} = 500$ K, $D = 10$, $f_{\mathrm{geom}} = 1$, $\Delta\nu_{(\mathrm{GHz})} = 1$, $N_B = 210$, and $n_a = n_m$, to get

$$\Delta T_b = \frac{3.2 B^2_{(\mathrm{km})}}{\sqrt{\Delta t_{(\mathrm{minutes})}}}\,\mathrm{K}\,.$$

Let us set $B_{(\mathrm{km})} = 0\farcs2\lambda_{(\mathrm{mm})}/\Theta$, where Θ is the desired resolution in arcseconds. Then for a 3σ detection we need

$$\Delta T_b(3\sigma) = \frac{0.38\lambda^2_{(\mathrm{mm})}}{\Theta^2\sqrt{\Delta t_{(\mathrm{minutes})}}}\,\mathrm{K}\,.$$

For a canonical eight-hour day's worth of integration we obtain

$$\Delta T_b(3\sigma) = 17\,\mathrm{mK}\,,$$

for $\lambda = 1$ mm and $\Theta = 1''$. For $T_D = 20$ K, this means we need $\tau_{1\,\mathrm{mm}} = 8.7 \times 10^{-4}$ or $N_{\mathrm{tot}} = 1.7 \times 10^{21}$ cm^{-2}.

This column density would be reached by our putative $1M_\odot$ protostar at 2.5×10^4 A.U. This would imply that such an object could be detected, but not resolved, at 25 kpc. More nearby objects could be resolved and studied in detail.

Experiment 3. Kinematic studies of protostellar fragments. Suppose we choose to do the kinematic studies in the CO $J = 2$–1 lines. Then, to obtain detailed kinematic information, we want a velocity resolution of 0.2 km s^{-1} and a spatial resolution of $0''.2$. This would require baseline lengths of 1.3 km for the $J = 2$–1 line of CO. The basic sensitivity equation presented in Experiment No. 2 becomes

$$\Delta T_b(1\sigma) = \frac{5.2(0''.2/\Theta)^2}{\sqrt{\Delta t_{(\mathrm{days})}(\nu_{(\mathrm{GHz})}/230)\Delta V_{(\mathrm{km\ s^{-1}})}}}\,\mathrm{K}.$$

For a 20 K line, eight hours of integration would achieve good signal-to-noise with $\Delta V = 0.2$ km s^{-1}.

Experiment 4. Determination of the physical conditions in protostellar fragments. First, to determine the column density distribution across the fragment, one would use molecular lines with $\tau \lesssim 1$. As the fragment contracts, many lines will become thick, so one would move to rarer isotopes. If $T_K = 20$ K, one would like to use lines with $T_R < 10$ K, in order to avoid saturation. The calculation for Experiment No. 3 then suggests integration times of several days, or a relaxation of the velocity resolution. At higher column densities the dust continuum would be the only probe of column density.

Modifying the calculation of Experiment No. 2 to achieve $0''.2$ resolution raises the $\Delta T_b(3\sigma)$ to 0.43 K and the required N_{tot} to 4.3×10^{22} cm^{-2}. Since the dust does not reach $\tau = 1$ until $N_{\mathrm{tot}} = 4 \times 10^{25}$ cm^{-2}, we have a column density probe which can work over three orders of magnitude to study the distribution over the fragment.

Second, determining the volume density, the ionization state, and the chemical abundances requires a multi-line study, combined with better theoretical underpinnings than currently exist. Observations of many lines will clearly be critical. Flexible spectrometers and the capability to observe in several bands simultaneously will certainly be helpful. For a concrete example, we consider the CS 2–1, 3–2, 5–4, and 6–5 lines. These have been observed in several dense regions and used to infer the presence of densities $n \approx 10^6$ cm^{-3} and to suggest the presence of the clumps we now are discussing. To observe the higher lines of this series, one needs relatively warm regions ($T_K = 30$–50 K). We suppose that the lines observed by Snell *et al.*[1] ($T_R^* = 1$–8 K) do not increase in brightness with decreasing beam size, to obtain a worst case sensitivity requirement. The most critical CS lines for constraining the highest densities are the higher J transitions at 245 and 290 GHz. Thus the site quality is an important consideration. If we take $T_{\mathrm{sys}} = 500$ K, we can use the equations from

Experiment No. 3 to arrive at $\Delta T_b(1\sigma) = 6.5$ K $(0\farcs2/\Theta)$ for $\Delta V = 0.5$ km s^{-1} and $\nu = 294$ GHz. Clearly, relaxing Θ to $\gtrsim 1''$ is the only way to make detection of these lines feasible. If, however, the filling factor for the current $1'$ beams is considerably less than unity, then the lines will be brighter for the interferometer, and the experiment will be easier.

Experiment 5. Study of absorption lines against continuum sources. The r.m.s. noise in an eight-hour integration with 0.5 km s^{-1} velocity resolution and $1''$ spatial resolution at 230 GHz is ~ 0.1 K. Given that one expects to find compact HII and dust regions with brightness temperatures greater than 50 K, the study of molecular absorption lines against these sources is feasible. For example, an A_v of 5–10 may correspond to an optical depth of ~ 1 in ^{13}CO $J = 1$–0 and would result in an absorption line with a width $\sim 60\%$ of the continuum level.

Experiment 6. Detecting recombination lines, in order to study the velocities of stellar winds. Here modest spectral resolution (6 km s^{-1}) and modest spatial resolution ($0\farcs6$) are sufficient. Using the sensitivity equation from Experiment No. 3, we have $\Delta T_b(1\sigma) = 0.4$ K at $\nu = 100$ GHz (H39α or H40α) in one day. At these frequencies one expects the line brightness to be roughly equal to the continuum brightness. Ultracompact HII regions and/or ionized stellar winds should be detectable in many outflowing regions, since we suspect that many are optically thick at centimeter wavelengths.

Experiment 7. Detection of protostellar clumps, bipolar outflows, or disks throughout our Galaxy. We showed in Experiment No. 2 that protostellar cores could be detected, but not resolved, at 25 kpc. At small distances, however, they can be resolved. The protostellar condensation in B335 produces a flux density of 0.5 Jy in the continuum at 1 mm. Since B335 is 400 pc away,

$$\Delta S_\nu = \frac{1.2(T_{\rm sys}/100)}{(D/10)^2\sqrt{\Delta t_{\rm (minutes)}\Delta\nu_{\rm (GHz)}}(N_B/210)(n_a/n_m)}\,{\rm mJy}$$

(see Hjellming's Chapter I). Our usual conventions lead to

$$\Delta S_\nu = \frac{0.3(T_{\rm sys}/500)}{\sqrt{\Delta t_{\rm (days)}}}\,{\rm mJy},$$

leading to a 3σ detection in one day, out to 10 kpc. The warmer condensations should be detectable to larger distances.

6. Summary of the Impact on Array Design

For the scientific problems considered by this Working Group, good performance at high frequencies is considerably more vital than having baselines longer than 1 km. The most important angular scales are $0\farcs2$ to $30''$. A few experiments require longer baselines. We need higher spectral resolution ($\Delta\nu$

as small as 10 kHz) than afforded by the "strawman" design. We would like to be able to observe in several frequency bands (e.g., J = 2–1 and 5–4 CS) simultaneously, and we certainly want a flexible IF and backend system so that many lines in the same band can be observed simultaneously. Double-sideband receivers will allow increased flexibility. It is also desirable to be able to do line and broadband continuum measurements simultaneously. Polarization studies are important for magnetic field measurements.

This Working Group's emphasis on high frequencies arises from two considerations: the realization that dust emission will be a very powerful tool; and the realization that CO J = 2–1 is always preferable to CO 1–0, as long as the atmosphere is good at 2–1. The latter point can be seen by comparing sensitivities at 2–1 and 1–0 for a *fixed* spatial resolution Θ and velocity resolution ΔV (km s^{-1}):

$$\frac{\Delta T_b(2\text{–}1)}{\Delta T_b(1\text{–}0)} = \frac{\Delta T_{\rm sys}(2\text{–}1)}{\Delta T_{\rm sys}(1\text{–}0)} \left(\frac{\nu(1\text{–}0)}{\nu(2\text{–}1)}\right)^{3/2}$$

(note that $(115/230)^{3/2} \approx 0.35$). Then for $T_{\rm rcvr} = 100(\nu_{\rm (GHz)}/100)$ K and $T_{\rm sys} = T_{\rm rcvr} e^{\tau_1 \sec\zeta} + T_{\rm atmo}(e^{\tau_1 \sec\zeta} - 1)$,

$$\frac{\Delta T_b(2\text{–}1)}{\Delta T_b(1\text{–}0)} \approx 0.35 \times \frac{530 e^{\tau_1(2\text{–}1)\sec\zeta} - 300}{415 e^{\tau_1(1\text{–}0)\sec\zeta} - 300}.$$

Since $\tau_1 \gtrsim 0.20$ for CO 1–0 (because of O_2), τ_1 for CO 2–1 need not be worse at a good site.

VI. Astrochemistry

Report of the Chemistry Working Group[†]

1. The Nature of Astrochemistry

The earliest successful model of interstellar chemistry was based on ion–molecule reactions, a theory which over the years has provided a satisfactory picture of many of the smaller interstellar molecules that are known, and some of the larger ones. This chemistry is based on the cosmic ray ionization of H_2 and of He, producing H_2^+, H_3^+, and He^+ ions which interact with many neutral atoms and molecules to produce a wide variety of molecular ions. Neutral species are formed from these ions by recombination with electrons. The major successes of this chemistry have been the semi-quantitative as well as qualitative predictions of HCO^+, HCS^+, $HCNH^+$, as well as neutral species such as HCN, HNC, OH, C_2H, CN, and others. The chemical fractionation with respect to deuterium of several species (DCO^+, N_2D^+, DCN, DNC, HDCO), and also with respect to ^{13}C in other species, is also well explained.

However, ion–molecule chemistry is beset by major uncertainties (e.g., unknown reaction rates, input atomic abundances, the question of whether steady state has been reached, and the role of interstellar grains). These presumably explain the severe difficulties in predicting abundances of species such as N_2H^+, NH_3, and CH, the CH/CH^+ abundance ratio, and the abundances of most sulfur-containing compounds. In addition there is evidence that clouds are far more heterogeneous, chemically, than is expected on the basis of standard ion–molecule chemistry. The limits of applicability of this most important interstellar chemistry have not been delineated, because of limitations both in basic laboratory data and in observations—especially those involving spatial resolution and sensitivity.

Many recent observational results point to the operation of additional types of interstellar chemistry. In particular, high temperature ("shock") chemistry seems indicated in many instances. The abundance of CH^+ in diffuse clouds can be explained only by high temperatures ($\gtrsim$ 1000 K). Recent observations of rotationally excited CH and of vibrationally excited HCN point to regions of extremely high temperatures and densities ($\gtrsim$ 2000 K and/or $\gtrsim 10^{10}$ cm^{-3}).[1,2] High temperature chemistry also applies to refractory compounds such as SiO, which are seen only in regions containing shocks. These regions cannot be adequately studied without the high spatial resolution planned for the MMA.

[†]Contributors: E. Herbst, Duke University; W. Irvine, University of Massachusetts; L. Snyder (Chairman), University of Illinois; B. Turner, NRAO; W. Welch, University of California at Berkeley; and R. Wilson, AT&T Bell Laboratories.

[1]Ziurys, L. M. and Turner, B. E. (1985), *Astrophys. J. (Letters)* **292**, L25.

[2]Ziurys, L. M. and Turner, B. E. (1986), *Astrophys. J. (Letters)* **300**, L19.

Another type of chemistry recently observed is that of collisional dissociative processes, in particular the breakup of H_2O to form excess amounts of OH within protostellar environments, in the interface regions between energetic bipolar particle flows and the ambient molecular cloud. Grain chemistry, involving either catalytic surface reactions or the sputtering of grains, is another type of chemistry that seems to explain certain phenomena such as the recent observations of enhanced NH_3 in certain high-temperature regions of Orion. Again, small regions are involved.

The chemistry of circumstellar shells differs from interstellar chemistry in that the interesting activity is believed to occur largely in the high temperature and high density regions close to the photosphere, where chemical equilibrium obtains. The equilibrium abundances that result may or may not persist throughout the envelope, owing to the possible absorption of some species onto grains, and to photochemical processes in the outer envelope.

Finally, an example of a chemistry that may not fit any of the above mentioned pictures is that of the recently speculated polycyclic aromatic hydrocarbons (PAHs), which may contain a significant fraction of the interstellar carbon.

1. High mass star-forming regions. Studies of star-forming regions have been aided greatly by interferometric observations. For example, the tendency for maps of a given region made in different molecular lines to differ from one another was already evident in single-dish maps. It is even more pronounced in the higher resolution interferometer pictures. This is evident from comparison of maps of Orion/KL in different molecular transitions. The Hat Creek maps of HCN (1–0), SiO ($v = 0$, $J = 2$–1), SO (2_2–1_1), and HCO^+ (1–0) are all available at a velocity of 9 km/sec with a resolution of 4 km/sec.[3,4,5] The 3 mm continuum has been mapped both at Owens Valley[6] and at Hat Creek[7]. The Hat Creek map is shown superposed on the NH_3 map[8] from the VLA, an integral over the whole (4,4) line, in Wright and Vogel[7]. The HCN and SO are very similar to each other, and both are very different from the compact thermal SiO and the extended HCO^+. All are "plateau" sources. The NH_3 "hot core" map is different from the others and rather like the thermal continuum. It is difficult to attribute all the differences to excitation effects. All the molecules require comparable collision rates for excitation, and one would be fooled if one mapped just one of these molecules and thought that one had an

[3]Plambeck, R. L., Wright, M. C. H., Welch, W. J., Bieging, J. H., Baud, B., Ho, P. T. P., and Vogel, S. N. (1982), *Astrophys. J.* **259**, 617.

[4]Wright, M. C. H., Plambeck, R. L., Vogel, S. N., Ho, P. T. P. and Welch, W. J. (1983), *Astrophys. J. (Letters)* **267**, L41.

[5]Vogel, S. N., Wright, M. C. H., Plambeck, R. L. and Welch, W. J. (1984), *Astrophys. J.* **283**, 655.

[6]Masson, C. R., Claussen, M. J., Lo, K. Y., Moffet, A. T., Phillips, T. G., Sargent, A. I., Scott, S. L., and Scoville, N. Z. (1985), *Astrophys. J. (Letters)* **295**, L47.

[7]Wright, M. C. H. and Vogel, S. N. (1985), *Astrophys. J. (Letters)* **297**, L11.

[8]Genzel, R., Downes, D., Ho, P. T. P., and Bieging, J. (1982), *Astrophys. J. (Letters)* **259**, L103.

accurate picture of the region where the H_2 density was of the order of 10^5 or 10^6 cm^{-3}. The study of this sort of region clearly requires the observation of many different molecular species. The interesting picture of the Orion infrared source IRc2 which is emerging from these observations indicates that IRc2 is surrounded by a dense disk of gas, with a high-velocity bipolar outflow. The disk is composed of molecules such as SO, HCN, SiO, and NH_3. The NH_3 seems to be central to the clumps or condensations in the disk, the OH masers are scattered around inside the dense gas disk, and the inner edges seem to support the SiO masers, which are within 35 A.U. of the infrared source IRc2. The outflow is traced in HCO^+, and it appears to originate either from the surface of the disk or from the central star itself. The diameter of activity is less than one arcmin and, within this region, IRc2 is believed to drive the flow.

In apparent contrast to the Orion picture, W3 is an example of high velocity flow with no constraining disk[9]; it has HCN emission as well as OH and H_2O masers. In general, OH, H_2O, and CH_3OH maser observations show that active star-forming regions typically contain dense clumps of gas. The clumping of molecular material is another aspect of interstellar chemistry (and structure) that is best studied using aperture synthesis techniques. These clumps of dense material would allow different types of chemistry to occur virtually side by side and would be indicators of structure and activity in interstellar sources. One current example is the discovery of small rotating ammonia clouds.[10] These cloudlets are of a size and mass to be possible sites of future star formation—in effect pre- proto-stellar objects. Another example is the formyl radical, HCO.[11] Recent higher spatial resolution observations of HCO in DR 21 have revealed all four strong hyperfine lines, for the first time in any source. Comparison of line strengths with previous lower spatial resolution observations indicate that HCO may exist in clumps throughout this source, and it serves to highlight the importance of beam size for the detection of such clumps and the molecules specific to them.

2. Cores of cold dark clouds. Relative to the giant molecular clouds, the dark clouds are nearby, less massive, and colder, and they lack formation sites for massive stars. They are excellent laboratories for astrochemistry, since high spatial resolution allows accurate determination of local physical conditions and the absence of high temperature processes leads to a simplification of the chemical models that need be considered. Although there are some basic similarities in the observed abundances in dark clouds with the more quiescent portions of large, warm molecular clouds, there are also fascinating differences, both among clouds and, apparently, within a given cloud.[12] The reasons for

[9]Wright, M. C. H., Dickel, H. R. and Ho, P. T. P. (1984), *Astrophys. J. (Letters)* **281**, L71.
[10]Matsakis, D. N., Palmer, P., and Harris, A. I. (1982), in *Symposium on the Orion Nebula To Honor Henry Draper*, Eds. A. Glassgold, P. Huggins, E. Schucking, *Annals of the New York Academy of Science* **395**, p. 210.
[11]Snyder, L. E., Schenewerk, M. S. and Hollis, J. M. (1985), *Astrophys. J.* **298**, 360.
[12]Irvine, W. M. (1985), in *Astrochemistry*, Eds. M. S. Vardya and S. P. Tarafdar, (Dordrecht: Reidel), p. 369.

such variations are not well understood, but are a subject of active study. Determination of isotope ratios can also provide critical tests of ion–molecule chemistry.[13]

Two well studied examples are TMC-1, in which Schloerb and Snell[14] find condensations ("clumps") with dimensions close to their beam size ($\sim 1'$, corresponding to linear sizes approximately equal to that of the Oort cloud and masses approximately equal to a few solar masses), and L134N, in which maps in species such as $C^{18}O$, SO, $H^{13}CO^+$, and C_3H_2 have quite different appearances[15]. To adequately evaluate chemical models, it is clear that multi-transition, multi-species maps are required in order to compare such physical conditions as kinetic temperature, density, and UV radiation field with the derived abundances.

Since structure is seen in these clouds down to the scale of current single-dish beams, higher angular resolution is clearly desirable. It is known that dark clouds are formation sites for low mass stars; and TMC-1 has been referred to as a "proto-solar nebula." A search for chemical effects in truly solar system-sized nebulae in such regions would be very exciting. At the distances of nearby dark clouds ($\sim$ 150 pc), the radius of Pluto's orbit would intercept an angle of about $1''$, so that study of a flattened solar nebula would require resolutions of $0''.2$ or better.

Dark clouds have been fertile sites for recent searches for new molecules, including both heavy organic species[16,17,18] such as CH_3C_4H and "non-terrestrial" species[19,20] such as C_3H and C_3H_2. Many of these have not been mapped, so their spatial scale is not known. It seems likely, however, from comparisons with better known molecules, that the prime requisite in searches for additional complex species will be sensitivity, rather than angular resolution—the antenna temperatures for the previous detections of C_3O and CH_3C_4H were on the order of only 30 mK. The 30–50 GHz region is crucial to searches for heavier molecules, as discussed below. Also, observed line widths in dark clouds may be as small as 0.2 km/s; high spectral resolution studies will therefore require $\sim$ 20 kHz resolution at 7 mm.

3. Evolved stars. High spatial resolution will provide an essential check on chemical models which predict abundance variation as a function of radius within the circumstellar molecular shells of evolved stars. The model tradi-

[13] *Cf.* Watson, W. D. and Walmsley, C. M. (1982), in *Regions of Recent Star Formation*, Eds. R. S. Roger and P. E. Dewdney, (Dordrecht: Reidel), p. 357.

[14] Schloerb, F. P. and Snell, R. (1985), *Astrophys. J.* **283**, 129.

[15] Swade, D. A., Schloerb, F. P., Irvine, W. M., Snell, R. L. (1987), preprint.

[16] Walmsley, C. M., Jewell, P., Snyder, L. E., and Winnewisser, G. (1984), *Astron. Astrophys. (Letters)* **134**, L11.

[17] Loren, R. B., Wootten, A. and Mundy, L. G. (1984), *Astrophys. J. (Letters)* **286**, L23.

[18] MacLeod, J. M., Avery, L. W., and Broten, N. W. (1984), *Astrophys. J. (Letters)* **282**, L89.

[19] Thaddeus, P., Gottlieb, C. A., Hjalmarson, A., Johansson, L. E. B., Irvine, W. M., Friberg, P., and Linke, R. A. (1985), *Astrophys. J. (Letters)* **294**, L49.

[20] Thaddeus, P., Vrtilek, J. M. and Gottlieb, C. A. (1985), *Astrophys. J. (Letters)* **299**, L63.

tionally used is the "freeze-out" chemical model, in which chemical species are formed under conditions of thermochemical equilibrium in the high temperature, high-density inner shell/photospheric region. These molecular species are then propelled outward by the stellar wind which produces the shell; as they move out in the shell, the density rapidly falls to a value where chemical reaction rates no longer compete with dynamical time scales; and the relative abundances are then "frozen" and become independent of the distance R from the central star.

Much indirect evidence suggests that this model fails to predict the chemistry accurately. Recent detections[2,21] of vibrationally excited HCN, CS, and SiS in the carbon-rich shell IRC10216 show that these species peak sharply in abundance toward the inner regions, and fall off rapidly with increasing R, in contrast to predictions. The failure to detect vibrationally excited CO indicates that CO has a much flatter distribution with R. SiC_2, a three-membered ring, is another species that shows intriguing spatial distributions quite at odds with the freeze-out model. A combination of millimeter-wave[22] and centimeter-wave[23] data gives a highly reliable rotational temperature of 150 K, suggesting that the SiC_2 abundance peaks at a fairly well-defined radius within the envelope, in contrast to the prediction of freeze-out models. The mechanism for formation of SiC_2 must be highly specific.

The angular size of IRC 10216, by far the most-studied evolved shell, is a maximum of 40″ in HCN, 30″ in several other species such as SiC_2, and much smaller in centrally condensed species such as the vibrationally excited ones. All of these species require interferometers for direct study. Further, all other evolved stars are considerably more distant, and thus much smaller in angular extent, than IRC10216. Only the first rudimentary studies of even IRC10216, at 10″ resolution by the Hat Creek interferometer, have nevertheless given important initial results, although only in the optically saturated lines of species such as HCN. To probe less abundant, optically thin species, which may be more centrally condensed, will require much greater angular resolution and much greater sensitivity. Such measurements, in many species and modes of excitation, will be needed to elucidate the many physical and chemical processes which appear actually to occur throughout the envelope, and to invalidate the simple freeze-out model. Among these processes are catalytic formation on grain surfaces, adsorption onto grains (particularly in the cooler, outer envelope), shock chemistry, and photo-dissociation in the outer envelope. A graphic example of the importance of the latter is given in the cover illustration [originally intended — Eds.] for these proceedings.

Much of the discussion so far has focused on carbon-rich stars, because the single well studied example, IRC10216, is such a star. Oxygen-rich stars also have circumstellar shells and their own unique chemistry, which besides CO,

[21]Turner, B. E. (1987), *Astron. Astrophys. (Letters)*, **182** L15; *ibid.*, **183** L23.
[22]Thaddeus, P., Cummins, S. E. and Linke, R. A. (1984), *Astrophys. J. (Letters)* **283**, L45.
[23]Snyder, L. E., Henkel, C., Hollis, J. M. and Lovas, F. J. (1985), *Astrophys. J. (Letters)* **290**, L29.

stresses H_2O, OH, and SiO among species accessible to radio observations. These species all exhibit powerful maser activity, and VLBI studies have already revealed important information, such as the fact that the OH masers lie outside the H_2O masers, and the SiO masers inside the H_2O masers. Such studies, while highly suggestive, are subject to interpretive uncertainties concerning the excitation of the masers. Studies of other molecules will add much complementary information; but as their signals will be much weaker, a large and sensitive interferometer will be required. Highly refractory, and hitherto undetected species such as metal oxides and hydroxides (MgO, MgOH, CaOH) may be detectable, according to predictions of thermochemical equilibrium. Intriguing details about the changing relative distributions of the masering OH, H_2O, and SiO species as functions of IR light cycle phase will also be possible, and will shed light on the pumping mechanisms.

The chemistry of evolved stars is singularly important, as these objects undergo copious mass loss to the interstellar medium, thus enriching the gas which is to form subsequent generations of stars. The entire nucleosynthetic history of our own and other galaxies depends on an accurate assessment of the composition of the molecular circumstellar gas. By their very nature, such shells are amenable to direct study only through use of large and sensitive interferometers.

4. The Sun. Spatial resolution of 8″ should allow confirmation of the refractory species claimed to exist in sunspots (e.g., SiO) and permit examination of their spatial distributions within the spots.

5. Extragalactic. Only a few simple molecules have so far been detected in other galaxies, but they provide essential tools for determining whether, and perhaps why, the chemistry in other galaxies differs from that of the Milky Way. Even so fundamental a species as CO is already known to be relatively lacking in several nearby and well known galaxies such as M31. It is not known whether molecular chemistry, as exemplified by CO, always is enhanced in spiral arms within a galaxy; the study of such arms in even the oldest galaxies requires spatial resolutions beyond those available with single-dishes.

HCO^+ is a tracer of cosmic rays, and gradients in HCO^+ abundance with galactocentric radius in other galaxies will answer such questions as whether cosmic ray densities correlate with the presence of supernova X-ray sources.

Isotope ratios are fundamental to nuclear processing in stars, in that they depend on the stellar mass distribution, the rate of star formation, and the rate of return of stellar material to the ISM. Models of the Milky Way predict gradients in certain key isotope ratios ($^{12}C/^{13}C$, $^{14}N/^{15}N$, $^{16}O/^{18}O$) with galactocentric radius, and it is difficult because of distance ambiguities to establish whether such gradients exist in our galaxy. Observations of other galaxies will provide this information more easily, and also they will indicate what differences there are between galaxies. Such differences in turn may reveal fundamental differences in the nature of star formation in galaxies. The high spatial resolution of an array is needed to obtain the necessary observational

information. Optical studies do not provide such information, because the isotopic lines are severely blended.

6. The solar system. The chemical composition of planetary and satellite atmospheres provides fundamental data for planetary science. The atmospheric composition is dependent (among other factors) on the overall composition of such a body, and so it reflects basic cosmogonical conditions. Moreover, the abundances of trace constituents probe both evolutionary history and important on-going physical and chemical processes. For example, day–night gradients in the abundance of CO in the Venus stratosphere provide information on both photochemistry and atmospheric circulation; and the $^{12}CO/^{13}CO$ ratio there may be different from the terrestrial value—this apparently reflects poorly understood fractionation processes during the lifetime of the planet, or conceivably in the solar nebula.[24,25] Likewise, the apparent detections (interferometrically) of CO on Titan and of the anomalous abundance of H_2O on Jupiter are examples of non-equilibrium abundances that must relate to important atmospheric processes such as deep circulation patterns of possible infall of material. Gradients across a planetary disk (e.g., the Jovian Great Red Spot) may be reflected in chemical anomalies of species such as phosphine (PH_3, detected in the millimeter transition on Jupiter[26], and in the infrared on Saturn[27]) or, in the case of Venus, of sulfur compounds producing the ultraviolet markings. Abundance measurements in these cases could test models of atmospheric/aerosol chemistry. Molecular lines should be observable in the atmospheres of both Io and Titan. Inversion of line profiles in all these cases provides the mixing ratio vs. altitude relations, which cannot be obtained from infrared spectroscopy.

To determine the requisite instrumental parameters, we note that the angular diameter of Titan is $\sim 1''$, while features such as the Great Red Spot are a few arcseconds across. Mapping of Venus (e.g., in CO) requires resolutions of approximately a few arcseconds. Planetary lines also impose stringent requirements on spectrometers. Pressure broadening is typically $\sim$ 2–3 GHz/bar, so bandwidths of this magnitude are extremely desirable.

There is suggestive evidence for the survival of interstellar molecular material in primitive solar system objects. The large values of the D/H ratio found in certain fractions of carbonaceous chondrites are particularly interesting, but models of cometary coma chemistry also point in this direction.[28] The most pristine material surviving today from the original solar nebula is believed to be in comets, so determining cometary chemical compositions is a critical problem. Not only may this provide boundary conditions on the solar

[24]Schloerb, F. P. (1985), in preparation.
[25]Clancy, R. T. and Muhleman, D. O. (1985), *Astrophys. J.* **273**, 829.
[26]Lellouch, E., Combes, F. and Encrenaz, T. (1984), *Astron. Astrophys.* **140**, 216.
[27]Haas, M. R. *et al.* (1984), in NASA Conference Publication CP-2353, *Airborne Astronomy Symposium*, Eds. H. A. Thronson and E. F. Erickson.
[28]Kerridge, J. F. and Chang, S. (1985), in *Protostars and Planets II*, Eds. D. Black and M. Matthews (Tucson: University of Arizona Press), p. 738.

nebula, but also it may conceivably lead to a means for relating the chemistry of comets to the chemistry of molecular clouds, hence allowing a determination of the type of cloud in which the solar system formed. Rotational transitions appear to hold the best promise for providing this type of information.[29] Because different molecules have different lifetimes in the solar radiation field, and because chemical reactions are expected in the inner coma, gradients in the chemical composition and excitation will provide important information on physical conditions and processes. For a moderately bright comet at a distance of 1 A.U., the molecular coma may vary in size from $\sim$ 1000 km (for species such as S_2 and NH_3) to $\sim$ 10,000 km (for HCN), corresponding to angular scales of $\sim 0\farcs1$ to $\sim 100''$.

2. Frequency Coverage

Unlike most other scientific areas which utilize well-chosen but specific molecular lines as probes of the physical conditions in dense clouds, the study of chemistry requires maximum frequency coverage. This is because the most important transitions of different types of molecules, under differing physical conditions, occur at wavelengths ranging from the centimeter to the submillimeter. This dependence of spectral features on molecular structure and physical conditions is most easily illustrated for linear molecules, and we choose these species for the following discussion. Non-linear molecules do not behave very differently, but they are more difficult to treat.

The integrated brightness temperature for a given molecular line is proportional to the square of the frequency of the line, multiplied by the population of the initial energy level involved in the transition. For a linear molecule in thermal equilibrium among its rotational energy levels, these two factors result in a transition frequency $\nu_{\max}$ of maximum intensity, where

$$\nu_{\max} \propto \sqrt{BT}\,. \tag{1}$$

In Expression 1, B, the rotation constant, is roughly proportional to the inverse cube of the number of heavy (non-hydrogen) atoms in the linear molecule. The frequency of the most intense spectral feature of a linear molecule is proportional to $\sqrt{B}$, or to $1/\sqrt{\mathcal{N}^3}$ where $\mathcal{N}$ is the number of heavy atoms. Larger molecules will have their strong spectral features at lower frequencies, *viz.*, toward the centimeter range, whereas smaller molecules will have their stronger features toward the millimeter and even the submillimeter range. Light hydrides such as NaH and MgH will have their lowest frequency (fundamental) transitions in the submillimeter region; observation of these particular species would be of extreme importance in determining metallic abundances in dense interstellar and circumstellar clouds.

A glance at Equation 1 reveals that, as temperature increases, so does $\nu_{\max}$. The result is that the study of the emission of a given molecule at higher temperatures is a means of specifically probing regions of higher temperature. In

[29]Snyder, L. E. (1982), *Icarus* **52**, 1.

particular, a change in temperature from say 10 K, which pertains throughout a typical cold interstellar cloud, to 300 K will result in an increase of ν_{max} by a factor of $\sqrt{30}$. Thus, the study of a single molecule in a heterogeneous source requires significant "frequency agility."

Perhaps more striking is the tremendous increase in sensitivity which these varied factors indicate for those particular species which may only form in small, high-temperature regions such as are produced by shocks, or that occur in the immediate vicinity of massive protostars. Highly refractory species such as metal compounds (MgO, CaO, FeO, PO, PN, NaO, NaOH), containing elements not yet detectable in dense clouds, may be examples of such species. If the highly excited regions are not larger in angular extent than the synthesized interferometer beam (as is expected), then the signal strength is dependent on the ratio of source solid angle to beam solid angle and thus varies as ν^2, where ν is the frequency. Further, the intrinsic brightness temperature of a transition of a linear molecule varies as ν or ν^2 as one goes up the rotational ladder, depending on whether the transition is optically thick or thin. At the high temperatures involved in these cases we can observe transitions that are much more highly excited than would be the case if the species occurred in low temperature regions. Thus the sensitivity for detection and study of refractory compounds which may occur only in small, highly excited regions will vary as ν^3 or ν^4 when studied with an interferometer at high frequencies—yielding many detections which otherwise would be impossible.

The above discussion has focused on why different frequency ranges are necessary for studying different molecules and/or different physical conditions. Frequency agility is also needed for individual molecules for the purpose of identification. It is difficult to establish the presence of a new interstellar molecule based on a one-line identification. Consider the ion HOC^+, which has been tentatively identified in Sgr B2 via a transition at 90 GHz. Confirmation will require observations of another transition at 270 GHz. In addition to the desirability of frequency agility for the purpose of identification, such a capability would be most useful for simultaneous mapping of two or more transition frequencies of a particular molecule in order to determine excitation conditions, and hence abundances.

Based on the above needs, the following general requirements are suggested:

(1) The basic IF passband preceding the correlator should be as wide as practical (1–2 GHz or more).
(2) Both sidebands of the first local oscillator should be observed, and they may be separated by oscillator phase switching.
(3) It should be possible to divide the correlator into a large number of separate bands (10–20), each of which can be tuned to a separate line.
(4) It should be possible to observe with more than one resolution in these different bands at the same time.
(5) Each band should have up to 64 channels.
(6) A bandwidth of 20–40 MHz for each band is desirable for velocity

coverage.

(7) The resolution in each band should be variable over half-a-dozen steps of a factor of two, so that very high velocity resolution may be obtained.

(8) Special attention must be given to spectral passband calibration.

3. Chemistry Summary

The following table summarizes those aspects of the MMA design which this Working Group deems essential to astrochemical studies:

1. Frequency Range:	33 GHz to 345 GHz: 33 GHz for the study of compact, heavy molecules; 345 GHz for study of small, tightly bound refractory molecules.
2. Frequency Agility:	E.g., both the upper and lower sidebands.
3. Bandwidth Flexibility:	Highest frequency resolution: 10 kHz. Greatest bandwidth $\approx$ 3 GHz (for the study of planetary atmospheres).
4. Angular Resolution:	One arcsecond for the projects discussed.
5. Collecting Area:	We can tolerate a minimum collecting area equivalent to that of a 46 meter dish, but we would prefer more. We need the best receivers available.
6. Site:	The 345 GHz boundary in Item 1 dictates a high, dry site.

VII. Nearer Extragalactic Objects

Report of the Working Group on Low Redshift Extragalactic Astronomy[†]

The millimeter array, as described in Chapter I, will acquire fundamentally new data on the structure and evolution of galaxies out to distances $z \approx 1$. It will become possible to obtain useful images of the molecular content of galaxies at a resolution of $0\farcs1$, a resolution attainable for imaging the extended structures of galaxies with one other instrument, the Space Telescope—and by no other instrument working at wavelengths outside the radio region. It will be possible to study the molecular star-forming material in the entire Shapley–Ames catalogue with resolution comparable to that of the best optical images, and with sensitivity sufficient to detect most giant molecular clouds in galaxies at distances less than 40 Mpc (considerably farther than the Virgo cluster). This instrument will lead to new understanding of evolutionary processes in galaxies, by allowing us to follow in detail the flow of interstellar matter through molecules into stars for a variety of galaxy types, in a wide range of galaxian environments.

1. General Considerations

The MMA will be able to collect useful data from galaxies, in both its continuum and line modes of operation. We therefore consider separately the science that can be addressed by operating in each mode. In the continuum, we recommend that the instrument be capable of observing to frequencies as high as possible, preferably to 350 GHz. Continuum observations would primarily be used for investigations of dust, compact non-thermal continuum sources, very young supernovae, and HII regions.

Line observations are likely to occur most frequently at CO transitions, and a capability of observing to 345 GHz ($J = 3$–2) is highly desirable, assuming that the instrument is situated at a sufficiently high site ($h \gtrsim 3{,}000$ m). The consensus of this Working Group is that the highest possible site is desirable, especially since little effective line work can be done at baselines $\gtrsim 3$ km (see below). We have considered the following classes of research which would be possible with the MMA:

(1) investigation of the global properties of disk galaxies;

[†]Contributors: T. Bania, Boston University; L. Blitz (Chairman), University of Maryland; P. Crane, NRAO; J. Gallagher, National Optical Astronomy Observatories; J. van Gorkom, NRAO; S. Gottesman, University of Florida; P. Ho, Harvard University; K. Y. Lo, California Institute of Technology; L. Rickard, Howard University; N. Scoville, California Institute of Technology; P. Solomon, State University of New York at Stony Brook; A. Stark, AT&T Bell Laboratories; R. Wilson, AT&T Bell Laboratories; and M. Wright, University of California at Berkeley.

(2) study of galactic centers, including active nuclei;
(3) study of galactic disks, including spiral structure; and
(4) study of molecular clouds and the interstellar medium.

We adopt the following parameters describing the $J = 1$–0 CO emission from particular classes of objects:

Table 1. $J = 1$–0 CO Parameters.

Type	Peak $\langle T \rangle$ (K)	ΔV (km sec^{-1})	Scale Size
Orion Core	100	10	0.5 pc
GMC (local)	2.5	5	50 pc
GMC (inner galaxy)	5	10	50 pc
Galactic Center (Milky Way)	5	250	150 pc
Central Molecular Annuli (e.g., N1068)	0.5	50	1 kpc
Global Integrated (Milky Way)	0.5	50	20 kpc
Global Integrated (Virgo Cluster)	0.2	250	5 kpc

From the Hjellming report (Chapter I of this volume), an eight-hour observation in a 300 m diameter, VLA-like Y configuration, together with natural weighting, provides $\Delta T_b = 0.64$ mK at 1 GHz frequency resolution and a spatial resolution of $1\farcs30$ for $T_{\rm rcvr} = 100$ K. ^{12}CO observations in good weather at this $T_{\rm rcvr}$ generally provide $T_{\rm tot} = 400$ K, although this might be better at a high site. Most extragalactic CO observations could combine orthogonal polarizations from dual channel receivers; the $\Delta T_{\rm rms}$ is lowered by $\sqrt{2}$. Therefore, since we require 3σ per pixel, the limiting sensitivity we consider is 1.5 mK per GHz of bandwidth at $1\farcs30$ resolution. This is equivalent to

$$\Delta T_{\rm rms}(3\sigma) = 5\sqrt{\frac{260}{V}}\ {\rm mK}\,,$$

on a 300 m baseline, where V is the velocity resolution of a particular observation or

$$\Delta T_{\rm rms}(3\sigma) = 5\sqrt{\frac{260}{V}}\ {\rm K}\,,$$

on a 3 km baseline, giving a resolution of $0\farcs13$. Of the sources listed in Table 1, the brightest sources are galactic centers; the extended emission at the center of the Milky Way is marginally detected in several pixels at a distance of 100 Mpc. Few sources are likely to be as much as ten times brighter (requiring an average $\langle T \rangle$ of 50 K over 150 pc), thus we expect little use of the MMA at baselines much larger than 3 km for extragalactic CO observations.

For nearly all problems we considered, we expect the best imaging results using the CO $J = 2$–1 line. We therefore recommend that the instrument be sited such that it is useful at 230 GHz for as large a fraction of the year as possible. Furthermore, because most galaxies are extended relative to the primary beam out to large redshifts, the mosaicing capability of the MMA will be essential for the overwhelming majority of extragalactic observations.

2. Line Observations

We list below the distances to which four classes of objects could be detected in CO with the MMA, as presently conceived:

Table 2. Maximum Practicable Distances of Observation in CO.

Object	Maximum Distance (Mpc)	Comment
Orion Core	3	(Local Group; 0.″1 resolution)
GMC	50	(includes Virgo Cluster; 1″ resolution)
Galactic Centers	300	(at 0.″1 resolution)
Integrated Galaxies	3000	(at 1″ resolution)

Since the parameters in our previous Table 1 do not correspond to the largest or brightest objects in each class, extreme examples could be detected at even larger distances. In each case above, the objects would subtend only one pixel at the limiting distance and could be resolved at smaller distances (except for GMCs which are resolved only at distances < 10 Mpc), assuming they are like their Milky Way counterparts. These distances assume observations made in the $J = 1$–0 line of CO. For observations in the $J = 2$–1 line, assuming equal signal strength and comparable system temperature, one would obtain four times the sensitivity for an object at the same distance—or, at the same sensitivity, one could observe objects twice as far as is shown in Table 2.

In the Milky Way a large fraction of the high surface-brightness CO is from GMCs. By extension, the MMA will be able to map most of the molecular emission from each of the galaxies in the Shapley–Ames catalogue. It will be possible to determine in detail the relationship molecular clouds have to spiral structure, how molecular gas is distributed in detail, and what relationship the molecular gas has to star formation and the general interstellar medium in galaxies of all morphological types in a large variety of environments. Because the integrated emission from galaxies can be detected to such large distances, it will be possible to investigate how the molecular content affects the evolution of galaxies. The integrated CO emission from an entire rich cluster of galaxies could be observed, for example, with a single eight hour integration if the MMA has a bandwidth of 5000 km s^{-1} and has 200 km s^{-1} filter widths. Furthermore, within individual galaxies, the global gas kinematics will be observable with unprecedented resolution. The determination of H_0, using tidally limited GMC diameters as objects of known physical size, may be possible with the MMA.

The structure of individual molecular clouds will be observable to a size scale of 2 pc for local group galaxies, and the counterparts of the galactic high latitude molecular clouds should also be detectable. Thus the structure of individual molecular clouds can be probed in many different galactic environments. Furthermore, with a broad bandwidth continuum channel it will be possible to map GMCs and the bright HII regions associated with them in a single observing period, to get a detailed look at the star formation process in a variety of environments. (Protostellar molecular disks, and bipolar outflows similar to those observed in the Milky Way would be marginally detectable,

but unrecognizable even in M31 and M33. Similarly, SiO masers from late type stars would be undetectable with the MMA even in M31 and M33.)

The MMA will be able to detect HCO^+ to a level $\sim 2\%$ of the CO brightness out to a distance of 10 Mpc, enabling the cosmic ray ionization rate and its variation in galactic disks to be determined. Also, it will be possible to observe and map the HCN and CS in galaxies within 10 Mpc if extrapolations based on current observational data are correct. Useful information on the ^{13}CO isotope will be obtainable for many galaxies, as with $C^{18}O$ in galactic centers. DCN emission should be detectable within the dense GMC cores of nearby galaxies.

When combined with HI, Hα, and radio continuum data, it will be possible to obtain a fairly complete picture of global properties of the interstellar medium, and the effects of spiral structure, HII regions, and supernovae in a large number of galaxies. The kinematic information obtained from the MMA will be superior to all of the other dense ISM tracers, however. For example, Hα is subject to severe extinction effects, and the spatial resolution at CO will be more than an order of magnitude greater than what is possible in HI at the VLA. The high spatial resolution is of critical importance in at least two areas: determining the variation of gas scale-height with radius in edge-on spirals, and the mapping of central bars. The former is an important datum in determining the structure of possible non-luminous halos, the latter in testing models of barred galaxies. High resolution studies of non-spiral systems will allow a detailed comparison to be made of properties as functions of morphological type.

Galactic centers are a main line of research for which the MMA will be uniquely suited, on scales from 5 pc at the Virgo cluster, to 100 pc at a distance of 200 Mpc. Studies of the centrally concentrated molecular gas of nuclear regions will show features at $0''.1$ resolution, a resolution complementary to the best currently planned optical facilities. These highly obscured regions are likely to be inaccessible at optical wavelengths. It may be possible to do absorption experiments toward galactic nuclei to determine whether circumnuclear gas is falling in or flowing out. Because of the brightness of the nuclear molecular gas, it will be possible to observe nuclear regions out to 300 Mpc. This volume contains a large number of galaxies with Seyfert and starburst nuclei. The MMA will doubtless yield new insight into these unusual phenomena.

3. Continuum Observations

Although we expect that the MMA will be used as a line instrument most of the time, the science it will do as a continuum instrument is also exciting. The MMA will, for example, be uniquely capable of arcsecond resolution imaging at $\lambda = 1$ mm of the dust emission in large GMCs and the nuclei of galaxies. Since the dust radiation is optically thin and relatively insensitive to temperature at these wavelengths, the data collected will be a reliable probe of the dust masses. Because dust emission decreases as λ^{-4}, the 1 mm capability of the full array is essential for these studies. GMC regions like W51, W59, and

Orion A, which contain $10^4 M_\odot$ of dust, could be detected to distances of $\sim$ 5 Mpc, encompassing M33 and IC342. Furthermore, the MMA will provide the opportunity to observe dust complexes in galactic nuclei out to cosmologically interesting distances ($\sim$ 200 Mpc!). Imaging of such regions at a resolution of 100 pc will be possible at the distance of the Virgo cluster.

The MMA will also be an important source of data for compact continuum sources in the centers of galaxies. In particular, elliptical galaxies sometimes contain compact nuclear radio sources with flat non-thermal spectra (e.g., Virgo A, Centaurus A, and Perseus A). The resolution provided by the high frequency of operation of the MMA, as well as the data gathered on polarization and high frequency variability, will increase the understanding of these phenomena.

Very compact HII regions will also be detectable in local group galaxies, and probably beyond. The compact stage of supergiant HII regions such as NGC 604 and 30 Doradus have never been observed. These are much more luminous than the most luminous galactic HII region. Since the most luminous of the galactic compact HII regions are near the detection limit of the MMA at the distance of M33, the precursors of NGC 604 type objects should be easily detectable.

Lastly, the MMA provides an important opportunity to observe the very early stages of radio supernovae, because millimeter wave observations make it possible to see through the circumstellar material at very early times. For example, the archetypical Type I radio supernova SN 1983n would have been transparent at 100 GHz within a few hours after the explosion, long before optical maximum. The millimeter observations may allow us to observe the initial acceleration of relativistic particles and give a new view of the properties of the expanding envelope of the star. Also, the early radio light curve will be determined by the mass-loss rate over the few years just preceding the explosion, yielding unique data on the final few moments of stellar evolution.

VIII. Distant Extragalactic Objects

Report of the Working Group on
High Redshift Extragalactic Astronomy[†]

1. Introduction

Our group considered and discussed which major scientific opportunities exist for the Millimeter Array in the wide redshift range $z > \sim 0.1$. We were assisted in our work by several members of other working groups, whose contributions were particularly important to Section 2 (Part 4) and Section 3, below.

We identified three general areas in which the MMA could make major scientific contributions:

(1) cosmology,
(2) the origin of structure in the Universe, and
(3) the nature of the "central engines" of QSOs, radio jets, and variable radio sources.

With one exception, noted below, the scientific goals we have in mind could be met entirely by continuum observations. Many of the projects that we have contemplated would, however, be at the limit of the sensitivity of the array. They likewise would require wide frequency coverage, but (again with one exception) no particular frequency, so that we would be free to observe at frequencies where the contributions due to foreground sources of emission, such as the atmosphere, are at a minimum. In addition, high redshift objects are uniformly distributed, so the latitude of the site that is chosen for the MMA is not of concern to us.

2. Cosmology

We shall begin by discussing scientific goals at the upper end of the redshift range we considered, particularly observations of the cosmic background radiation. To first order this relic of the hot Big Bang is completely isotropic, although large scale anisotropy introduced by the velocity of the solar system has been detected. Our interest is, instead, in anisotropies of small angular scale. We consider two possible sources of small scale anisotropy: intrinsic fluctuations in the intensity or temperature of the radiation introduced when it last interacted with matter (probably at a redshift $z \approx 1000$), and small "cool spots" in the radiation introduced by the subsequent inverse Compton scattering of the radiation by hot plasma, especially in clusters of galaxies (the *Sunyaev–Zel'dovich effect*).

[†]Contributors: J. Condon, NRAO; W. Cotton, NRAO; H. Martin, NRAO; C. Masson, California Institute of Technology; F. Owen, NRAO; B. Partridge (Chairman), Haverford College; and R. Sramek, NRAO.

1. Intrinsic fluctuations. If the matter content of the Universe, or more specifically the baryon content, was inhomogeneously distributed at the time that the cosmic background radiation last interacted with it, then fluctuations in the temperature of the background ought to have resulted. Since the Universe is manifestly inhomogeneous now, we expect it was also to some degree inhomogeneous earlier. To produce the presently observed large-scale structure, such as galaxies and clusters of galaxies, we expect the fractional density inhomogeneity $\Delta\rho/\rho$ at $z < 1000$ to be roughly 10^{-3}. The corresponding temperature fluctuations $\Delta T/T$ would be smaller: predicted values range from 3×10^{-4} to a few times 10^{-6}, depending on the cosmological model and other astrophysical variables. Whatever their amplitude, detection of intrinsic fluctuations is a vital step in understanding how and when large-scale systems in the Universe formed. Such observations provide the only direct handle on the early history of astronomical systems, permitting us to study them by redshifts several hundred times greater than the redshifts of most distant observed discrete objects. In addition, study of the amplitude and spectrum of such fluctuations may help elucidate some fundamental questions in particle physics, since (1) the relationship between $\Delta\rho$ and ΔT depends in part on the presence of a cosmologically important density of massive neutrinos, axions, or other fundamental particles, and (2) the nature of the mass spectrum $\Delta\rho(M)$, and hence that of the spectrum of fluctuations, may be determined very early on in the history of the Universe, when particle physics was dominant.

Because of their importance, intrinsic fluctuations have been searched for actively. The lowest limit on $\Delta T/T$ is now at just about 10^{-5} on scales of 1!5–4!5 (see Figure 1 for comparison with some recent theoretical models). This filled-aperture measurement was made at a wavelength $\lambda = 1.5$ cm, and is close to the state-of-the-art sensitivity for such measurements. Measurements at longer wavelengths, where receiver noise and atmospheric emission present fewer problems, are already running into the problem of confusion due to faint radio sources. We note that estimates of the radio source confusion suggest that, at wavelengths shorter than ~ 1 cm, confusion will present no problem for observations at a sensitivity $\sim 10^{-6}$ in $\Delta T/T$. For this reason and others, we believe that the MMA will be a powerful tool in the search for intrinsic fluctuations.

2. The Sunyaev–Zel'dovich effect. When cosmic background photons encounter hot plasma, for instance the intergalactic plasma in clusters of galaxies, they undergo inverse Compton scattering caused by the electrons of the plasma. This process increases the energy of the photons but conserves photon number. The effect is to shift an initially blackbody spectrum to higher frequencies, resulting, as shown in Figure 2, in a small temperature decrement, or cool spot in the radiation, if it is observed in the Rayleigh–Jeans regime through a cluster. (For all $\lambda \gtrsim 1$ mm, the Sunyaev–Zel'dovich effect produces a temperature decrement.) The magnitude of the effect is directly proportional to the integral of the pressure through the intergalactic plasma, and thus it provides a useful diagnostic tool for probing the plasma properties. Of more general

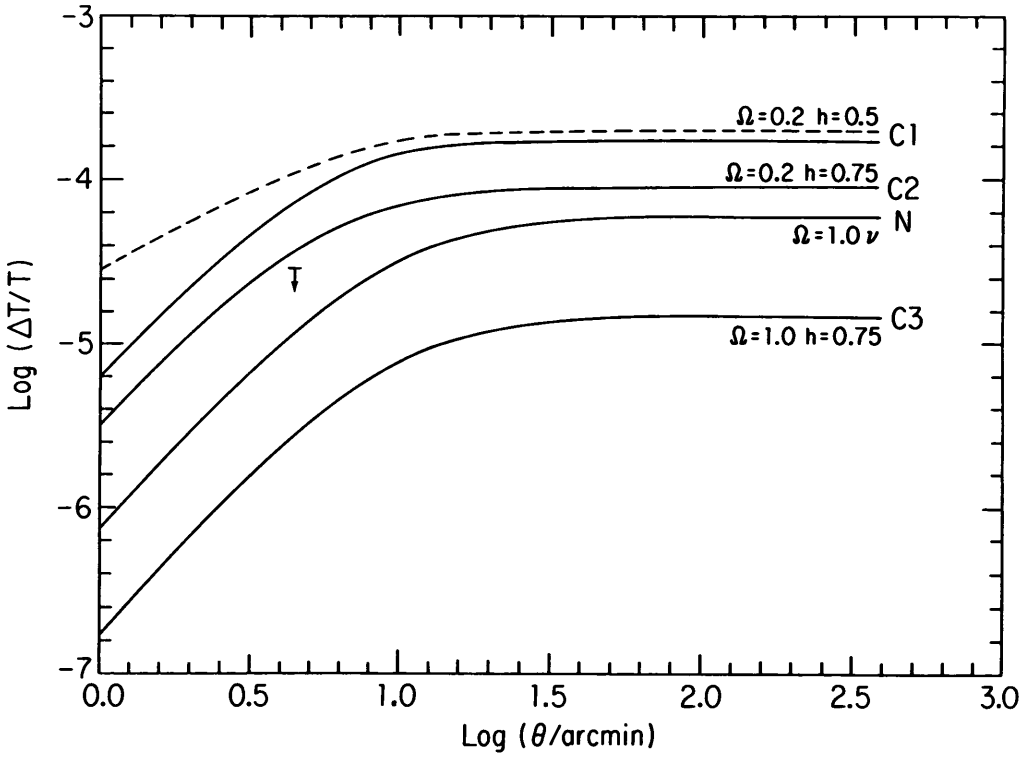

Figure 1. An array of models for intrinsic $\Delta T/T$ fluctuations in the cosmic background radiation, showing the increase in $\Delta T/T$ as Θ approaches 10′. The single observational limit is by Uson and Wilkinson (*Astrophys. J.*, **283** (1984) 471). Figure adapted from Bond and Efstathiou (*Astrophys. J. (Letters)*, **285** (1984) L45).

interest is the fact that observations of the Sunyaev–Zel'dovich effect provide a means to measure distances to clusters—distances which are independent of any of the intermediate rungs on the cosmic distance ladder. This possibility arises because the amplitude of the Sunyaev–Zel'dovich effect depends on the parameters of the plasma, but is independent of the distance. On the other hand, the measured X-ray flux from the hot intergalactic plasma does depend on the distance. Observations to date are not sufficiently sensitive to give us good distance estimates even to nearby clusters, and therefore the power of this method in determining the basic cosmological parameter H_0 has not yet been utilized. The X-ray measurements necessary to refine our values of H_0 should be available within the next decade, thanks to planned space missions. What about the microwave observations? Two problems face us: the contribution from radio sources within the cluster and from background sources, and the need to map the cluster so as to obtain information about the distribution of the cluster plasma. The latter requirement is important because the X-ray flux and the Sunyaev–Zel'dovich signal depend on different powers of the plasma density, so that the distribution of hot plasma in the clusters must either be mapped or modeled. The high frequency at which the MMA will be able to

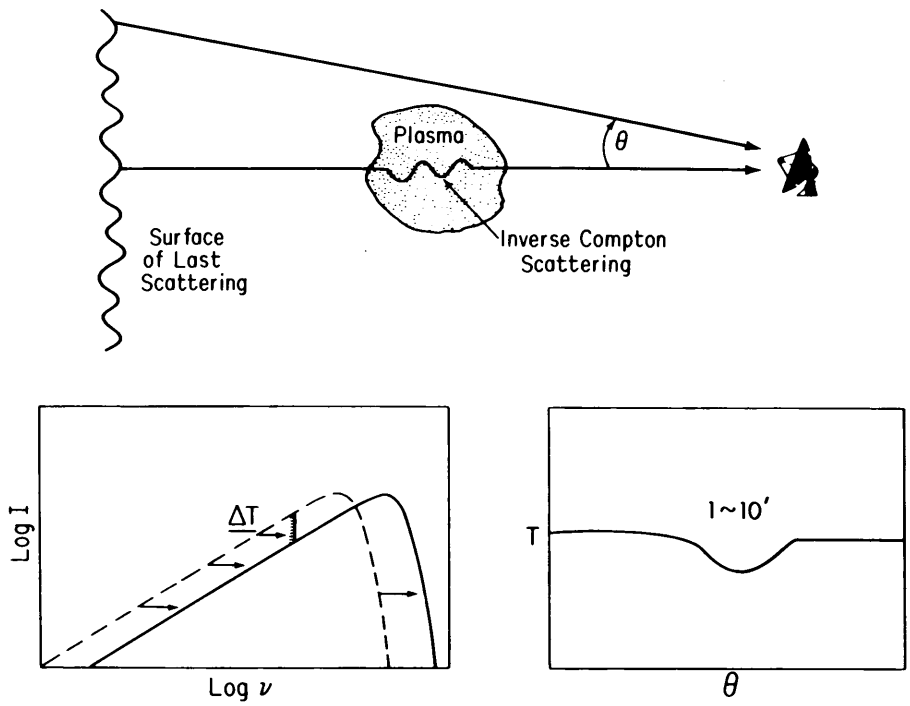

Figure 2. The Sunyaev–Zel'dovich effect, produced by the inverse Compton scattering of cosmic background photons by electrons within the hot intergalactic plasma in clusters of galaxies.

operate will help substantially with the first of these two problems. Even in the 30–50 GHz window, we expect to find few sources brighter than 1 mJy. The ability of the MMA to make accurate maps will also help with both problems mentioned above. Sources can be located and excised from the data, and then it will be possible to map the amplitude of the temperature decrement with adequate accuracy. Since the amplitude of the Sunyaev–Zel'dovich effect falls off slowly with distance from the cluster center, the area to be mapped is several times the cluster core radius R_c. R_c is typically > 1 arcmin, so regions of $\gtrsim 10'$ extent will need to be mapped at a few arcsecond resolution.

Although the amplitude of the signals expected from typical clusters of galaxies is somewhat higher than the amplitude of intrinsic fluctuations, say, $\Delta T/T \approx 1\text{–}3 \times 10^{-4}$, the effect is still not an easy one to observe, as experience with both filled aperture and interferometric observations has shown. We believe the planned capabilities of the MMA make it a uniquely powerful instrument to detect and map the Sunyaev–Zel'dovich effect, and thus to provide an independent measurement of H_0.

In addition, since the Sunyaev–Zel'dovich effect is independent of distance, we should be able to measure the effect in both nearby and cosmologically distant ($z \approx 1$) clusters. If the corresponding X-ray measurements can be made, we may then be able to determine H_0 at different redshifts, and from

these values deduce limits on a second important cosmological quantity, the deceleration parameter q_0.

We should also note here that the Sunyaev–Zel'dovich effect may arise in other contexts, such as elliptical galaxies that are X-ray sources, and possibly in larger scale structures like superclusters.

3. Requirements for the MMA. Both of these experiments will require the highest possible continuum sensitivity. A system temperature of order 50 K and a bandwidth of 1 GHz should be adequate. Because of confusion, wavelengths below 1 cm are favored. Finally, as noted above and as illustrated in Figure 1, the angular scales at which these effects appear are up to 10′–30′. All of these considerations point in the direction of working at 9 mm as a reasonable compromise. We shall adopt that assumption as a basis for the following remarks.

In the search for intrinsic fluctuations on angular scales of $\sim 5'$ or less, the MMA must provide sensitivity to extended sources. Using the instrument as an interferometer will help avoid some of the systematic error encountered in single-dish observations (see below). Nevertheless, a search for fluctuations at the level of a few times 10^{-6} in $\Delta T/T$ will require not only high sensitivity, but also very careful control of systematic errors. Here we have particularly in mind the problem of antenna or correlator cross-talk. In order to make useful observations, these systematic effects will need to be held to a level of at most a few one-hundredths of a milli-Kelvin.

As noted above, the most promising angular scale on which to search for intrinsic fluctuations is 10′–30′. This scale is larger than any that is currently anticipated for the MMA. Our Working Group considered this problem at some length and discussed a variety of means of increasing the angular scale capability of the MMA. The most straightforward approach would be to use 10 meter antennas (or possibly smaller antennas in a central subarray) to make independent measurements of the background temperature of the sky at an array of points spaced by 10′–30′ apart. To control atmospheric emission, beam switching would be necessary. If this technique is to be applied, it sets constraints on permissible residual errors in systematic offsets in beam switched operation. Such measurements would not be possible unless the offsets were limited to $\lesssim 0.1$ mK, and $\lesssim 0.03$ mK would be desirable. Such an instrument could then reach the desired sensitivity level of $\Delta T/T \approx 3 \times 10^{-6}$. To control systematics such as back- and side-lobe pickup, the back-lobe region of the telescopes should be kept clean. In addition, we believe that observations requiring such high sensitivity as this would be precluded if radomes are used to house the antennas.

Another alternative allowing larger angular scales would be to add to the MMA a tertiary array consisting of yet smaller elements—elements small enough that their primary beams at $\lambda = 9$ mm would be $\sim 30'$. A set of small antennas with diameters less than a meter, or a set of conical horns, are two possibilities. We recommend further study of this alternative. Another possibility would be to adapt the feed elements of the central element so that

they could view the sky directly. Note that measurements on short baselines, as well as a larger beam, are desirable. We believe these questions are thus left to a future engineering study, but we do wish to emphasize that useful observations of intrinsic fluctuations in the cosmic background, and observations of the Sunyaev–Zel'dovich effect in nearby clusters, can be made only if the angular scales to which the instrument is sensitive can be increased by factors of 3–5.

4. Redshifted molecular lines. Another cosmological experiment made possible by the sensitivity of the MMA is a search for molecular lines, in absorption, at large redshifts. As one instance, note that the 2.6 mm CO line is shifted into the 30–50 GHz band at redshifts of order $z = 2$. Absorption-line systems at approximately this redshift have been detected in the optical in some background QSOs, and in some cases they suggest hydrogen column densities as high as 10^{22} cm^{-2}. Such a high column density suggests that the absorber must be a galaxy (or a galaxy halo). It is interesting to inquire whether galaxies at such large redshifts contain CO and other molecular species.

We note also that some lines currently inaccessible because of their high frequency, such as the carbon line at 492 GHz, or because of atmospheric blockage, such as the O_2 or H_2O lines, may be redshifted into an accessible millimeter band and hence be available for investigation.

3. Primeval Galaxies

A fundamental problem in astronomy concerns the origin of galaxies. We have available a range of models explaining the formation of galaxies, but, unlike the situation with respect to stars, we have no direct observations of this process. This is because galaxy formation occurred long in the past. A variety of arguments suggest that most galaxies form their first generation of stars at an epoch corresponding to redshifts $3 \lesssim z \lesssim 30$. The presently available upper limits on fluctuations in the cosmic background make the interval $3 \lesssim z \lesssim 10$ appear more plausible.

Models of primeval galaxies suggest a large energy release during the formation period—of order 10^2–10^3 times the present luminosity of galaxies, over a period of 10^8–10^9 years. A major component of the luminosity is the emission from massive stars; hence a very high UV flux in the rest frame of the objects is predicted. At $z = 3$–10 the UV emission is shifted to the optical. Optical searches for primeval galaxies, however, have failed to locate them. There is a natural explanation for this failure: absorption of the UV photons by interstellar dust in the star-forming galaxies. This dust must re-radiate thermally, with a peak in the submillimeter region.

Strong support for this basic picture is provided by our best local analogues of primeval galaxies, the star-burst galaxies. These are bright IRAS sources at $\lambda = 100$ μm, and in many cases they have spectra still rising at 100 μm, suggesting a dust temperature > 30 K. Even these local sources are highly luminous—of order 100 Jy at 100 μm if at a distance of 100 Mpc.

Whether we adopt these figures or make projections from models of primeval galaxies, we arrive at the same conclusion: primeval galaxies at $z \approx$ 3–10 may be detectable at 100–300 GHz using the MMA. The angular scale of the images will be $> 5''$ (depending on the intrinsic properties, on z, and on cosmological parameters like H_0 and q_0). The number per square degree also depends on the cosmological parameters, but it is large enough (of order 100 deg^{-2}) to permit searches for such sources in regions that are free of other sources. The predicted flux density lies in the range 0.3–30 mJy. Particularly if the flux lies at the lower end of this range, the MMA will have to be pushed to its limits in sensitivity.

The advantages of the MMA over other planned and current instruments are its ability to map a two-dimensional region of the sky at adequate sensitivity, and the greater freedom of millimeter wave observations (compared to submillimeter ones) from emission by Galactic IR cirrus. In addition, a wide range of available frequencies is an advantage, since the peak of thermal dust emission depends on two unknown factors, the redshift of the primeval galaxies and the characteristic temperature of their dust:

$$\nu_{\rm peak} = \frac{60T}{1+z}\,{\rm GHz}.$$

If these predictions are correct, then these dusty primeval galaxies at high redshifts may be the dominant contributors to radio source confusion at $\lambda =$ 1–3 mm.

4. The Physics of Radio Sources

We consider here the use of the MMA both to map radio sources and to make high-frequency, high-sensitivity flux density measurements of unresolved sources.

1. Mapping of radio jets and lobes. Key understanding of radio sources comes from the ability to map them at high frequencies. High frequency observations will permit us to study the energetic particles thought to be responsible for the radio emission as they were when they were "younger"—that is, at epochs closer to the time of injection. The characteristic break in the radio spectrum (i.e., the abrupt change in spectral index) of these synchrotron sources occurs at a frequency ν_0 which is related to the age of the radiating particles according to $\nu_0 \propto t^{-2}$. Higher frequency observations will thus permit us to look more closely at the accelerating "engines" in the cores of these sources. Observations over a wide range of frequencies will permit us to follow the energy loss or aging of the particles in the jets of extragalactic radio sources. MMA maps will thus complement and strengthen VLA results. Such combined observations will increase our understanding of both the physics of the central "engines" of radio sources and the plasma physics of the jets and lobes themselves.

While the planned-for resolution of the MMA approximately matches that of the VLA, it is known from VLBI observations that radio sources (including

jets) have structure on angular scales as small as 10^{-3} arcsec. To understand the fine structure of jets, and in particular to investigate conditions near the central "engines" of these sources, higher resolution is needed than is provided for by the "benchmark" instrument that we considered. One solution, which we believe merits careful consideration, is to link the MMA to the VLBA, whose antennas will function to 90 GHz with an acceptable efficiency of 25–30%. The combined instrument would permit observations at 3 mm or 9 mm over a range of angular scales of $\sim 10^6 : 1$.

To make such a link work, baselines of order 3–30 km are required in order for the MMA to tie in with the shortest VLBA spacings. In addition, since the center of the VLBA array is at the VLA, and the shortest baselines are centered there, there is a strong argument for siting the MMA near the VLA. This is the one situation we have discussed in which we believe a scientific goal dictates a specific location of the MMA.

We also wish to note that long-baseline synthesis observations of such sources ought to be feasible, because of the possibility of using self-calibration. Most such sources have one or more bright radio sources present which can be used for self-calibration.

Finally, siting the MMA near the center of the VLBA offers a side benefit—the MMA in its 90 meter configuration could then be used on occasion as a phased-array element in the VLBA network itself.

2. Unresolved sources. We have discussed two classes of unresolved or "point" sources: radio quiet QSOs, and variable sources. In both cases, it is the combination of the high frequency response and the high sensitivity of the MMA that opens up new scientific possibilities.

Radio quiet QSOs are those whose radio flux densities (at centimeter or longer wavelengths) fall below their optical flux densities (some striking examples are shown in Figure 3). In general, the optical spectra of radio quiet QSOs show an increase in flux as the frequency of observation decreases. Some of these sources were observed by IRAS, which showed that the trend continues to $\lambda = 100$ μm, or $\nu = 3{,}000$ GHz. Where and why does the spectrum break in the radio quiet QSOs? It is observations in the millimeter range that will tell us.

In addition, the central, high-luminosity, broad emission-line region of these objects is not accessible to radio observations at $\lambda \approx 1$ mm, because of free–free opacity. At millimeter (and possibly at submillimeter) wavelengths, we may be able to probe the central "engines" of these QSOs as well. The spectral signature of the radio quiet QSOs in the 30–300 GHz range will provide an important diagnostic.

The same may be said for variable radio sources. High frequency observations will detect younger electrons, nearer to the accelerating region. They may also make possible a bridge, in understanding, between radio variability and optical variability—which in many sources now appear unrelated.

The shorter radiative lifetime in the millimeter region also means that high frequency observations will be less influenced by left-over emission from previ-

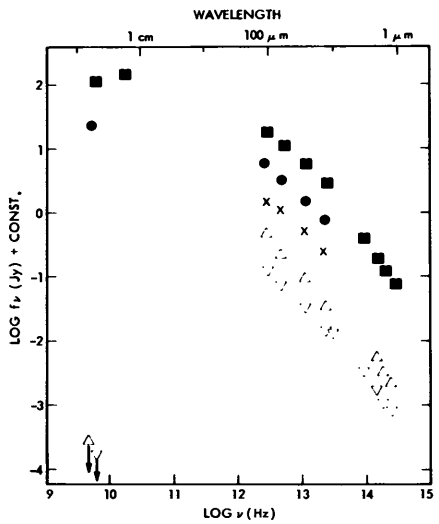

Figure 3. Spectra of radio quiet and radio bright QSOs (from Neugebauer *et al.* (1984), *Astrophys. J. (Letters)* **278**, L83).

ous outbursts—thus a "cleaner" signal will result.

All these considerations, and the expectation of higher fractional variability in the millimeter than in the centimeter region, also make the MMA an attractive instrument for monitoring gravitationally lensed sources. Studies of the variability of lensed sources will provide useful data both on cosmological parameters like Ω_0 and on the properties of the foreground, lensing, objects.

For many of the observations discussed in this section, a high frequency capability is important. On the other hand, because of the intrinsically broadband nature of the emission mechanisms involved, the gain in moving from the 200–290 GHz atmospheric window to 345 GHz is not vital.

3. Source counts. We also discussed use of the MMA to make source counts at millimeter wavelengths. Its high resolution makes it unsuitable for such work. At 9 mm, our estimate is that a rapid sky survey with the 10 m antennas used independently would turn up one source only every few hours, assuming an integration time, per survey area, of one second. Sources with flux density $S \gtrsim 0.6$ Jy could be detected. At $\lambda \lesssim 9$ mm, the instrument would not be at all useful in making source counts—hence our emphasis above on its power to improve our knowledge of *known* radio sources.

4. Polarization studies. Many of the kinds of extragalactic radio sources we discussed are polarized, and linear polarization is an important diagnostic of radio-frequency emission mechanisms. If the MMA is to be used fruitfully for polarization studies, then the uncertainties in the instrumental polarization of the array need to be reduced to the 0.1% level. The instrumental polarization itself can and probably will be > 0.1%, but it must be stable and be determinable to the 0.1% level.